On Thinning Ice: Modeling Sea Ice in a Warming Climate

Kenneth M. Golden
Department of Mathematics, University of Utah

Antarctic Sea Ice and Southern Ocean Seminar
16 February 2022

Worby

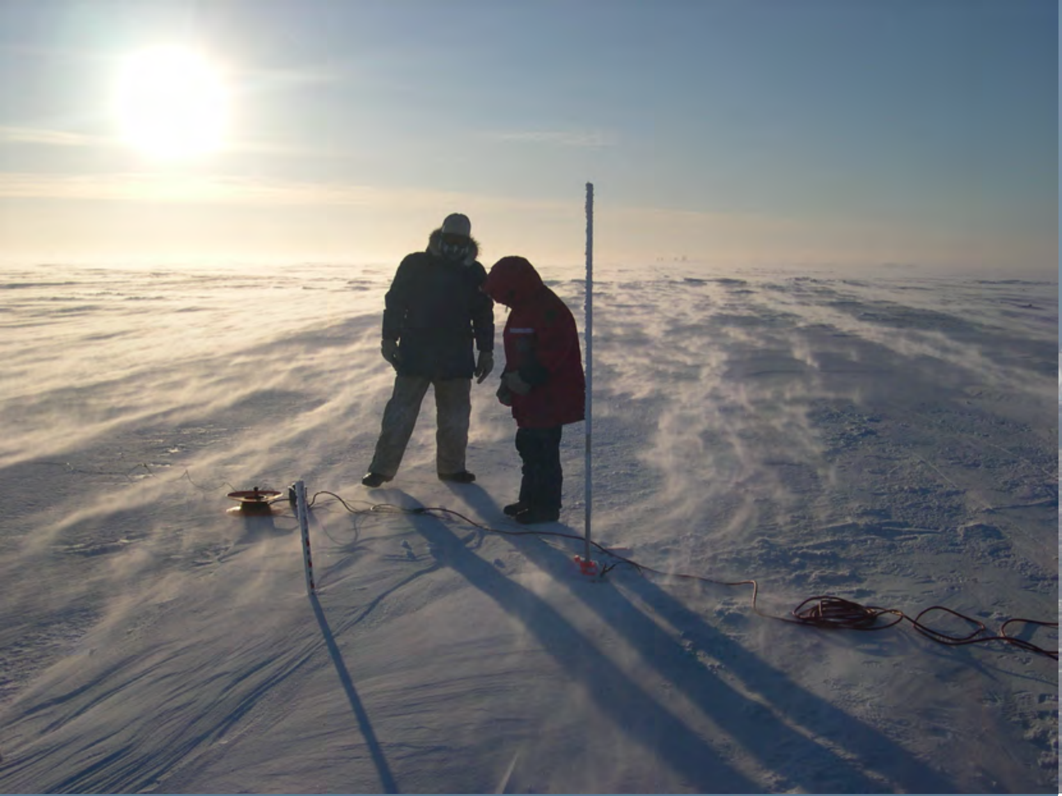

sea ice may appear to be a barren, impermeable cap ...

brine inclusions in sea ice (mm)

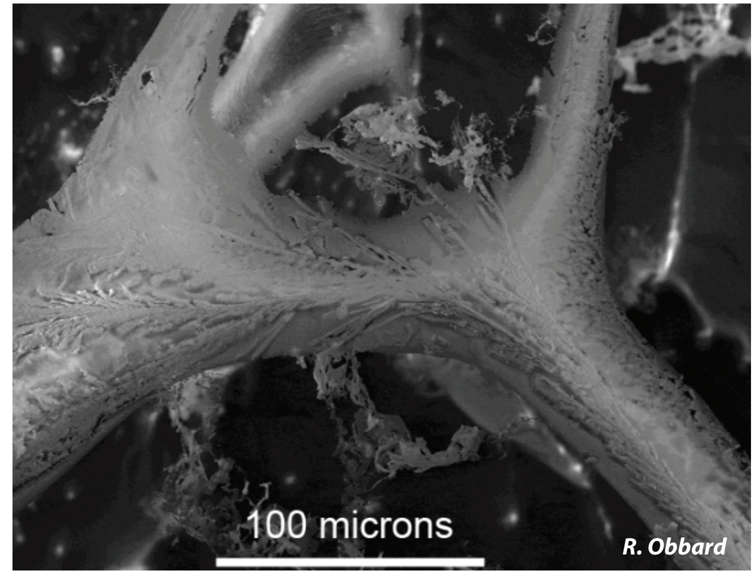

micro - brine channel (SEM)

brine channels (cm)

horizontal section

vertical section

sea ice is a porous composite

pure ice with brine, air, and salt inclusions

fluid flow through the porous microstructure of sea ice governs key processes in polar climate and ecosystems

evolution of Arctic melt ponds and sea ice albedo

nutrient flux for algal communities

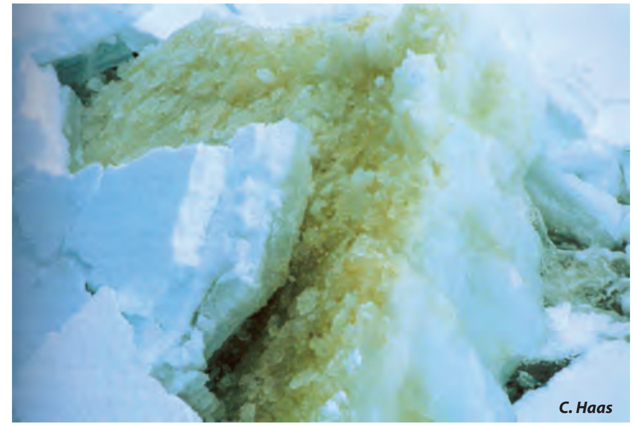

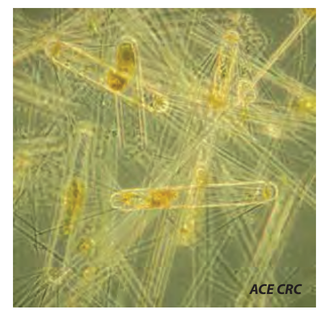

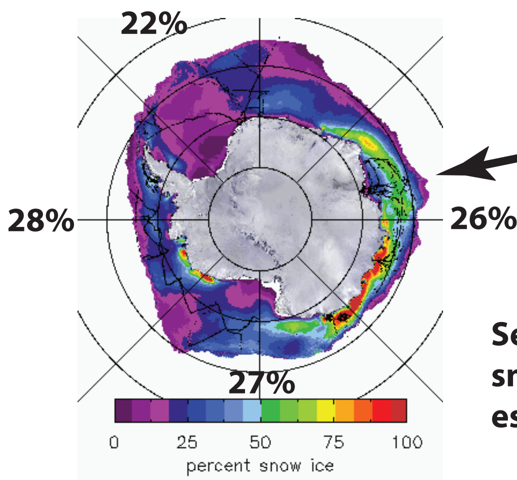

T. Maksym and T. Markus, 2008

September snow-ice estimates

Antarctic surface flooding and snow-ice formation

- evolution of salinity profiles

- ocean-ice-air exchanges of heat, CO_2

Sea Ice is a Multiscale Composite Material

microscale

brine inclusions

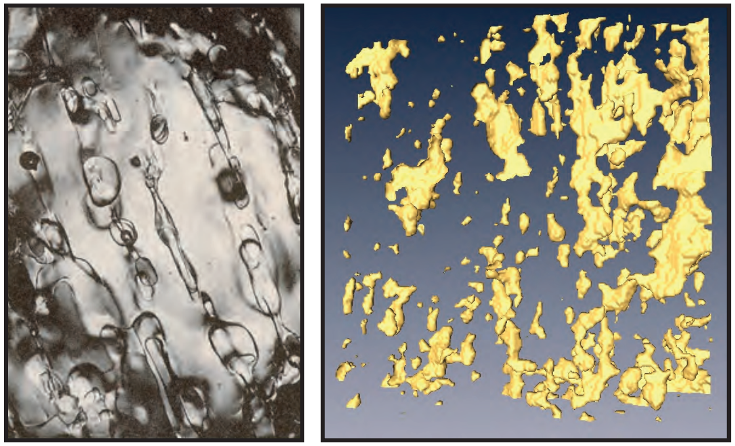

Weeks & Assur 1969

H. Eicken
Golden *et al. GRL* 2007

polycrystals

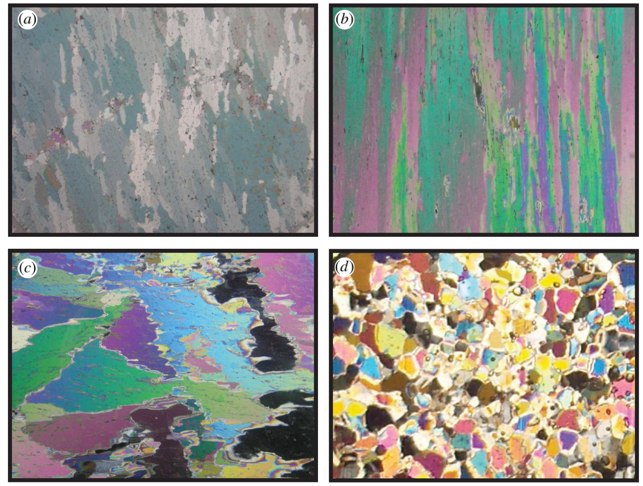

Gully *et al. Proc. Roy. Soc. A* 2015

brine channels

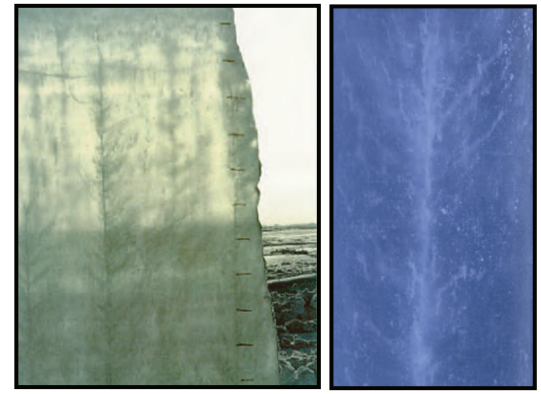

D. Cole **K. Golden**

millimeters **centimeters**

---

mesoscale

Arctic melt ponds

K. Frey

Antarctic pressure ridges

K. Golden

meters

macroscale

sea ice floes

J. Weller

sea ice pack

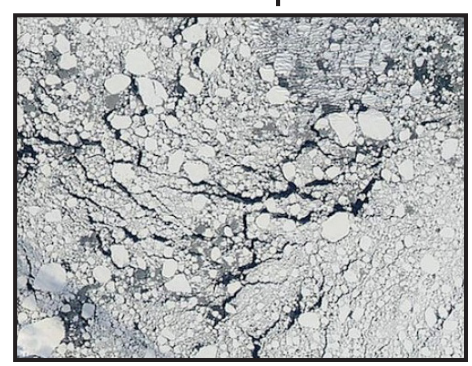

NASA

kilometers

Arctic sea ice extent September 15, 2020

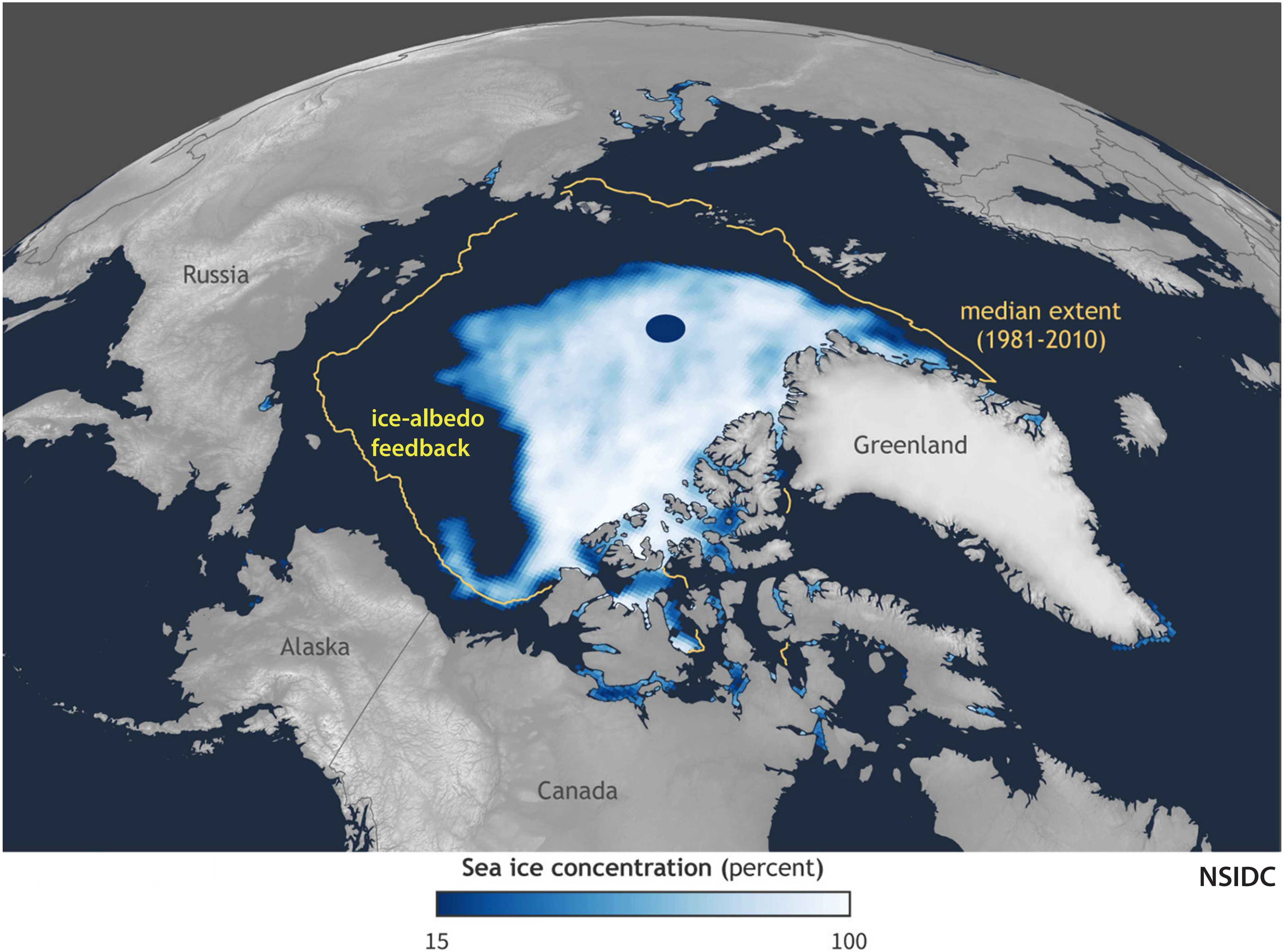

Predicting what may come next requires lots of math modeling.

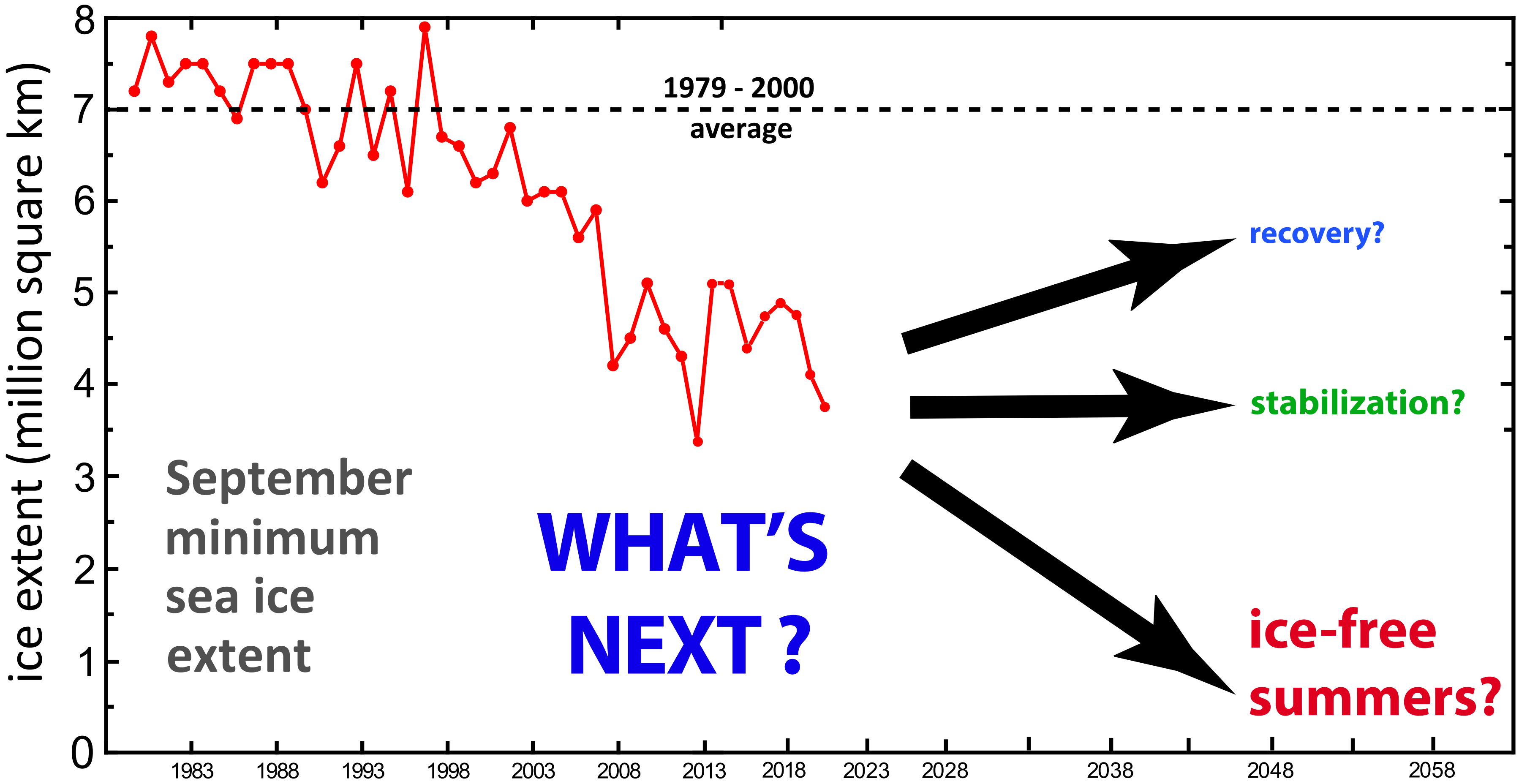

National Snow and Ice Data Center (NSIDC)

HOMOGENIZATION for Composite Materials

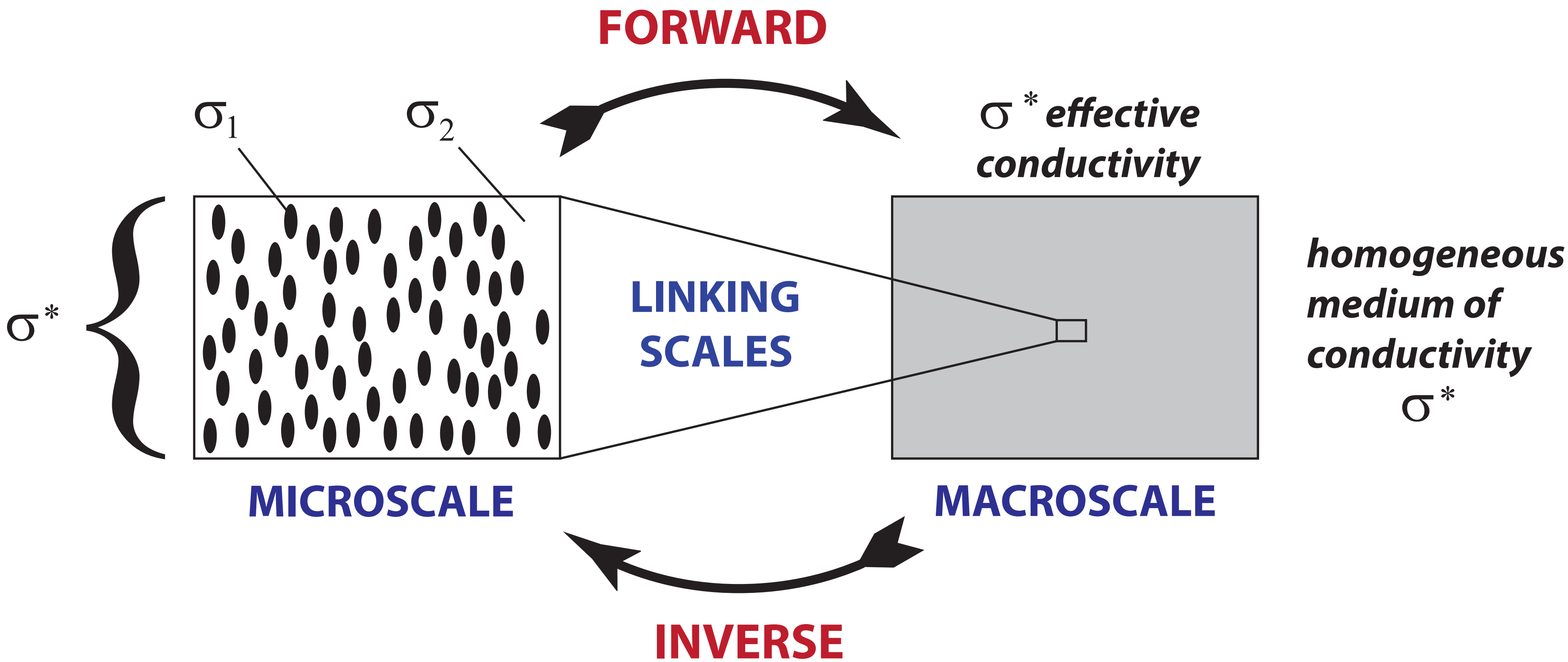

Maxwell 1873 : effective conductivity of a dilute suspension of spheres
Einstein 1906 : effective viscosity of a dilute suspension of rigid spheres in a fluid

*Wiener 1912 : arithmetic and harmonic mean **bounds** on effective conductivity*
*Hashin and Shtrikman 1962 : variational **bounds** on effective conductivity*

widespread use of composites in late 20th century due in large part to advances in mathematically predicting their effective properties

What is this talk about?

Using methods of **homogenization and statistical physics** to model sea ice effective behavior and advance representation of sea ice in climate models, process studies, ...

MODELING SEA ICE

microscale

↓

mesoscale

↓

macroscale

A tour of key sea ice processes on micro, meso, and macro scales.

What is our research about?

Using methods of **homogenization and statistical physics** to model sea ice effective behavior and advance representation of sea ice in climate models, process studies, ...

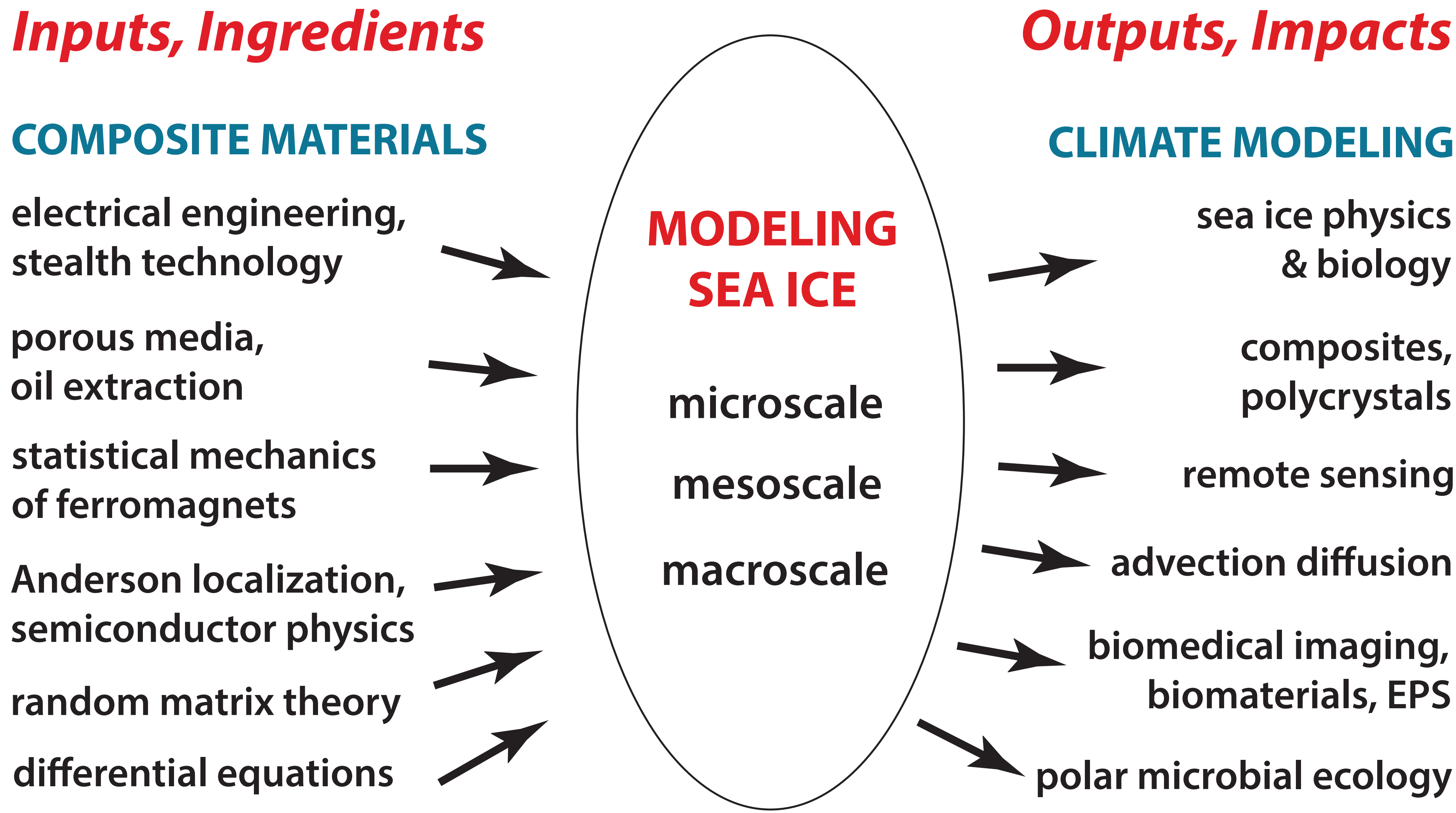

What is our research about?

Inputs, Ingredients

COMPOSITE MATERIALS

Outputs, Impacts

CLIMATE MODELING

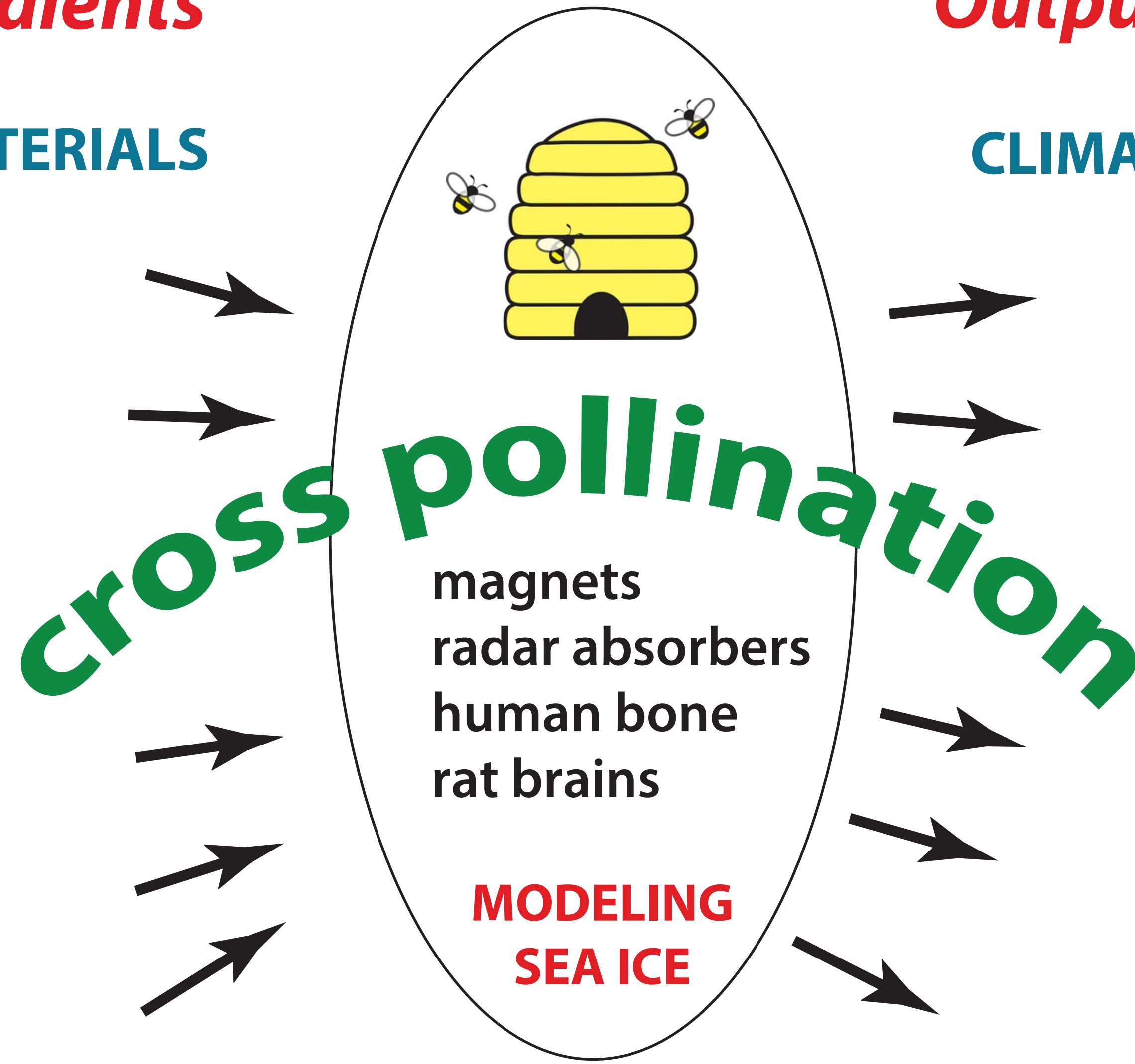

Modeling sea ice drives advances in many areas of science and engineering.

microscale

brine volume fraction and ***connectivity*** increase with temperature

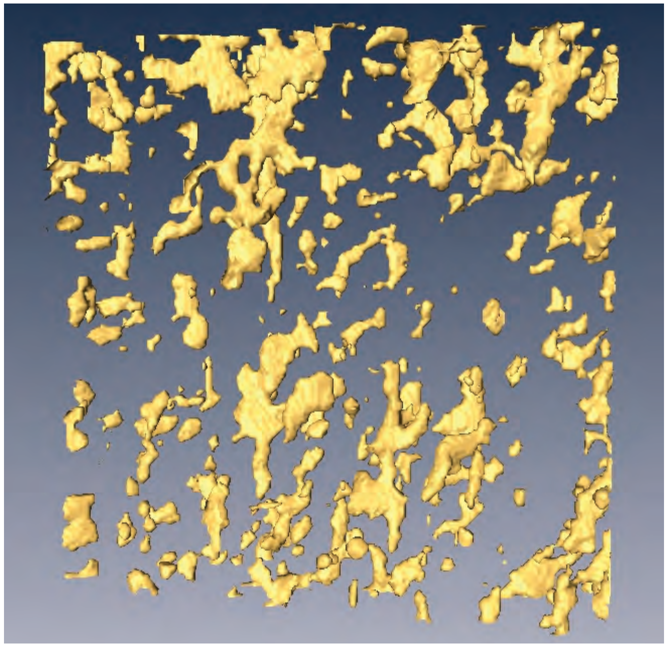

T = -15 °C, $\phi = 0.033$

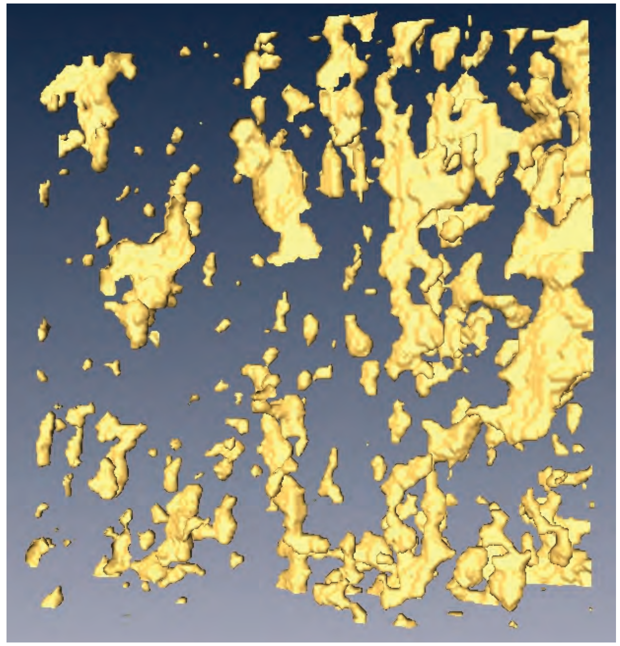

T = -6 °C, $\phi = 0.075$

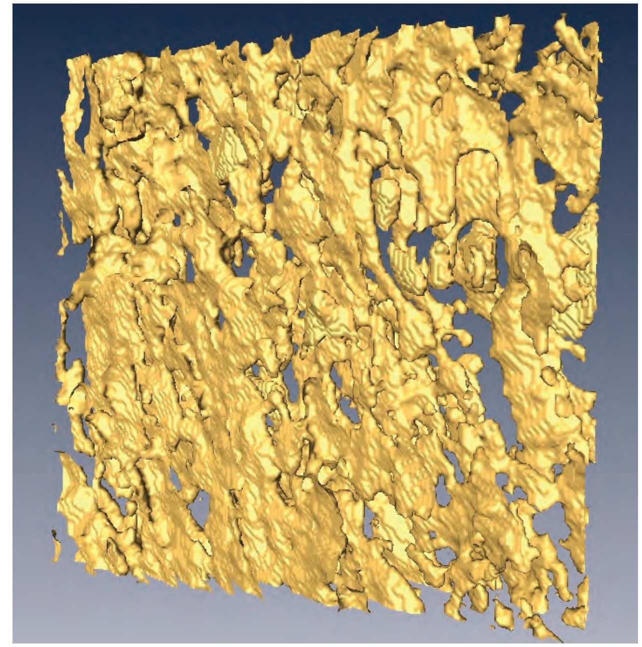

T = -3 °C, $\phi = 0.143$

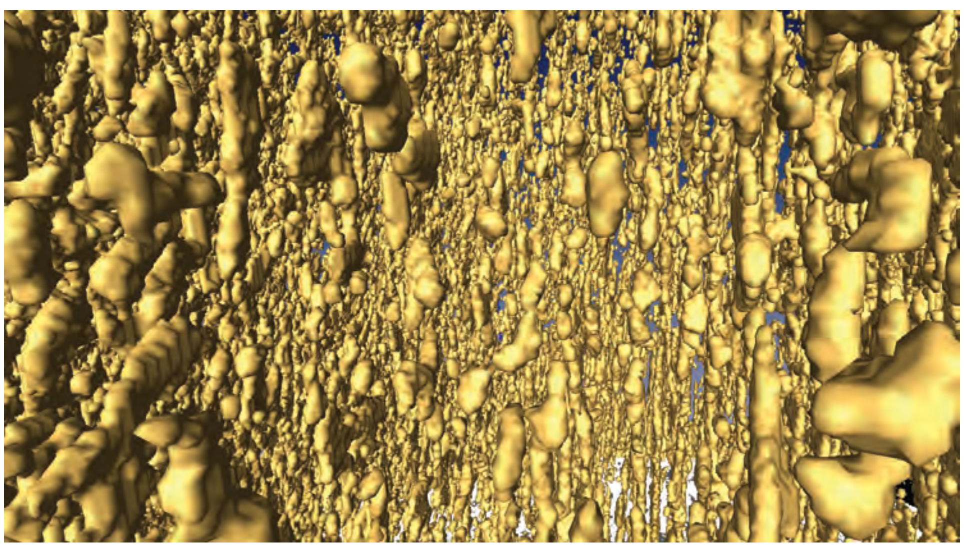

T = -8 °C, $\phi = 0.057$

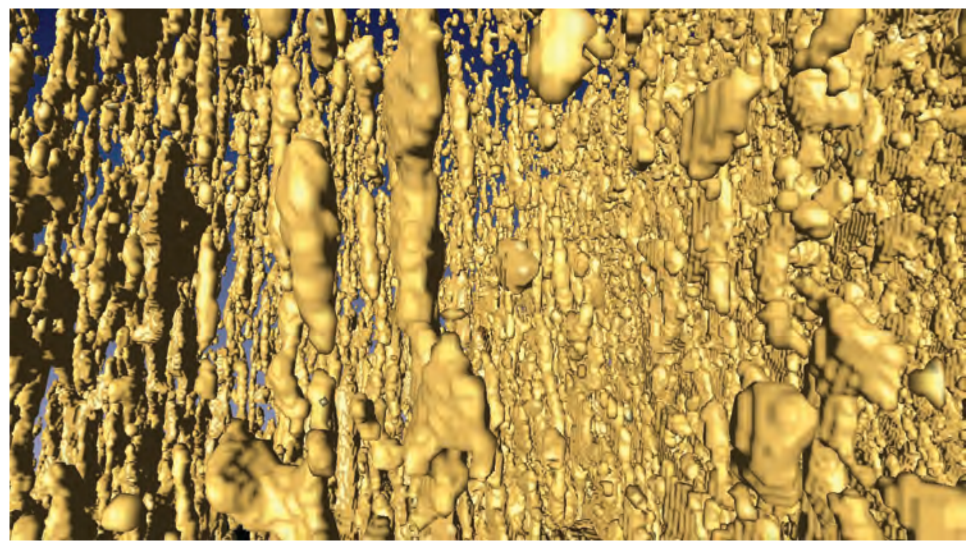

T = -4 °C, $\phi = 0.113$

X-ray tomography for brine in sea ice

Golden *et al.*, *Geophysical Research Letters*, 2007

fluid permeability of a porous medium

how much water gets through the sample per unit time?

Darcy's Law

for slow viscous flow in a porous medium

averaged fluid velocity

pressure gradient

$$\mathrm{v} = -\frac{\mathbf{k}}{\eta}\,\nabla p$$

viscosity

$\mathbf{k}$ = fluid permeability tensor

HOMOGENIZATION

mathematics for analyzing effective behavior of heterogeneous systems

Critical behavior of fluid transport in sea ice

impermeable permeable

Arctic field data

vertical fluid permeability k (m^2)

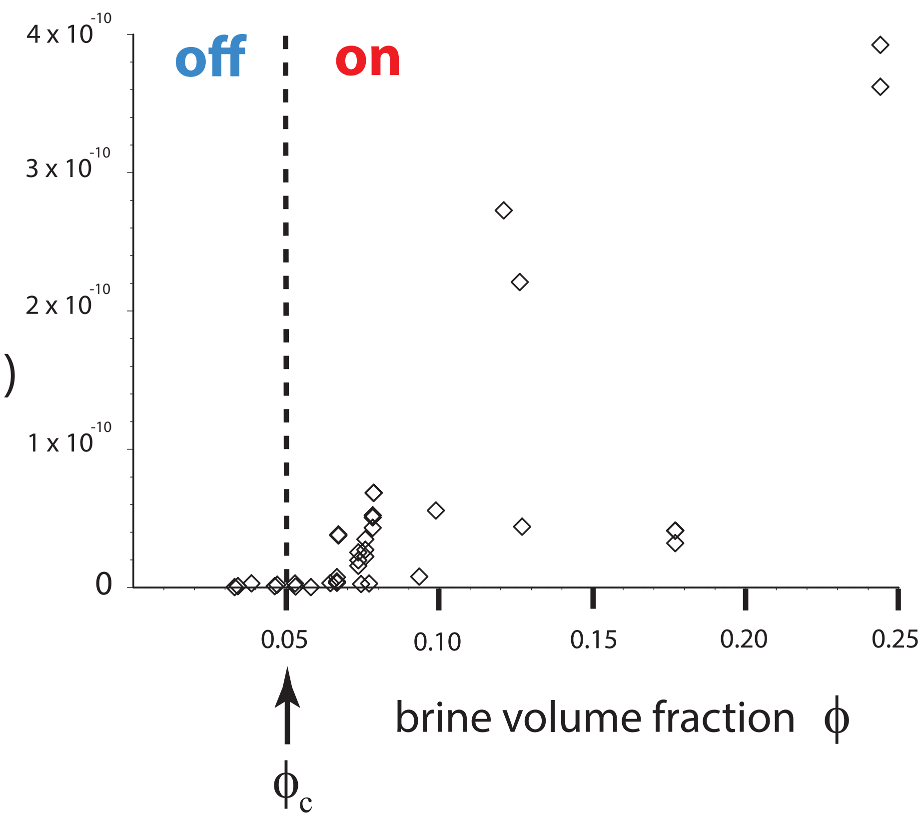

"on - off" switch for fluid flow

critical brine volume fraction $\phi_c \approx 5\%$ $\longleftrightarrow$ $T_c \approx -5^\circ$C, $S \approx 5$ ppt

RULE OF FIVES

Golden, Ackley, Lytle Science 1998
Golden, Eicken, Heaton, Miner, Pringle, Zhu GRL 2007
Pringle, Miner, Eicken, Golden J. Geophys. Res. 2009

sea ice algal communities

D. Thomas 2004

nutrient replenishment controlled by ice permeability

biological activity turns on or off according to ***rule of fives***

Golden, Ackley, Lytle ***Science 1998***

Fritsen, Lytle, Ackley, Sullivan ***Science 1994***

critical behavior of microbial activity

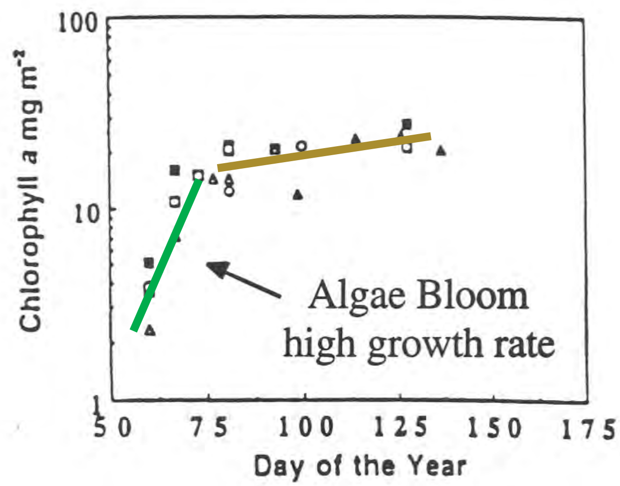

Convection-fueled algae bloom
Ice Station Weddell

percolation theory

probabilistic theory of connectedness

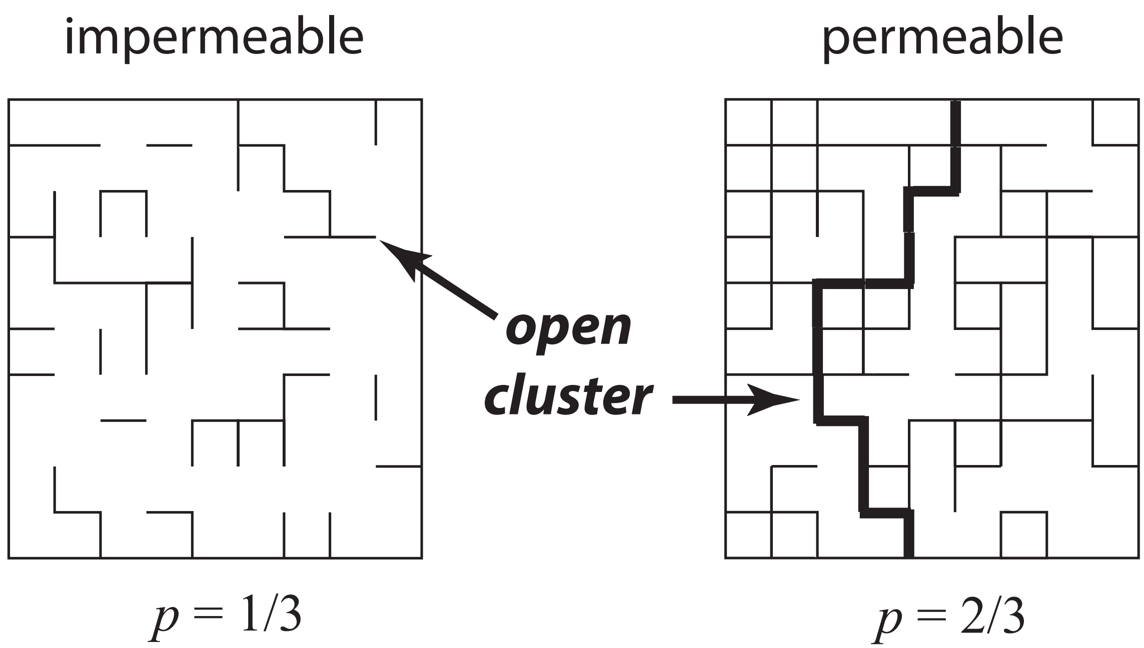

bond → **open** *with probability p*
closed *with probability 1-p*

percolation threshold

$$p_c = 1/2 \quad \text{for} \quad d = 2$$

smallest *p* for which there is an infinite open cluster

Continuum percolation model for *stealthy* materials applied to sea ice microstructure explains **Rule of Fives** and Antarctic data on ice production and algal growth

$\phi_c \approx 5\,\%$ Golden, Ackley, Lytle, *Science*, 1998

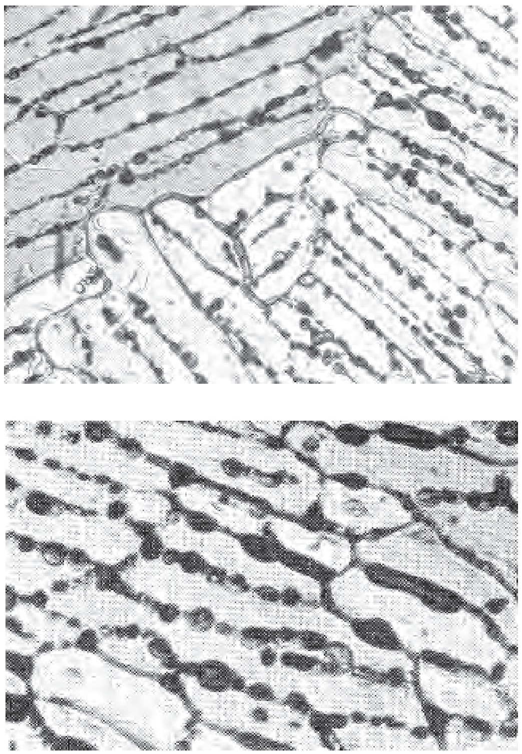

sea ice

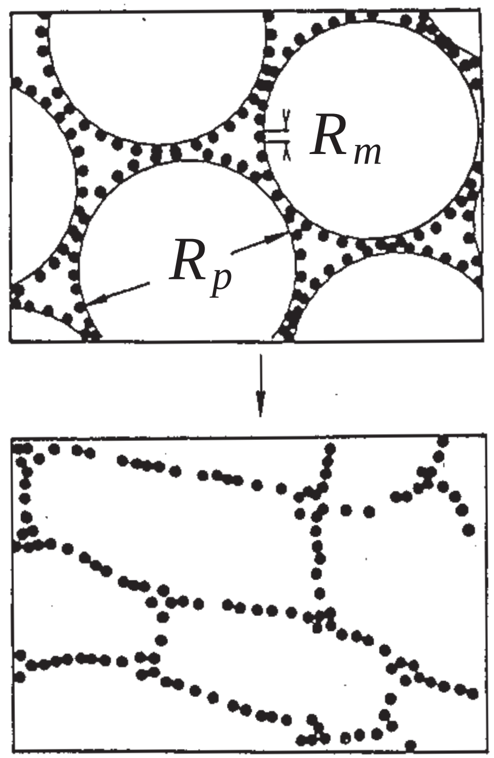

compressed powder

radar absorbing composite

sea ice is radar absorbing

Thermal evolution of permeability and microstructure in sea ice

Golden, Eicken, Heaton*, Miner, Pringle, Zhu, Geophysical Research Letters 2007

microscale

governs

mesoscale processes

melt pond evolution

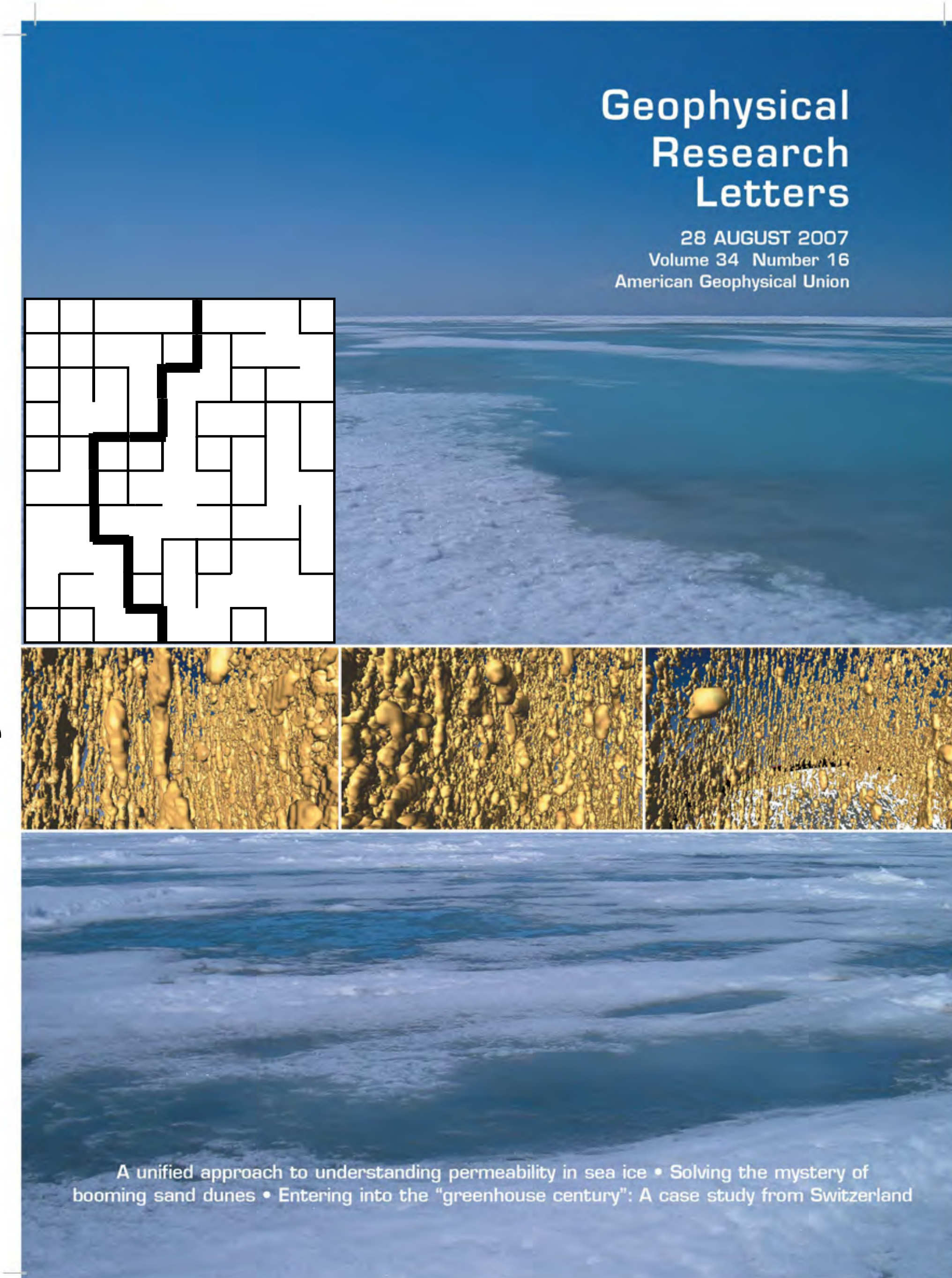

percolation theory for fluid permeability

$$k(\phi) = k_0 (\phi - 0.05)^2$$

critical exponent t

$$k_0 = 3 \times 10^{-8} \ \mathrm{m}^2$$

from critical path analysis in hopping conduction

hierarchical model

rock physics

network model

rigorous bounds

X-ray tomography for brine inclusions

confirms rule of fives

Pringle, Miner, Eicken, Golden J. Geophys. Res. 2009

theories agree closely with field data

Sea ice algae secrete extracellular polymeric substances (EPS) affecting evolution of brine microstructure.

How does EPS affect fluid transport? **How does the biology affect the physics?**

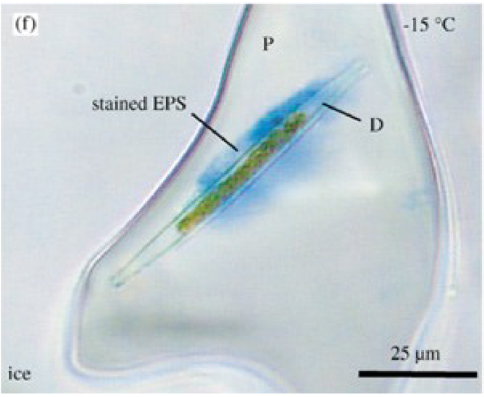

Krembs

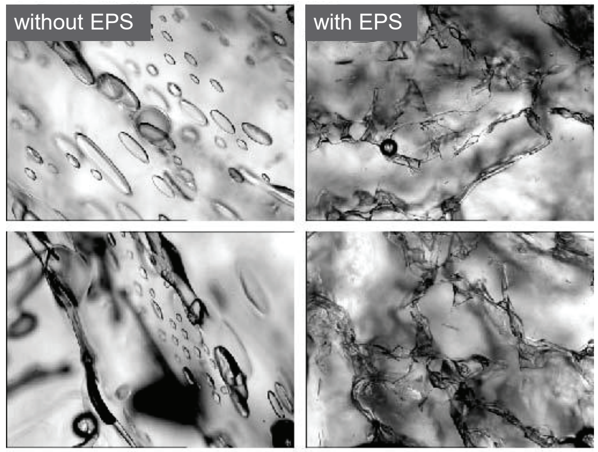

Krembs, Eicken, Deming, PNAS 2011

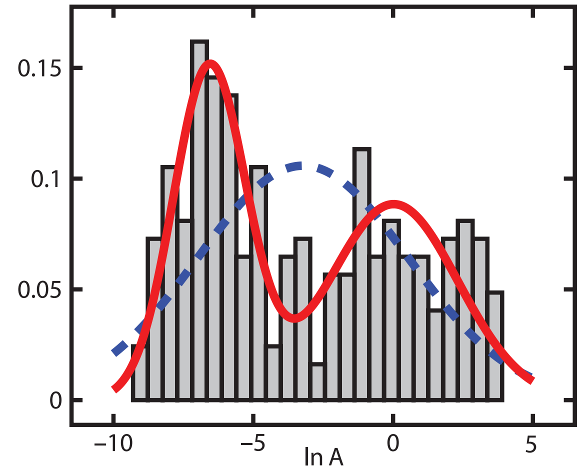

RANDOM PIPE MODEL

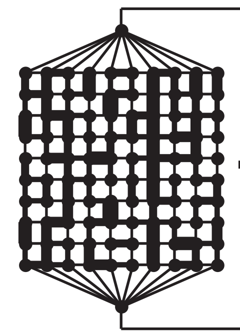

- 2D random pipe model with bimodal distribution of pipe radii
- Rigorous bound on permeability *k;* results predict observed drop in *k*

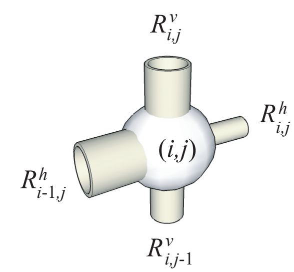

Steffen, Epshteyn, Zhu, Bowler, Deming, Golden
Multiscale Modeling and Simulation, 2018

Zhu, Jabini, Golden, Eicken, Morris
Ann. Glac. 2006

Thermal evolution of the fractal geometry of the brine microstructure in sea ice

N. Ward, D. Hallman, H. Eicken, M. Oggier and K. M. Golden, 2022

$T = -12\ ^\circ\mathrm{C},\ \phi = 0.033$

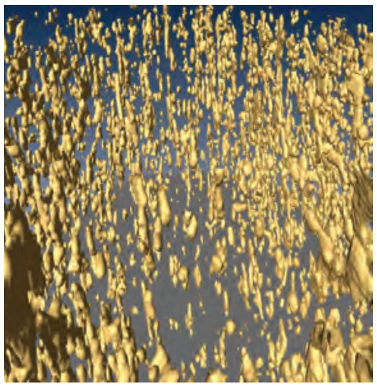

$T = -8^\circ\mathrm{C},\ \phi = 0.057$

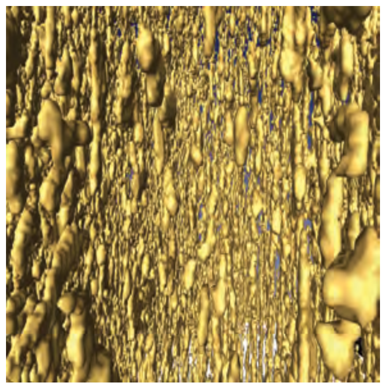

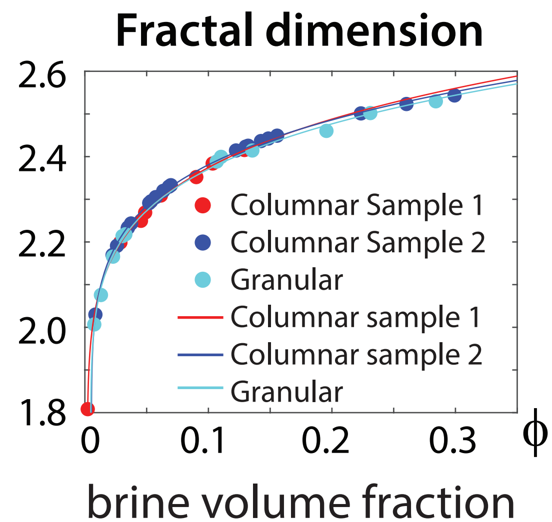

X-ray tomography

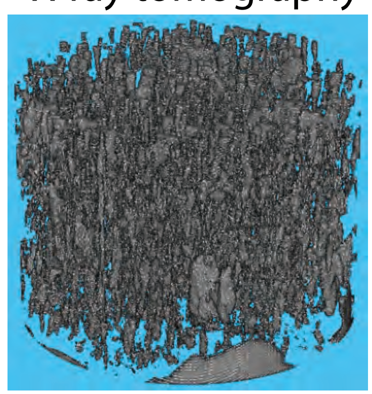

DLA model

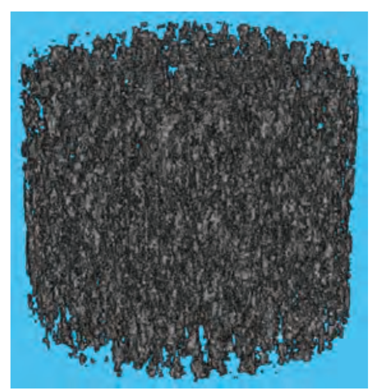

Arctic and Antarctic field experiments

develop electromagnetic methods of monitoring fluid transport and microstructural transitions

extensive measurements of fluid and electrical transport properties of sea ice:

2007	*Antarctic*	*SIPEX*
2010	*Antarctic*	*McMurdo Sound*
2011	*Arctic*	*Barrow AK*
2012	*Arctic*	*Barrow AK*
2012	*Antarctic*	*SIPEX II*
2013	*Arctic*	*Barrow AK*
2014	*Arctic*	*Chukchi Sea*

photo by Jan Lieser

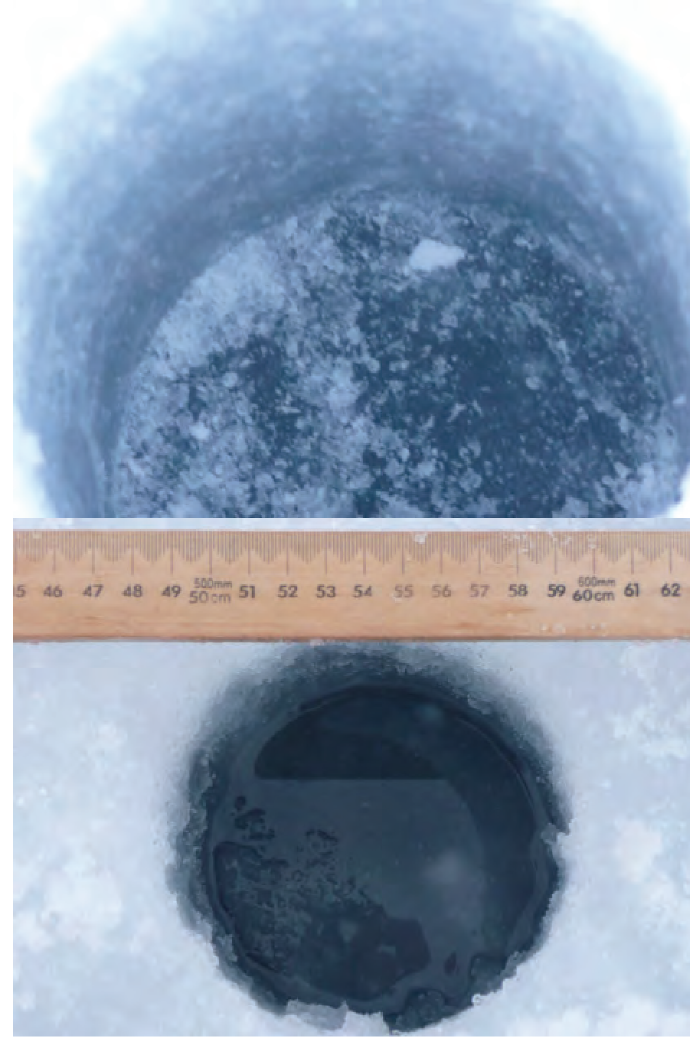

measuring
fluid permeability
of Antarctic sea ice

SIPEX 2007

electrical measurements

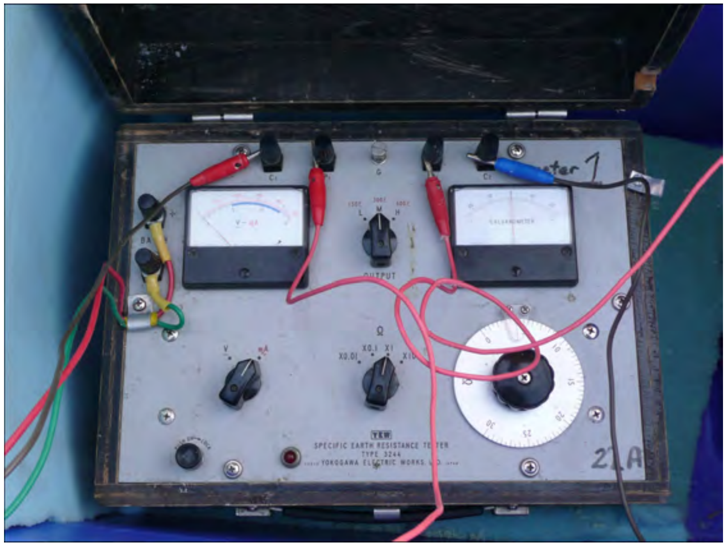

Wenner array

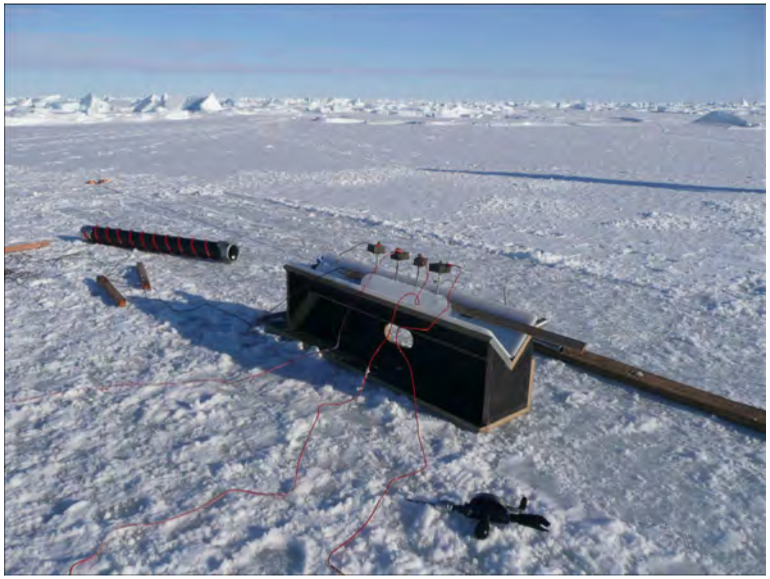

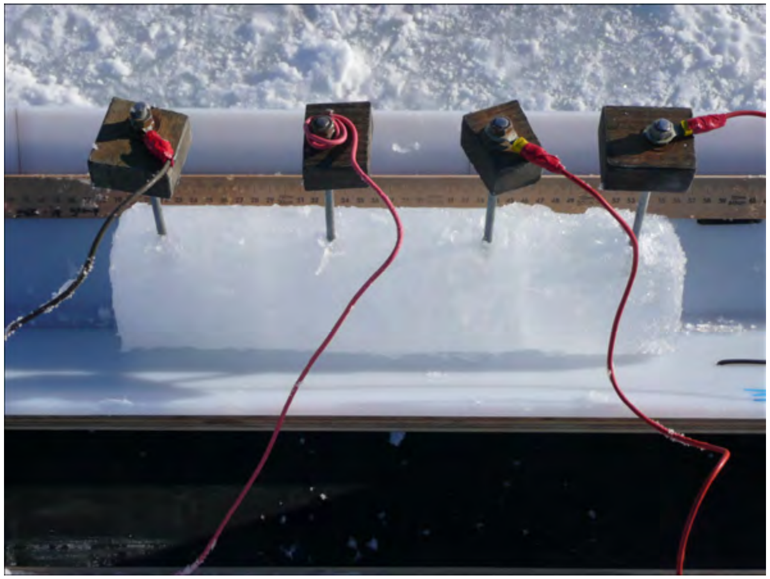

vertical conductivity

Zhu, Golden, Gully, Sampson ***Physica B*** 2010

Sampson, Golden, Gully, Worby ***Deep Sea Research*** 2011

cross borehole tomography

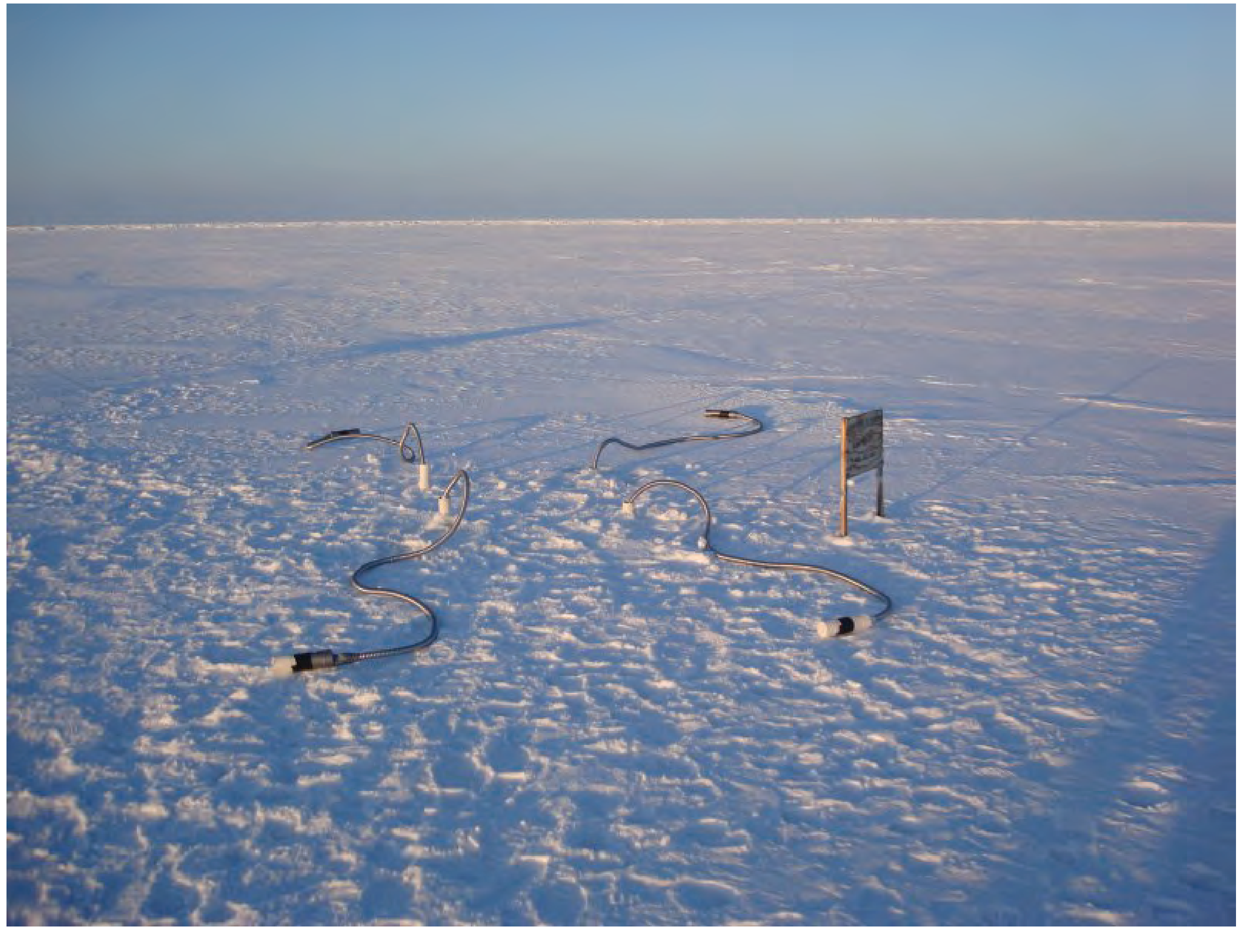

Ingham, Jones, Buchanan
Victoria University, Wellington, NZ

critical behavior of electrical transport in sea ice

electrical signature of the on-off switch for fluid flow

same universal critical exponent as for fluid permeability

studied for over 50 years but no previous observations or theory of critical behavior

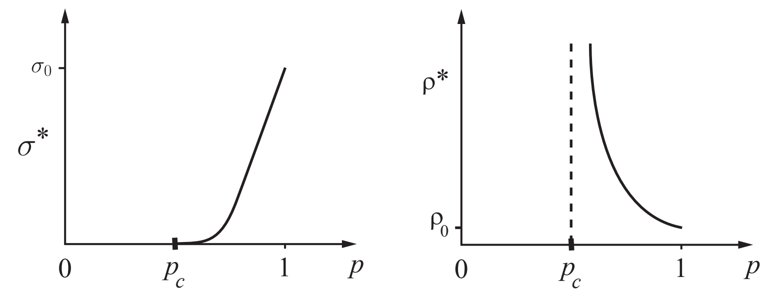

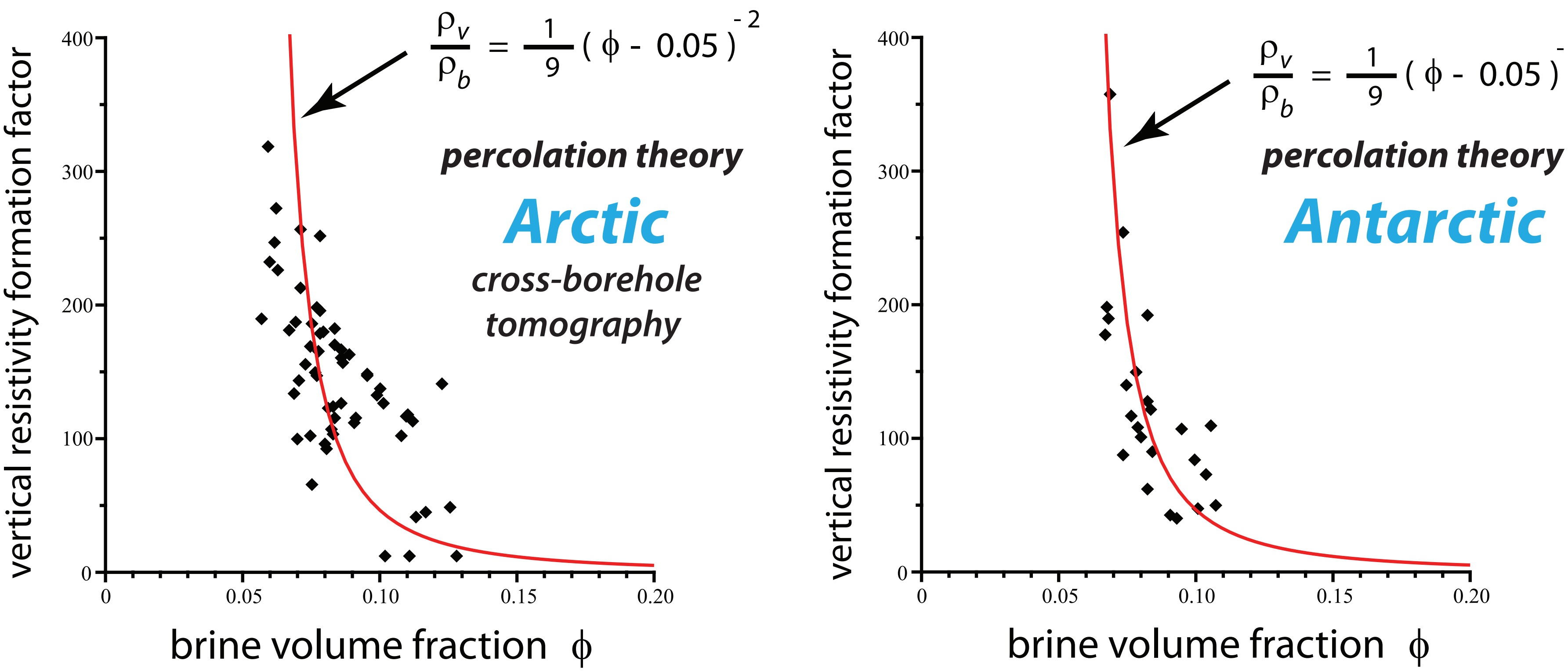

Golden, Eicken, Gully, Ingham, Jones, Lin, Reid, Sampson, Worby 2022

Measuring sea ice thickness

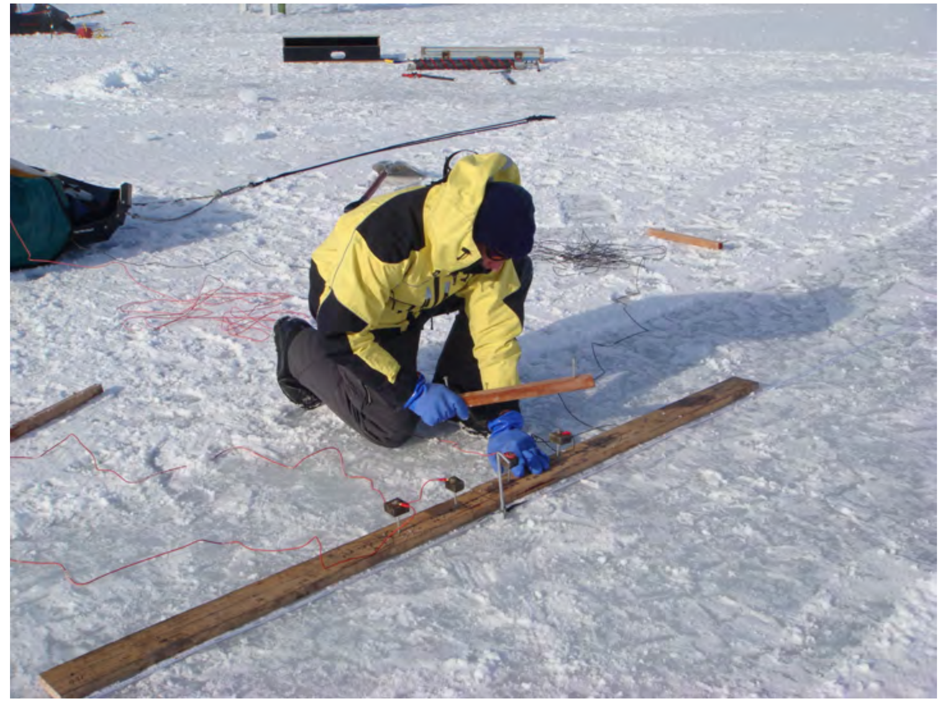

Golden

Modeling of anisotropic electromagnetic reflection from sea ice
Golden & Ackley, JGR 1981

measure sea ice thickness using 100 MHz waves

Model sea ice as a two phase composite of pure ice with anisotropic ellipsoidal brine inclusions; use mean field theory to estimate complex permittivity

Explained marked anisotropy in bottom return in terms of relation between E field polarization and current-induced anisotropy in brine microstructure (c-axis direction).

Weeks & Gow, 1979
Kovacs & Morey, 1978

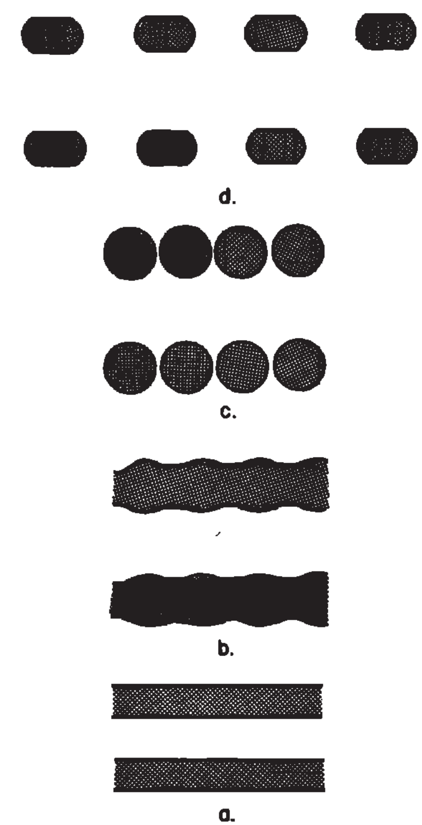

Fig. 4. Brine layers (top view) near the bottom of sea ice (*a*) begin to 'neck' with decreasing temperature further up in the ice sheet(s) and freeze out into cylinders (*c*) and elliptical cylinders (*d*) [from *Anderson and Weeks*, 1958].

Bounds on the complex permitttivity of polycrystalline sea ice with anisotropy in the horizontal plane
K. McLean, E. Cherkaev, K. M. Golden, 2022

Remote sensing of sea ice

sea ice thickness
ice concentration

INVERSE PROBLEM

Recover sea ice properties from electromagnetic (EM) data

ε^*

effective complex permittivity
(dielectric constant, conductivity)

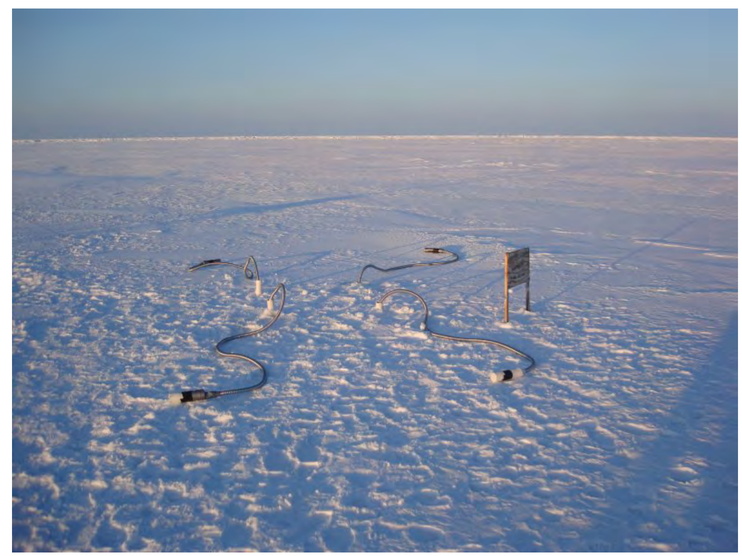

brine volume fraction
brine inclusion connectivity

Effective complex permittivity of a two phase composite in the quasistatic (long wavelength) limit

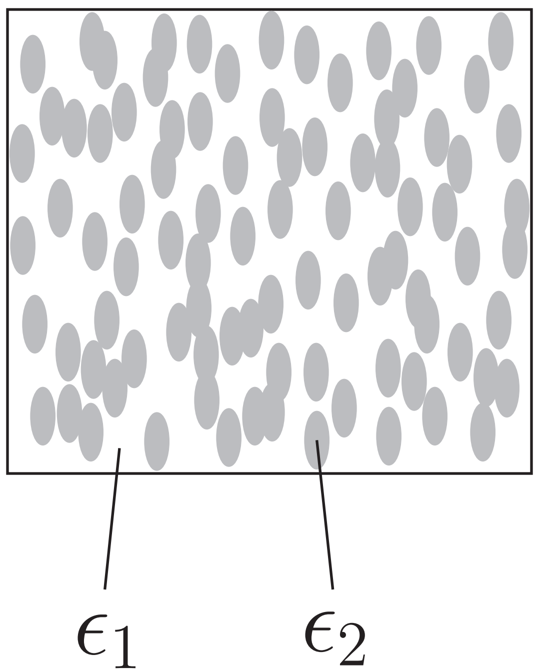

$$\epsilon^*$$

$$D = \epsilon E$$

$$\nabla \cdot D = 0$$

$$\nabla \times E = 0$$

$$\langle D \rangle = \epsilon^* \langle E \rangle$$

p_1 , p_2 = volume fractions of the components

$$\epsilon^* = \epsilon^* \left(\frac{\epsilon_1}{\epsilon_2} \; , \text{ composite geometry } \right)$$

What are the effective propagation characteristics of an EM wave (radar, microwaves) in the medium?

Analytic Continuation Method for Homogenization

Bergman (1978), Milton (1979), Golden and Papanicolaou (1983), Theory of Composites, Milton (2002)

Stieltjes integral representation for homogenized parameter

separates geometry from parameters

geometry

$$F(s) = 1 - \frac{\epsilon^*}{\epsilon_2} = \int_0^1 \frac{d\mu(z)}{s - z} \qquad s = \frac{1}{1 - \epsilon_1/\epsilon_2}$$

material parameters

μ

- spectral measure of self adjoint operator $\Gamma\chi$
- mass $= p_1$
- higher moments depend on n-point correlations

$\Gamma = \nabla(-\Delta)^{-1}\nabla\cdot$

$\chi =$ characteristic function of the brine phase

$E = s\,(s + \Gamma\chi)^{-1} e_k$

$\Gamma\chi$: **microscale $\longrightarrow$ macroscale**

$\Gamma\chi$ ***links scales***

Golden and Papanicolaou, Comm. Math. Phys. 1983

This representation distills the complexities of mixture geometry into the spectral properties of an operator like the Hamiltonian in physics.

forward and inverse bounds on the complex permittivity of sea ice

forward bounds

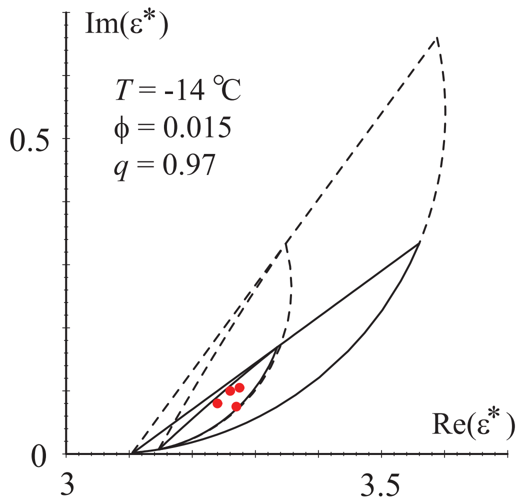

4.75 GHz data

matrix particle

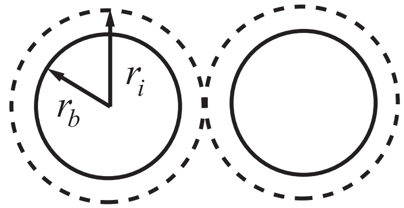

$$q = r_b / r_i$$

$$0 < q < 1$$

Golden 1995, 1997

inverse bounds

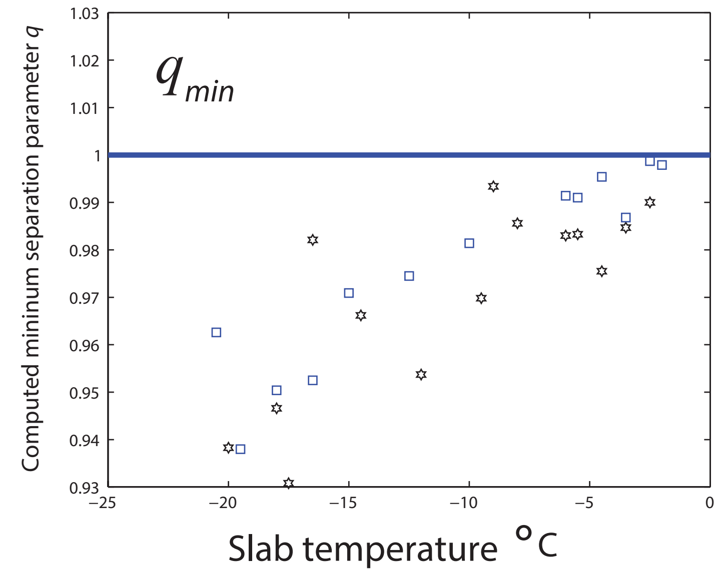

Inverse Homogenization

Cherkaev and Golden (1998), Day and Thorpe (1999), Cherkaev (2001), McPhedran, McKenzie, Milton (1982), *Theory of Composites*, Milton (2002)

ε^* ⟶ ***composite geometry*** **(spectral measure μ)**

inverse bounds and recovery of brine porosity

Gully, Backstrom, Eicken, Golden
Physica B, 2007

inversion for brine inclusion separations in sea ice from measurements of effective complex permittivity ε^*

rigorous inverse bound on spectral gap

construct algebraic curves which bound admissible region in (p,q)-space

Orum, Cherkaev, Golden
Proc. Roy. Soc. A, 2012

SEA ICE

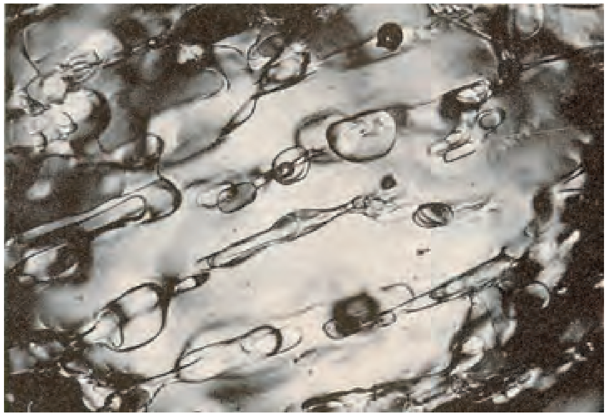

HUMAN BONE

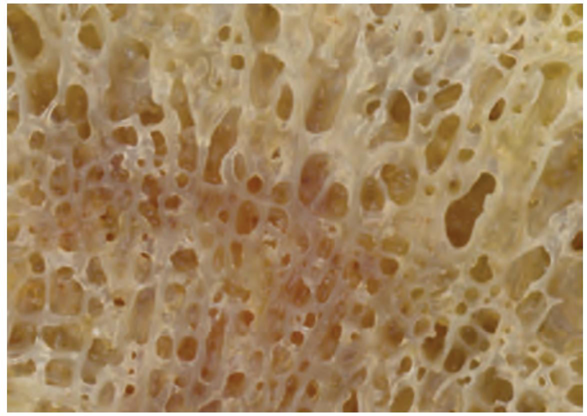

spectral characterization of porous microstructures in human bone

young healthy trabecular bone

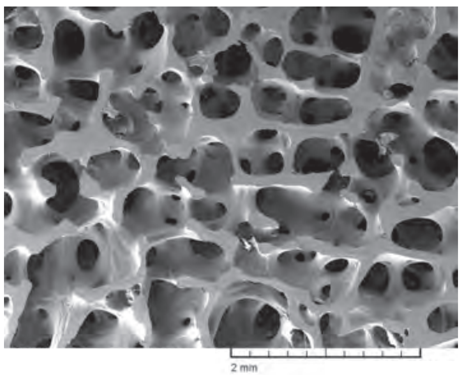

old osteoporotic trabecular bone

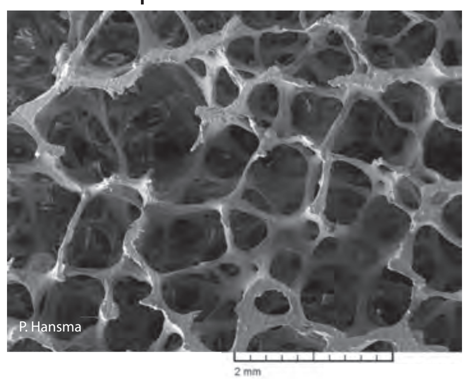

reconstruct spectral measures from complex permittivity data

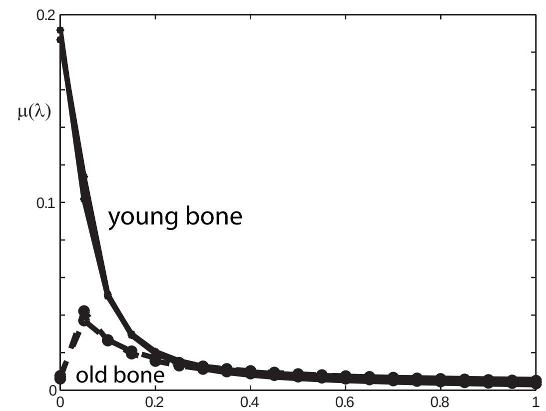

use regularized inversion scheme

apply spectral measure analysis of brine connectivity and spectral inversion to electromagnetic monitoring of osteoporosis

Golden, Murphy, Cherkaev, J. Biomechanics 2011

the math doesn't care if it's sea ice or bone!

direct calculation of spectral measures

Murphy, Hohenegger, Cherkaev, Golden, *Comm. Math. Sci.* 2015

- depends only on the composite geometry
- discretization of microstructural image gives binary network
- fundamental operator becomes a random matrix
- spectral measure computed from eigenvalues and eigenvectors

once we have the spectral measure μ it can be used in Stieltjes integrals for other transport coefficients:

electrical and thermal conductivity, complex permittivity, magnetic permeability, diffusion, fluid flow properties

earlier studies of spectral measures

Day and Thorpe 1996
Helsing, McPhedran, Milton 2011

Spectral computations for sea ice floe configurations

spectral measures

eigenvalue spacing distributions

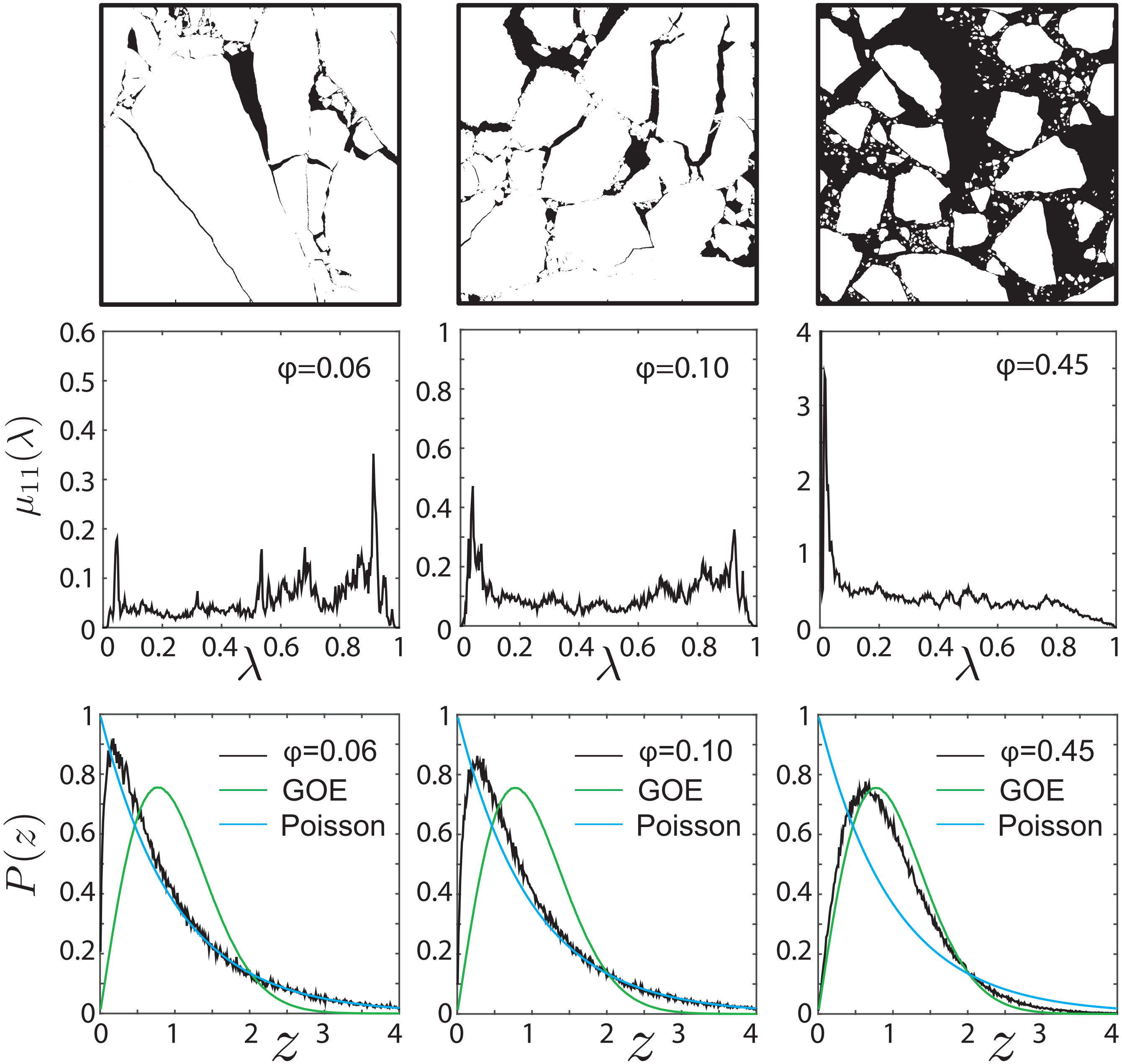

UNIVERSAL Wigner-Dyson distribution

uncorrelated → **level repulsion**

Eigenvalue Statistics of Random Matrix Theory

Wigner (1951) and Dyson (1953) first used random matrix theory (RMT) to describe quantized energy levels of heavy atomic nuclei.

$[\mathbf{N}]_{ij} \sim N(0,1)$, $\mathbf{A} = (\mathbf{N}+\mathbf{N}^T)/2$ ***Gaussian orthogonal ensemble (GOE)***

$[\mathbf{N}]_{ij} \sim N(0,1)+iN(0,1)$, $\mathbf{A} = (\mathbf{N}+\mathbf{N}^\dagger)/2$ ***Gaussian unitary ensemble (GUE)***

Short range and long range correlations of eigenvalues are measured by various eigenvalue statistics.

Spacing distributions of energy levels for heavy atomic nuclei

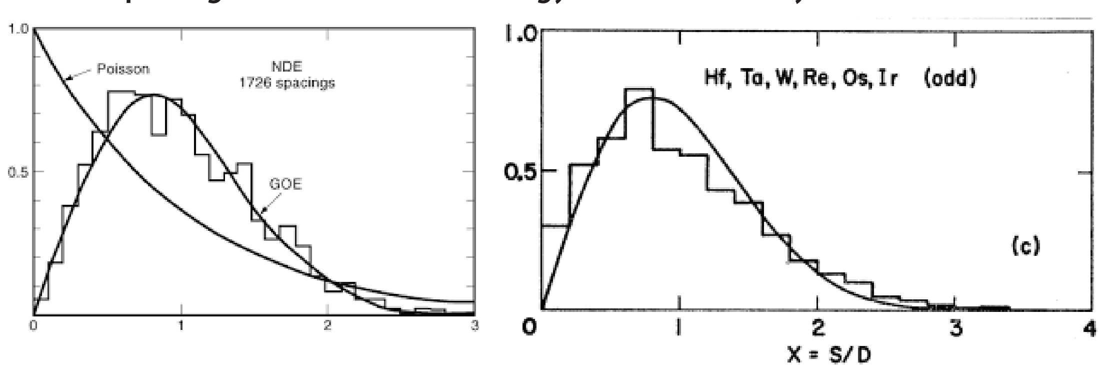

Spacing distributions of the first billion zeros of the Riemann zeta function

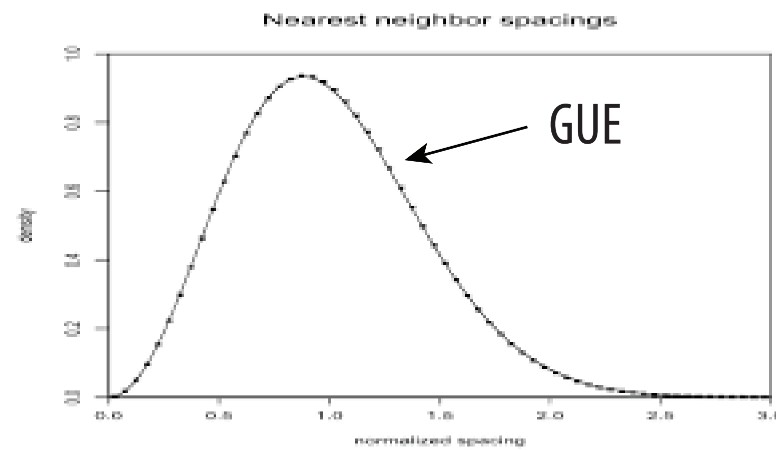

Universal eigenvalue statistics arise in a broad range of “unrelated” problems!

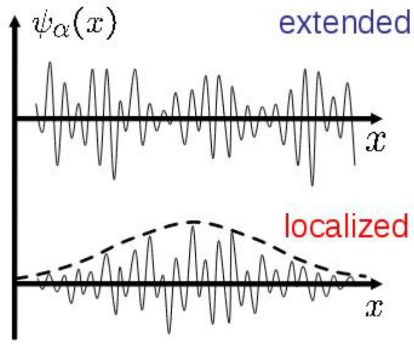

electronic transport in semiconductors

metal / insulator transition

localization

Anderson 1958
Mott 1949
Shklovshii et al 1993
Evangelou 1992

Anderson transition in wave physics:
quantum, optics, acoustics, water waves, ...

---

from analysis of spectral measures for brine, melt ponds, ice floes

we find percolation-driven

Anderson transition for classical transport in composites

Murphy, Cherkaev, Golden Phys. Rev. Lett. 2017

PERCOLATION TRANSITION → universal eigenvalue statistics (GOE)
extended states, mobility edges

-- but with NO wave interference or scattering effects ! --

Order to disorder in quasiperiodic composites

Morison, Murphy, Cherkaev, Golden, *Commun. Phys.* 2022

Parameterized Moiré Pattern Creates Tunable Microgeometry

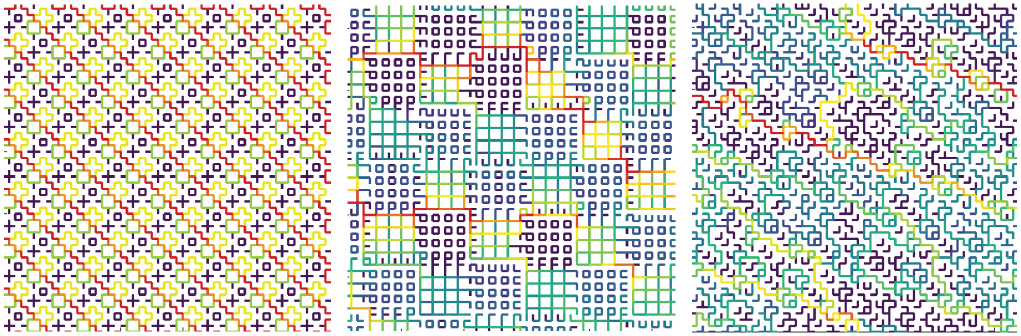

Anderson transition as QP is tuned

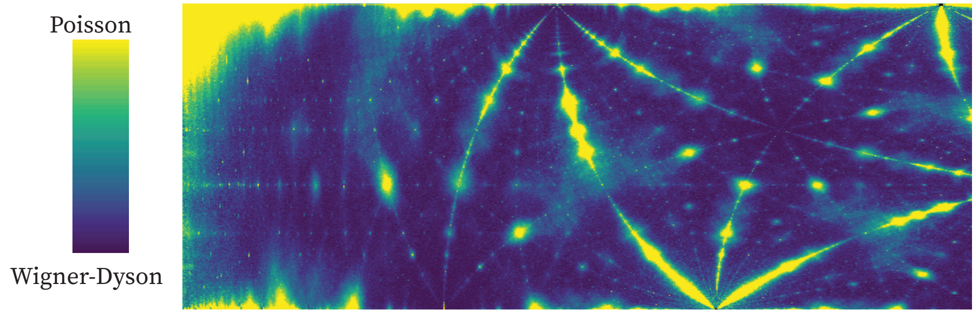

parameter space

periodic → **quasiperiodic**

electric field strength

spectral measure

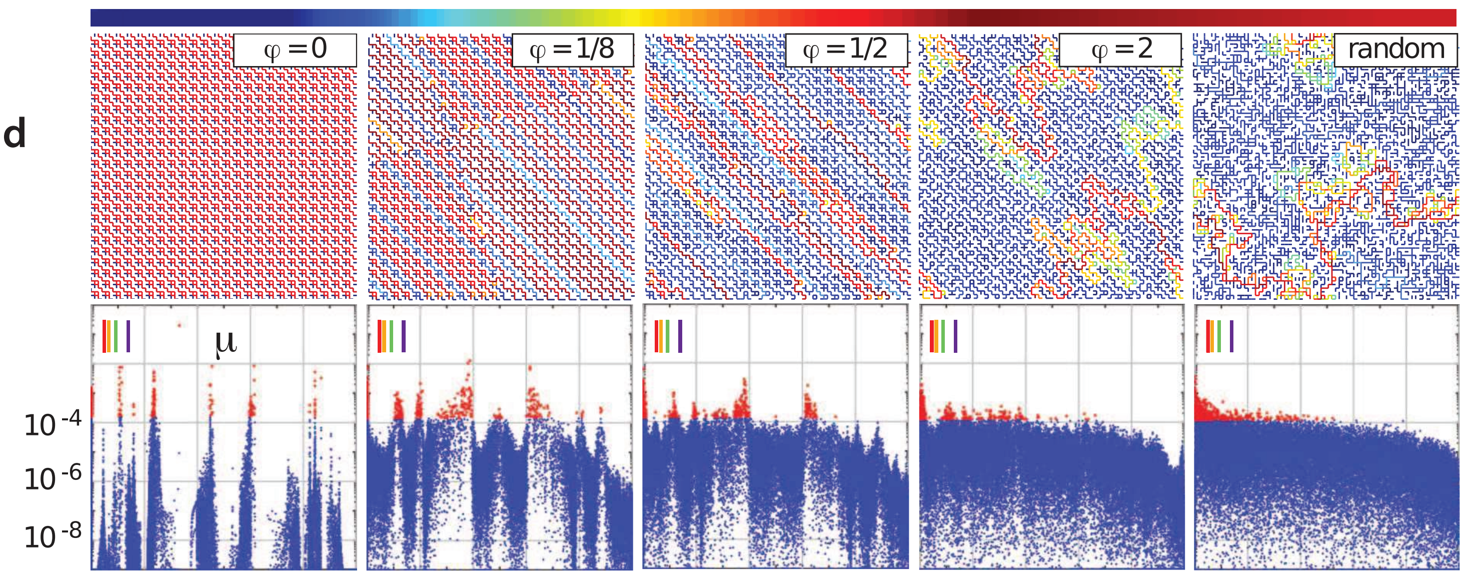

RRN at percolation threshold

we bring the framework of solid state physics of electronic transport and band gaps in semiconductors to classical transport in periodic and quasiperiodic composites

photonic crystals and quasicrystals

twisted bilayer graphene

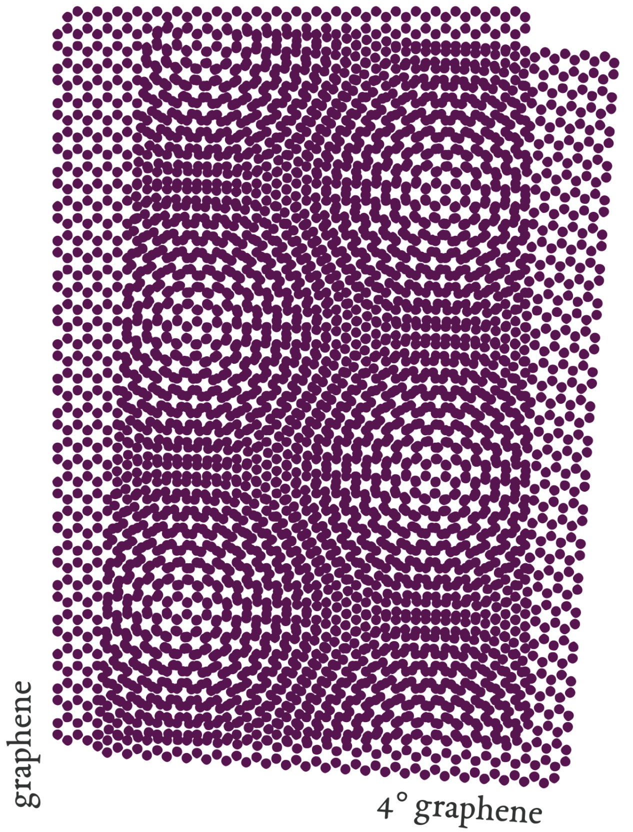

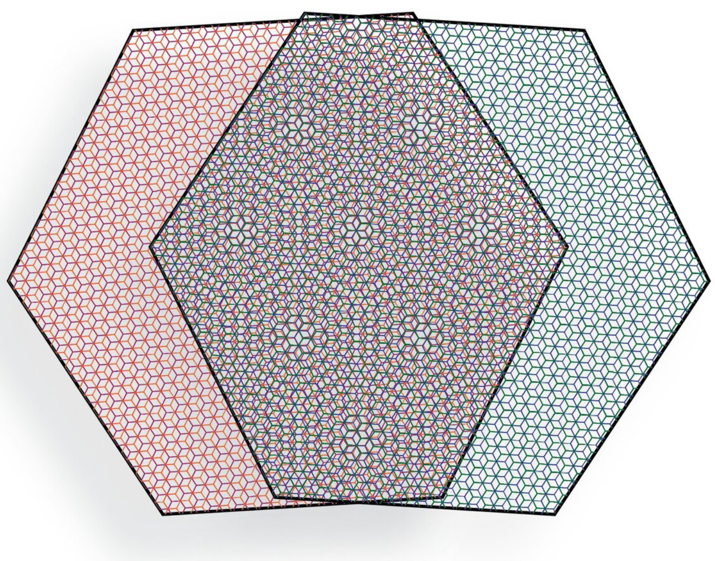

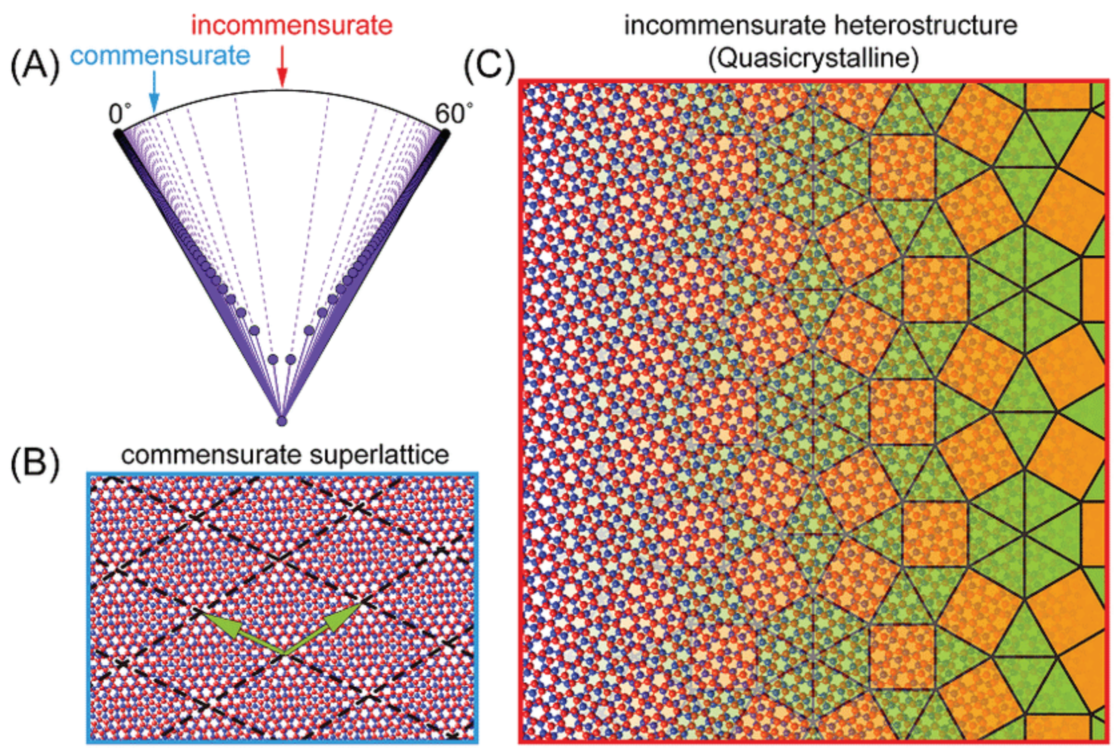

Yao et al., 2018

Homogenization for polycrystalline materials

Two-component composites

Local conductivity

σ_1 σ_2

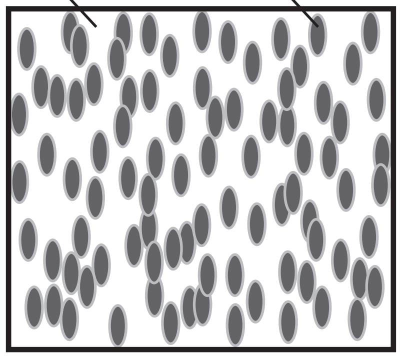

inhomogeneous medium

Homogenize

σ^* ***effective conductivity***

homogeneous medium

Find the homogeneous medium which behaves macroscopically the same as the inhomogeneous medium

Polycrystalline media

Conductivity of crystal directions

σ_1 σ_2

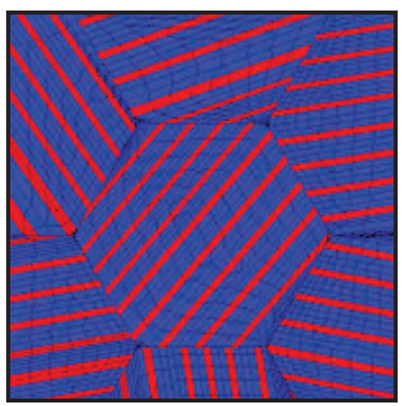

inhomogeneous medium

Homogenize

σ^* ***effective conductivity***

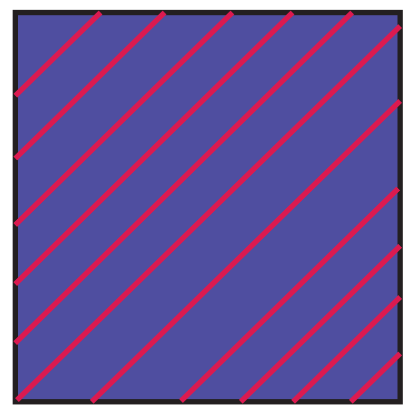

homogeneous medium

Bounds on the complex permittivity of polycrystalline materials by analytic continuation

Adam Gully, Joyce Lin,
Elena Cherkaev, Ken Golden

- **Stieltjes integral representation for effective complex permittivity**

  Milton (1981, 2002), Barabash and Stroud (1999), ...

- **Forward and inverse bounds**

  orientation statistics

- **Applied to sea ice using two-scale homogenization**

- **Inverse bounds give method for distinguishing ice types using remote sensing techniques**

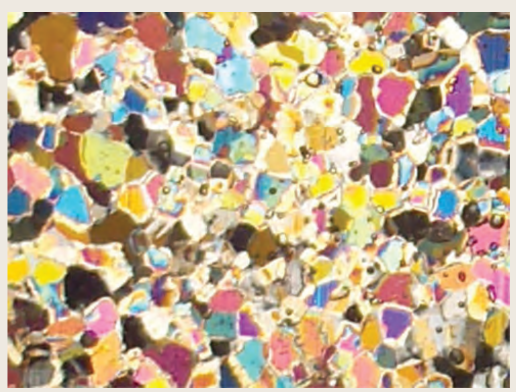

Proc. Roy. Soc. A 8 Feb 2015

Proc. R. Soc. A | Volume 471 | Issue 2174 | 8 February 2015

ISSN 1364-5021 | Volume 471 | Issue 2174 | 8 February 2015

PROCEEDINGS A

350 YEARS OF SCIENTIFIC PUBLISHING

An invited review commemorating 350 years of scientific publishing at the Royal Society

A method to distinguish between different types of sea ice using remote sensing techniques

A computer model to determine how a human should walk so as to expend the least energy

THE ROYAL SOCIETY PUBLISHING

21/01/15 1:47 PM

higher threshold for fluid flow in granular sea ice

microscale details impact "mesoscale" processes

nutrient fluxes for microbes
melt pond drainage
snow-ice formation

columnar

granular

5%

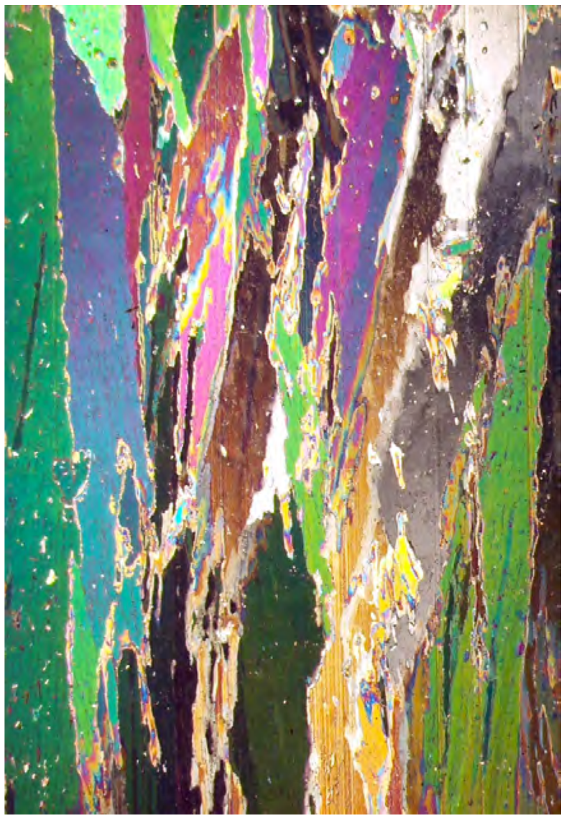

10%

Tison

Golden, Sampson, Gully, Lubbers, Tison 2022

electromagnetically distinguishing ice types

Kitsel Lusted, Elena Cherkaev, Ken Golden

mesoscale

wave propagation in the marginal ice zone (MIZ)

first theory of key parameter in wave-ice interactions only fitted to wave data before

Keller, 1998
Mosig, Montiel, Squire, 2015
Wang, Shen, 2012

Analytic Continuation Method

Bergman (78) - Milton (79)
integral representation for ε^*
Golden and Papanicolaou (83)

Milton, *Theory of Composites* (02)

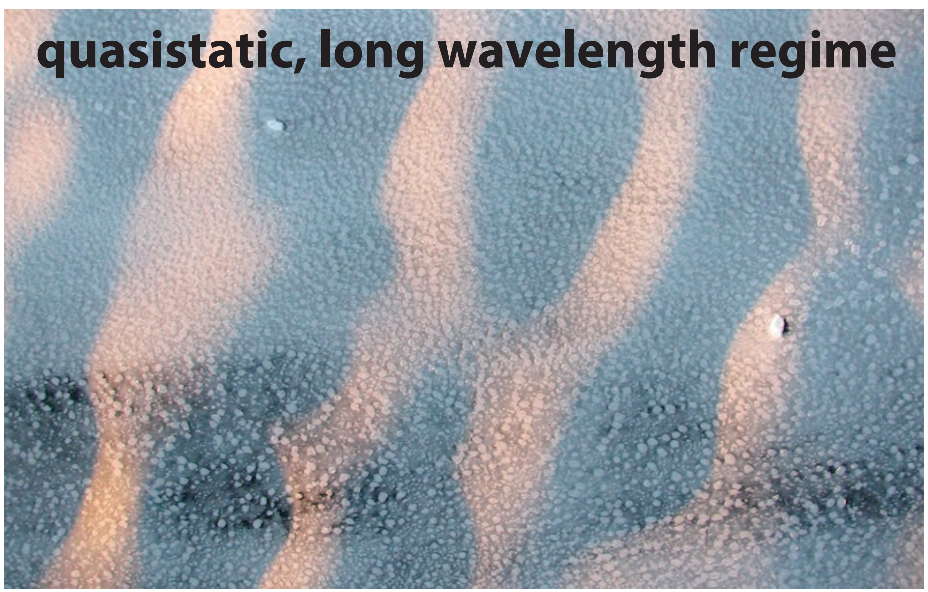

homogenized parameter depends on sea ice concentration and ice floe geometry

like EM waves

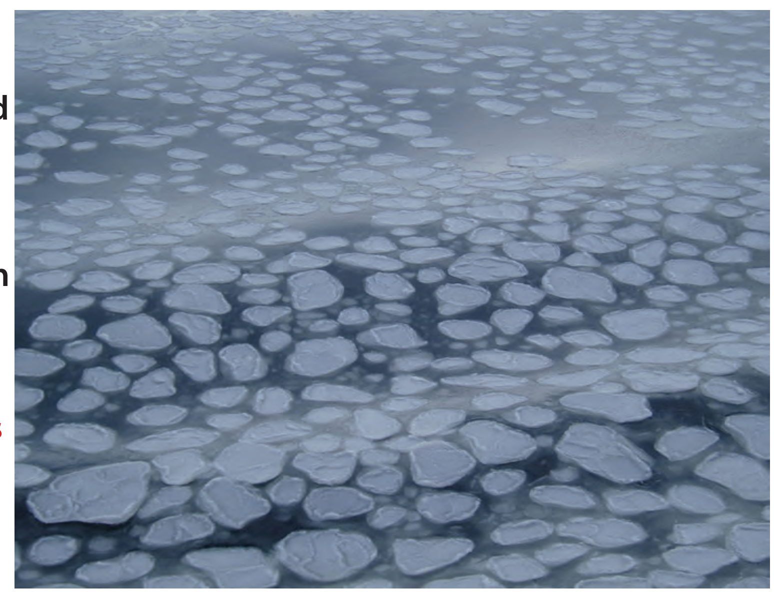

advection enhanced diffusion

effective diffusivity

nutrient and salt transport in sea ice
heat transport in sea ice with convection
sea ice floes in winds and ocean currents
tracers, buoys diffusing in ocean eddies
diffusion of pollutants in atmosphere

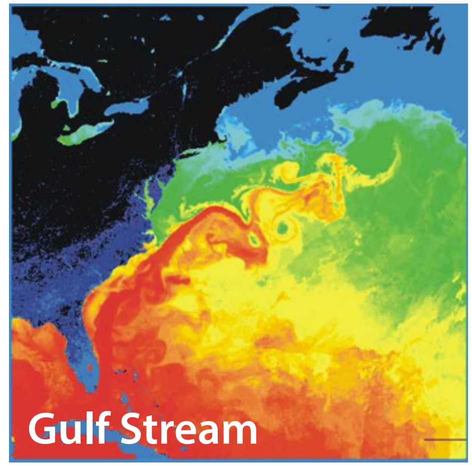

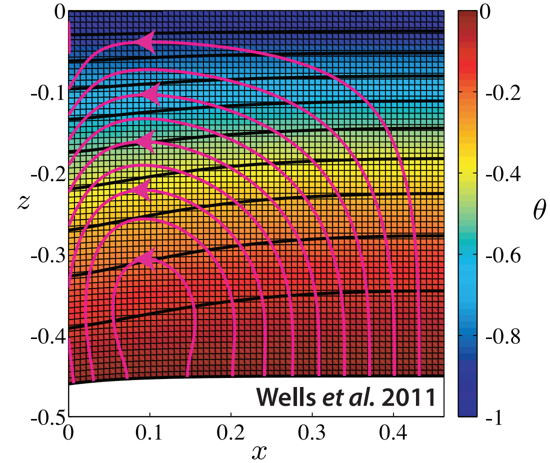

advection diffusion equation with a velocity field $\vec{u}$

$$\frac{\partial T}{\partial t} + \vec{u} \cdot \vec{\nabla} T = \kappa_0 \Delta T$$

$$\vec{\nabla} \cdot \vec{u} = 0$$

homogenize

$$\frac{\partial \overline{T}}{\partial t} = \kappa^* \Delta \overline{T}$$

κ^* ***effective diffusivity***

Stieltjes integral for κ^* with spectral measure

Avellaneda and Majda, PRL 89, CMP 91

Murphy, Cherkaev, Xin, Zhu, Golden, *Ann. Math. Sci. Appl.* 2017
Murphy, Cherkaev, Zhu, Xin, Golden, *J. Math. Phys.* 2020

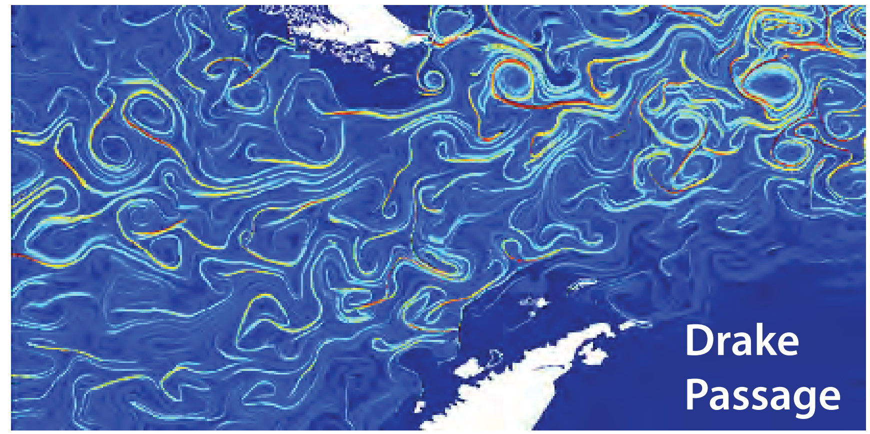

tracers flowing through inverted sea ice blocks

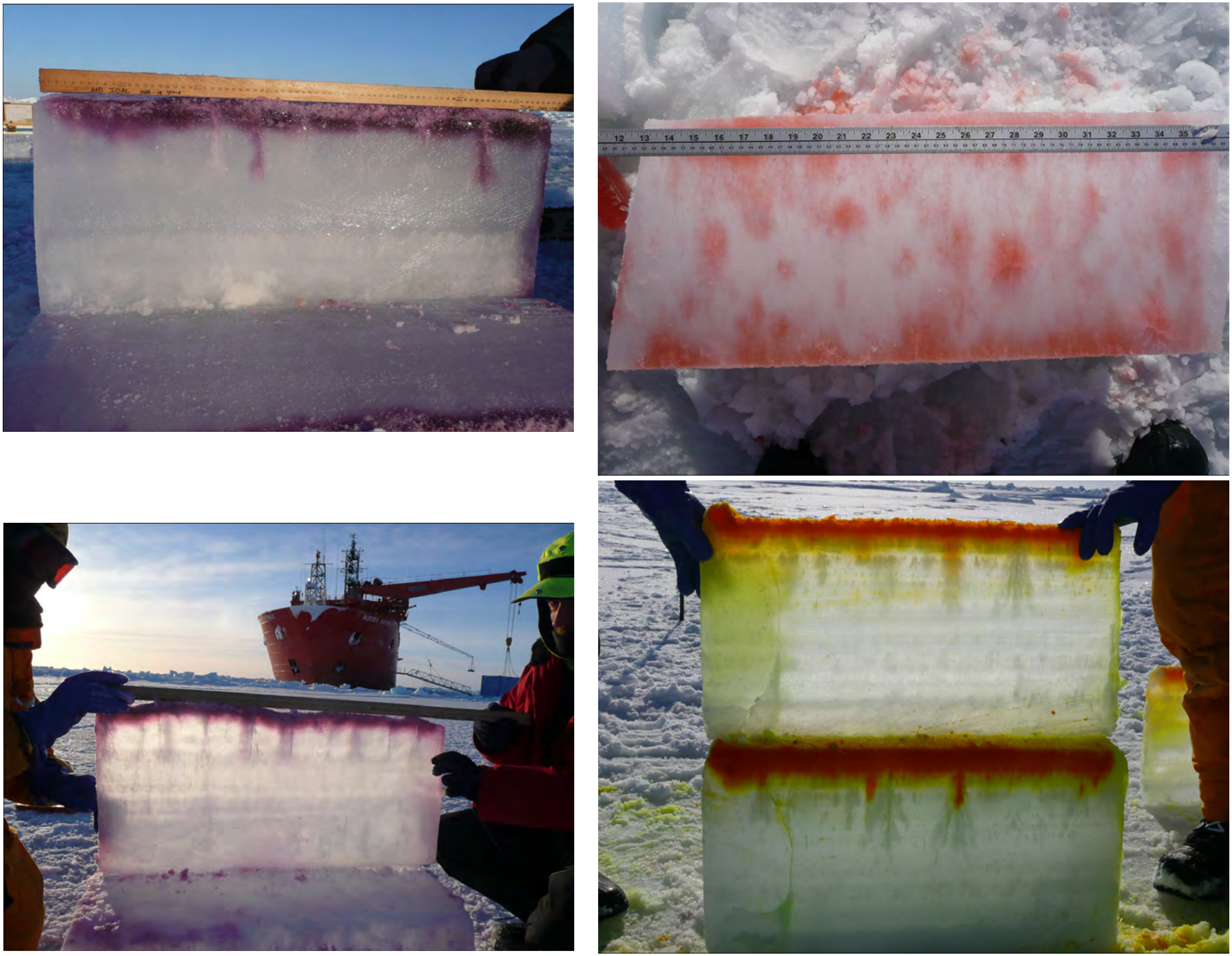

ANZFLUX drift camp

snow loading, surface flooding and subsequent snow - ice formation

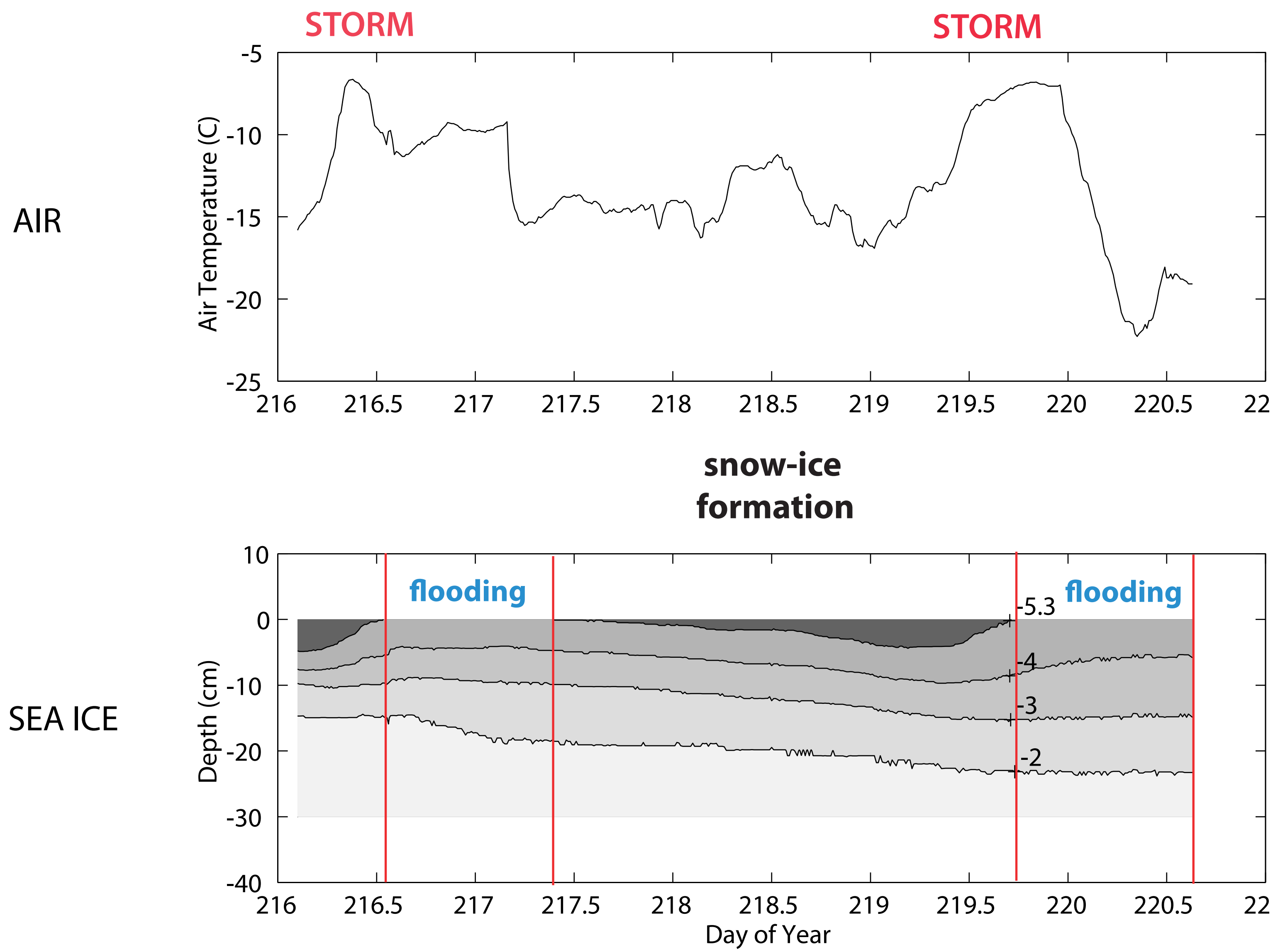

Rigorous bounds on convection enhanced thermal conductivity of sea ice

Kraitzman, Hardenbrook, Dinh, Murphy, Zhu, Cherkaev, Golden 2022

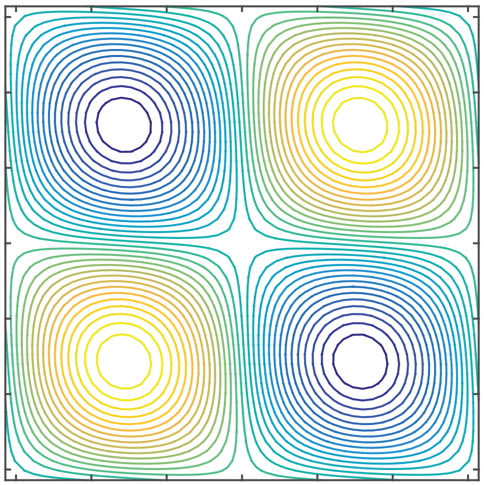

cat's eye flow model for brine convection cells

similar bounds for shear flows

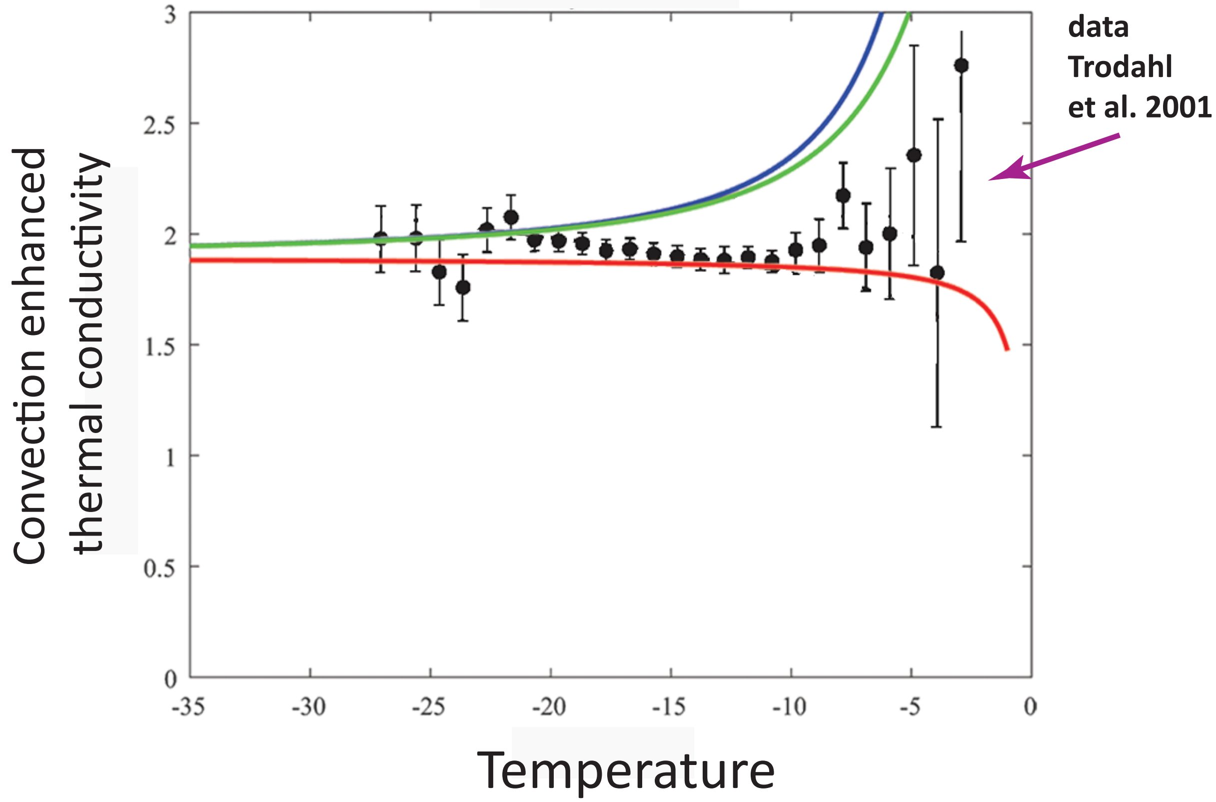

rigorous Padé bounds from Stieltjes integral + analytical calculations of moments of measure

Lytle & Ackley 1996

melt pond formation and albedo evolution:

- ***major drivers in polar climate***
- ***key challenge for global climate models***

numerical models of melt pond evolution, including topography, drainage (permeability), etc.

Lüthje, Feltham, Taylor, Worster 2006

Flocco, Feltham 2007

Skyllingstad, Paulson, Perovich 2009

Flocco, Feltham, Hunke 2012

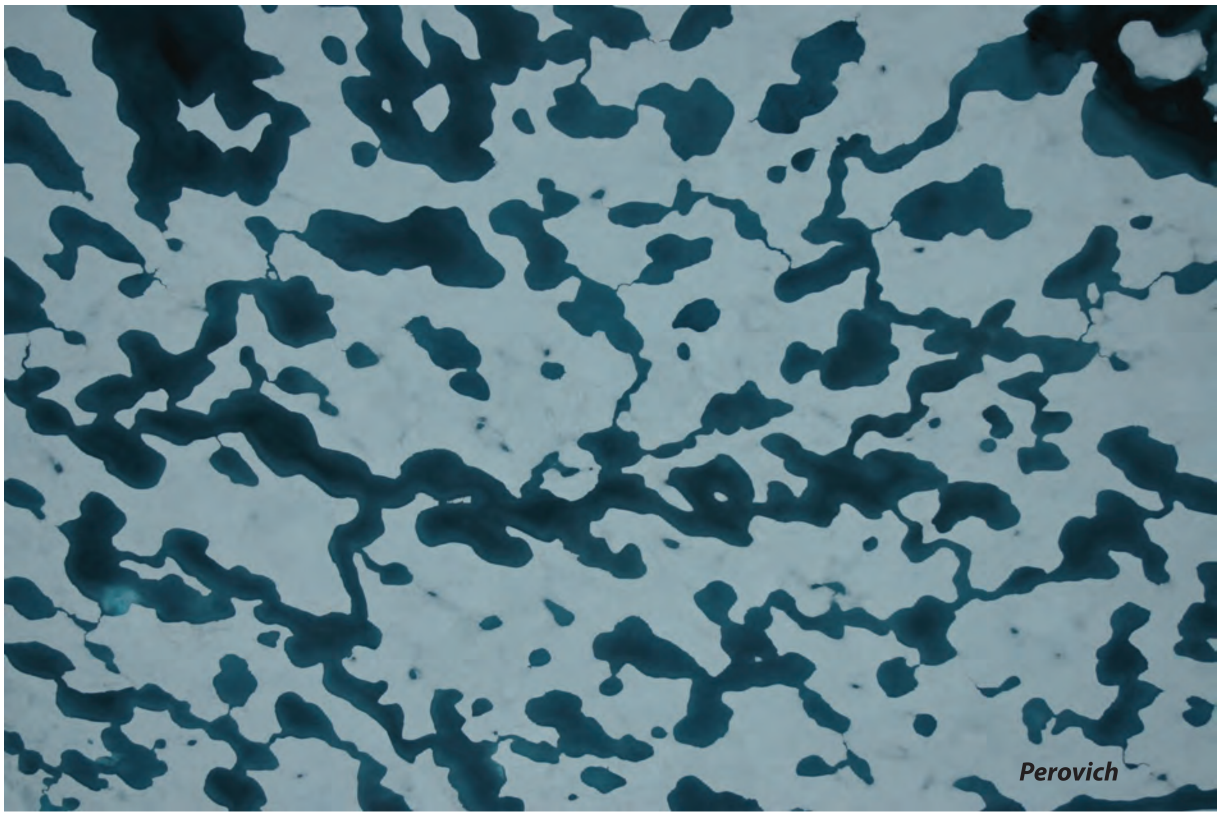

Are there universal features of the evolution similar to phase transitions in statistical physics?

fractal curves in the plane

they wiggle so much that their dimension is >1

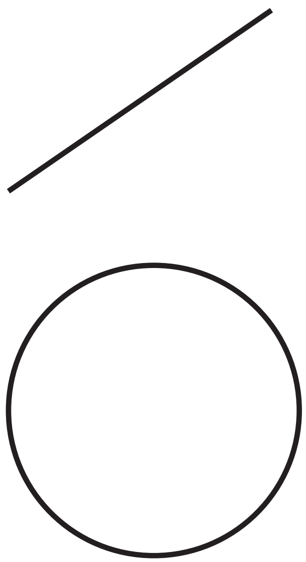

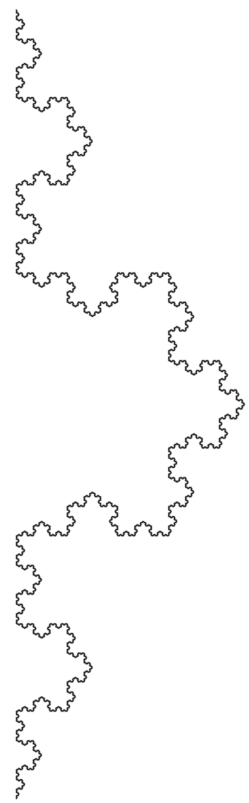

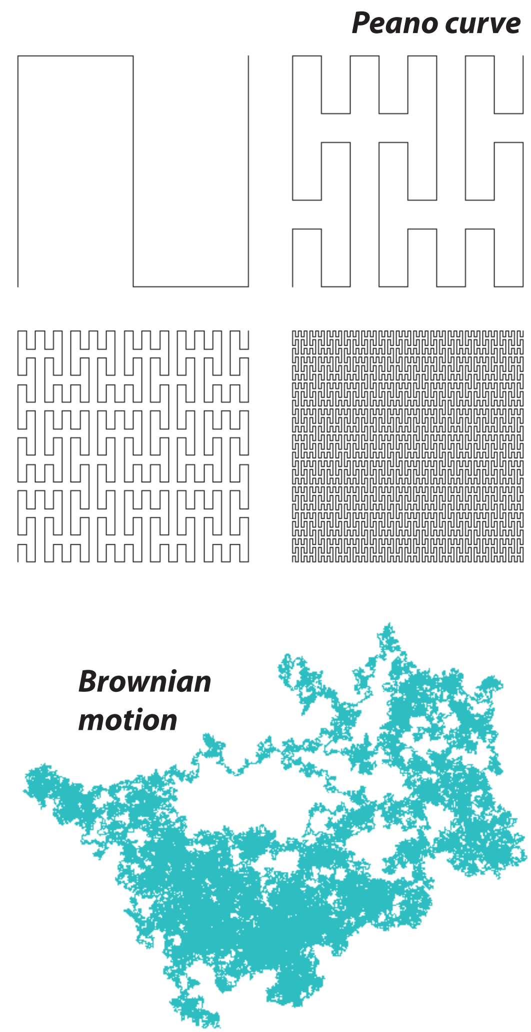

simple curves

D = 1

Koch snowflake

D = 1.26

space filling curves

D = 2

Transition in the fractal geometry of Arctic melt ponds

Christel Hohenegger, Bacim Alali, Kyle Steffen, Don Perovich, Ken Golden

The Cryosphere, 2012

complexity grows with length scale

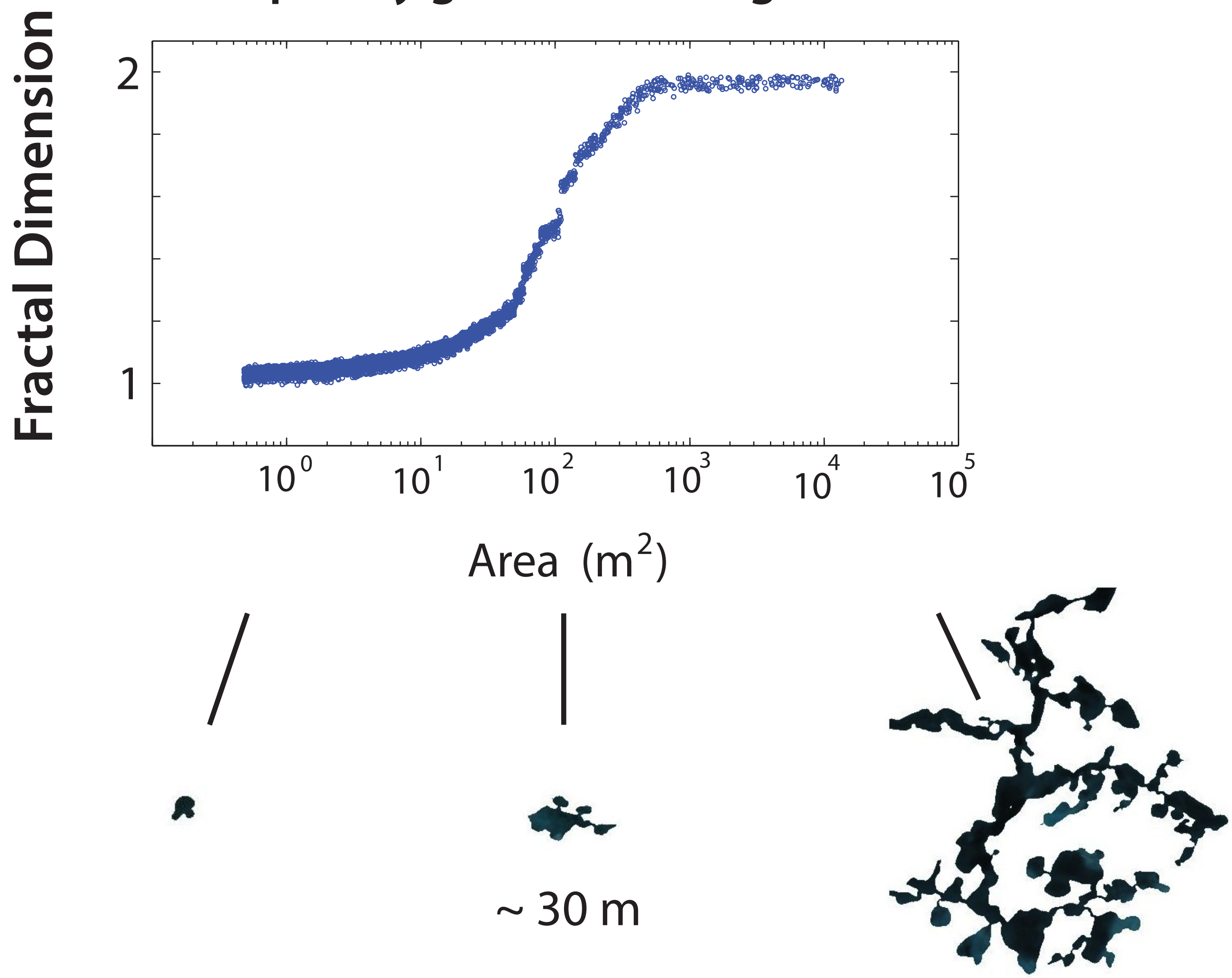

simple pond ***transitional pond*** ***complex pond***

Continuum percolation model for melt pond evolution

level sets of random surfaces

Brady Bowen, Court Strong, Ken Golden, J. Fractal Geometry 2018

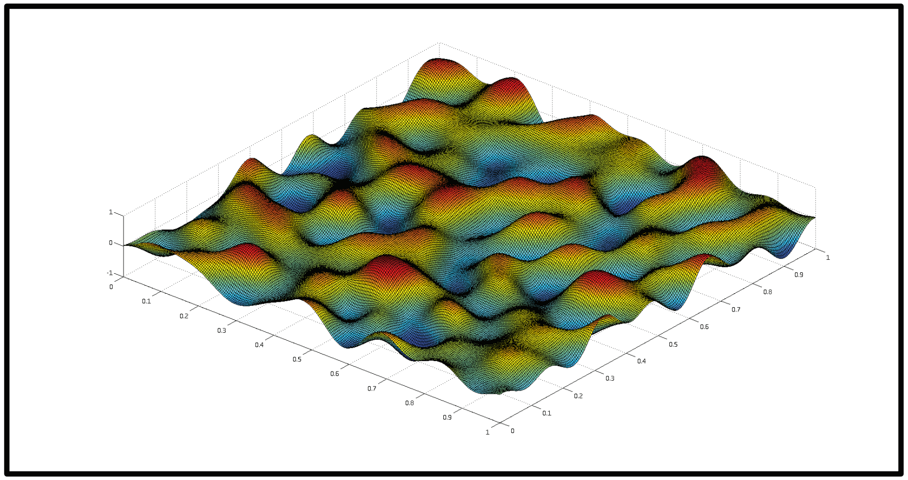

random Fourier series representation of surface topography

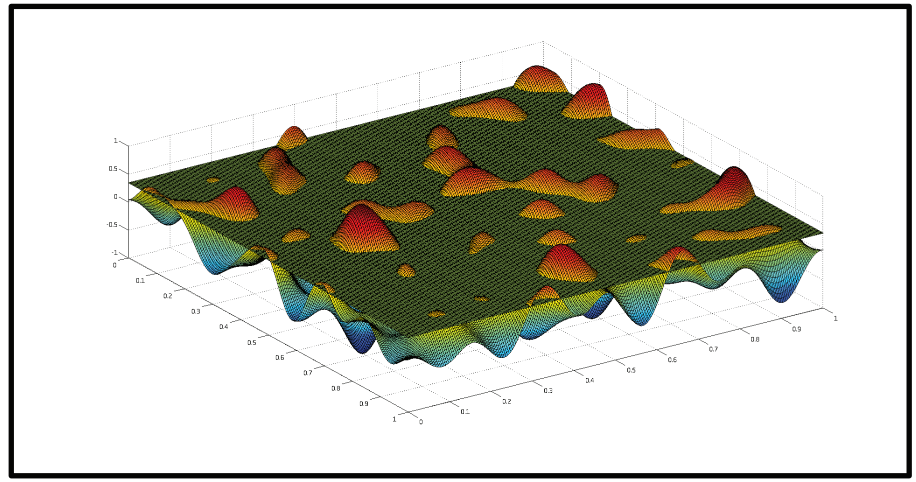

intersections of a plane with the surface define melt ponds

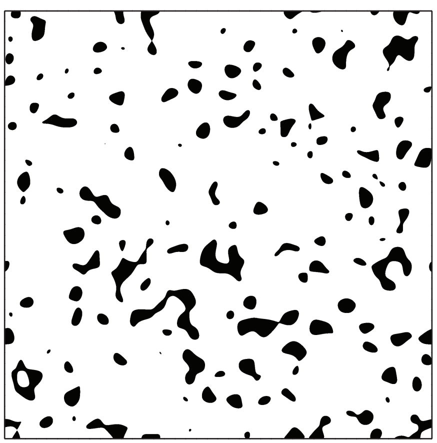

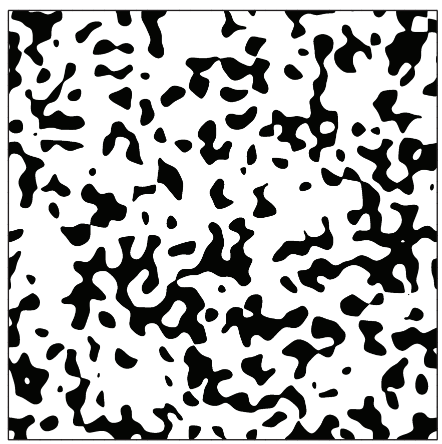

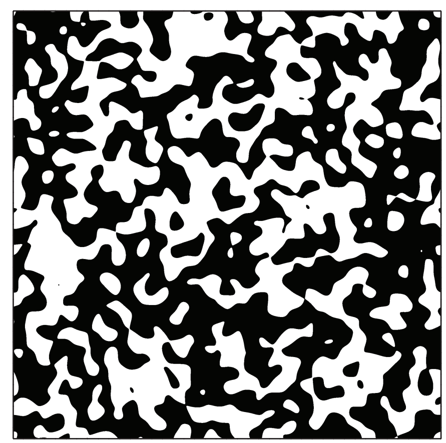

electronic transport in disordered media *diffusion in turbulent plasmas* *Isichenko, Rev. Mod. Phys., 1992*

fractal dimension curves depend on statistical parameters defining random surface

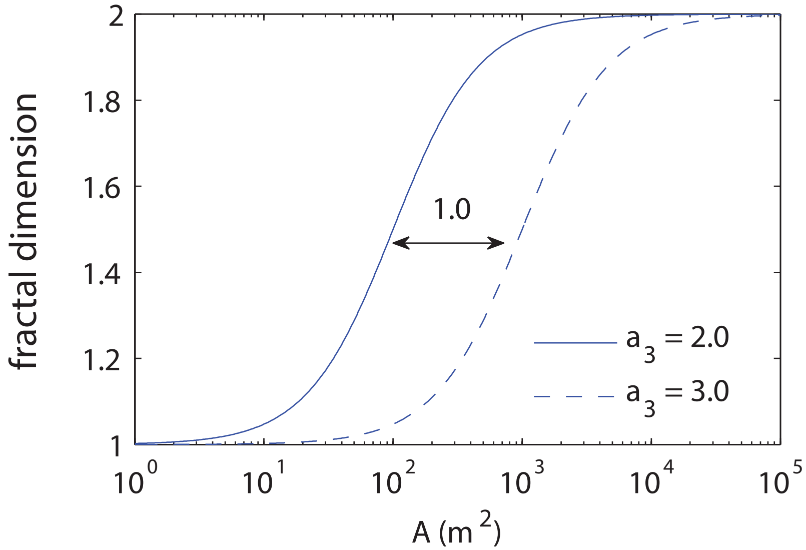

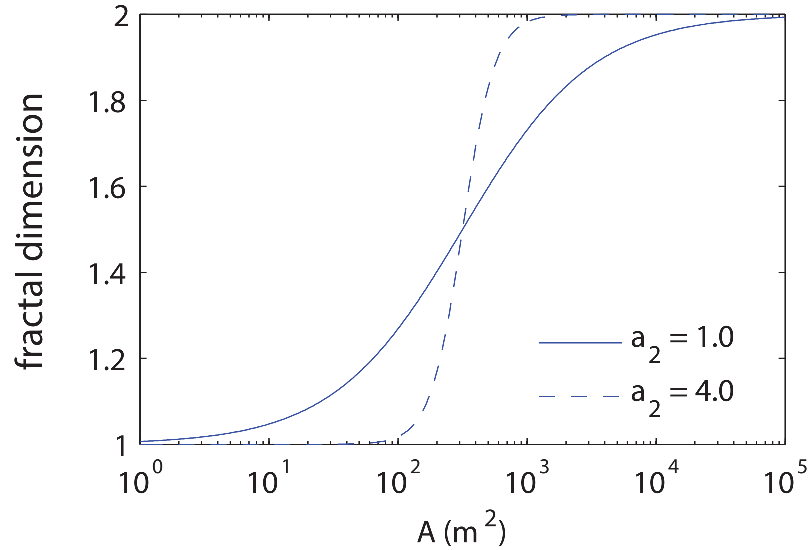

Saddle points of the sea ice surface and the fractal geometry of Arctic melt ponds

Physical Review Research (invited, under review)

Ryleigh Moore, Jacob Jones, Dane Gollero,
Court Strong, Ken Golden

Several models replicate the transition in fractal dimension, but none explain how it arises.

We use Morse theory applied to the random surface model to show that saddle points play the critical role in the fractal transition.

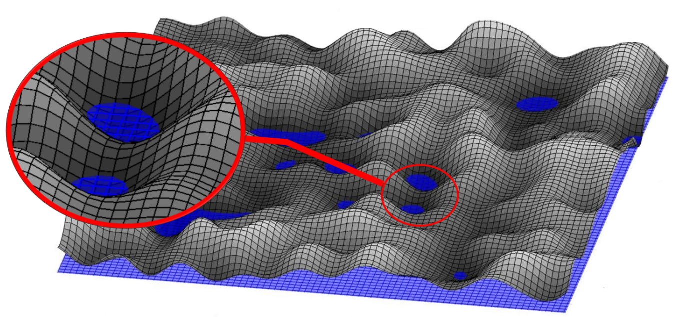

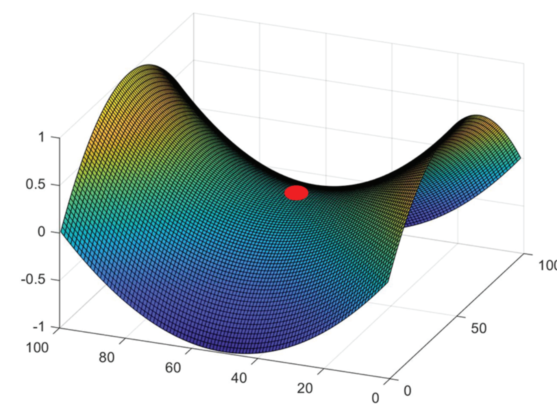

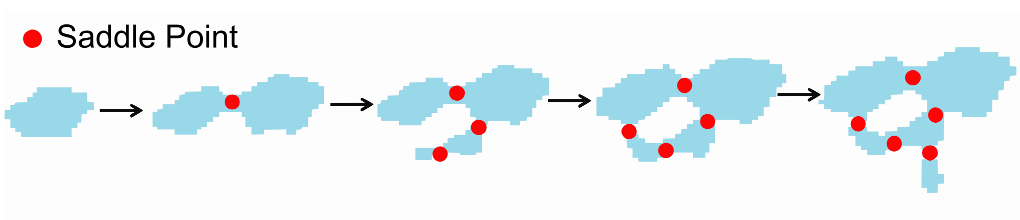

ponds coalesce
(change topology) and
complexify at saddle points

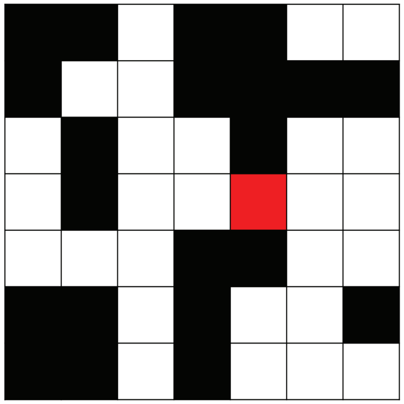

- Ponds connect through saddle points (Morse Theory).
- Red bonds in lattice percolation theory ~ saddle points.

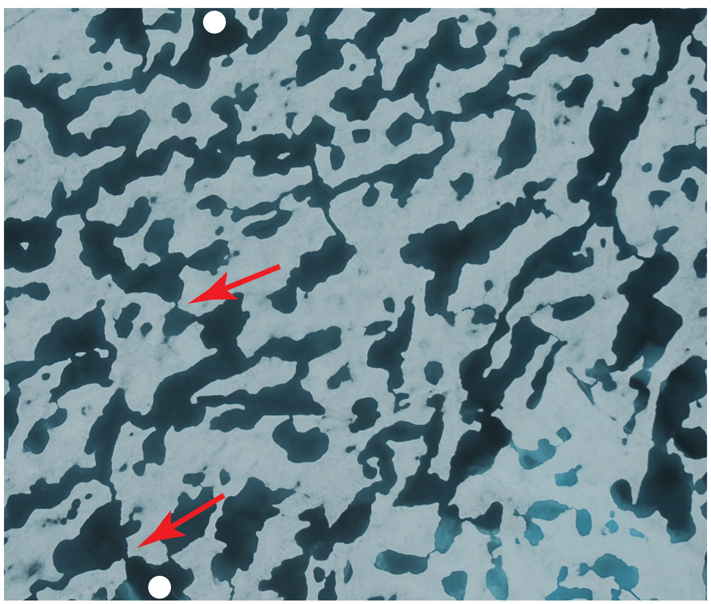

Perovich

saddles

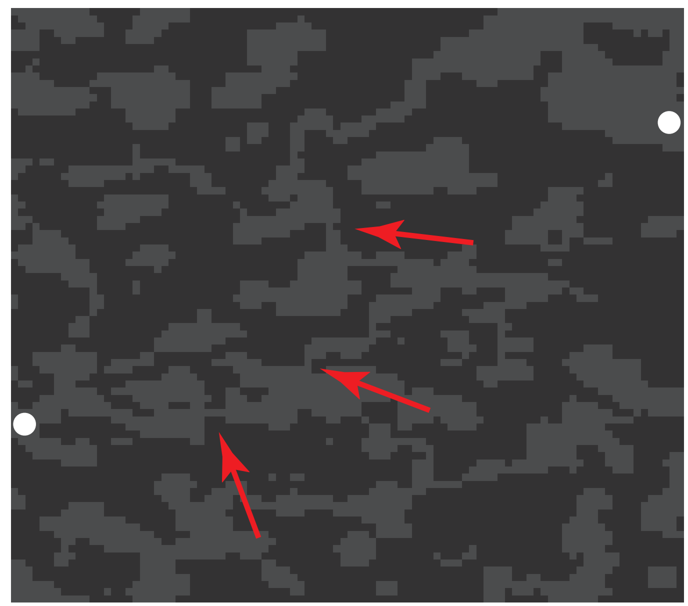

“red squares”

Main results

Isoperimetric quotient - as a proxy for fractal dimension - takes discrete jumps up when ponds coalesce at saddle points.

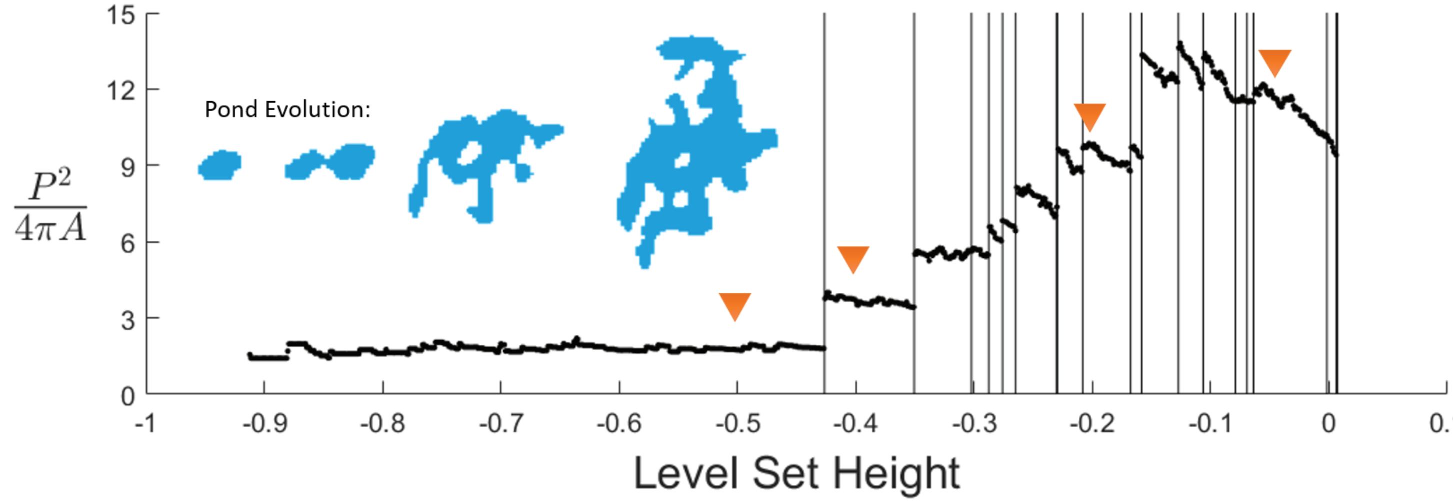

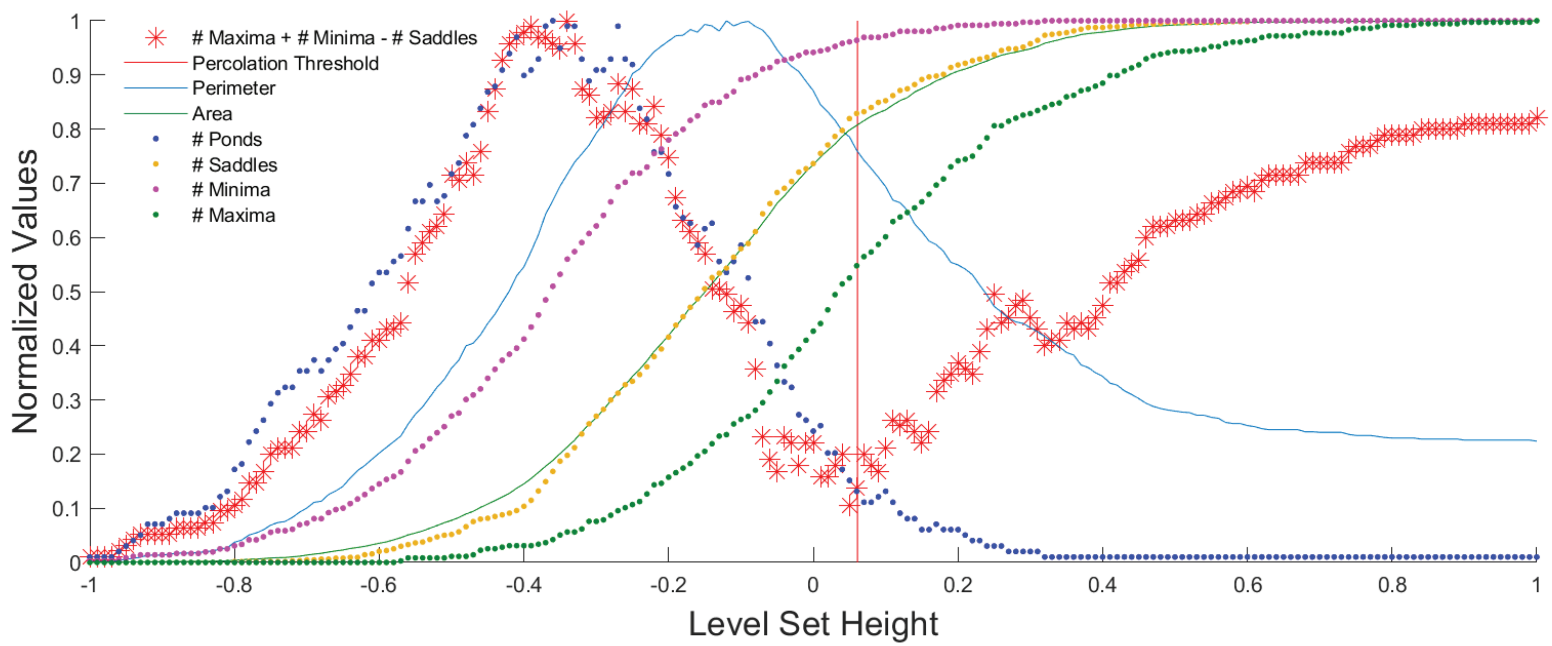

Euler characteristic reaches minimum at percolation threshold.

Horizontal fluid permeability "controlled" by saddles ~ electronic transport in 2D random potential.

Ising Model for a Ferromagnet

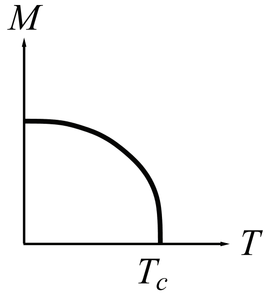

Curie point
critical temperature

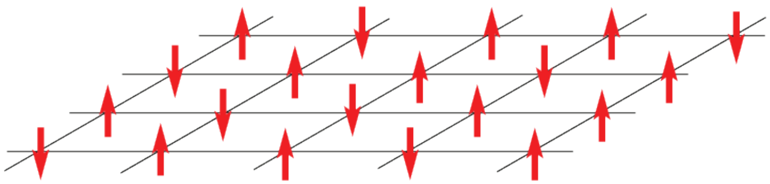

applied magnetic field H

$$s_i = \begin{cases} +1 & \text{spin up} \\ -1 & \text{spin down} \end{cases}$$

blue
white

$$\mathcal{H} = -H\sum_i s_i - J\sum_{<i,j>} s_i s_j$$

nearest neighbor Ising Hamiltonian

$$M(T,H) = \lim_{N\to\infty}\frac{1}{N}\left\langle \sum_j s_j \right\rangle$$

effective magnetization

Ising Model for a Ferromagnet

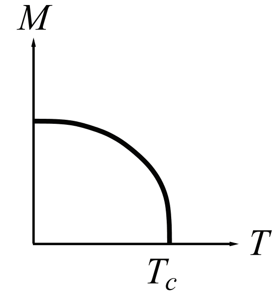

Curie point
critical temperature

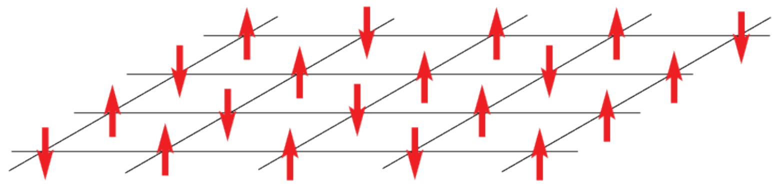

applied magnetic field

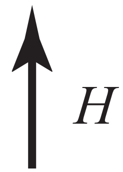

$$s_i = \begin{cases} +1 & \text{spin up} \\ -1 & \text{spin down} \end{cases}$$

blue

white

$$\mathcal{H} = -H \sum_i s_i - J \sum_{<i,j>} s_i s_j$$

nearest neighbor Ising Hamiltonian

islands of like spins

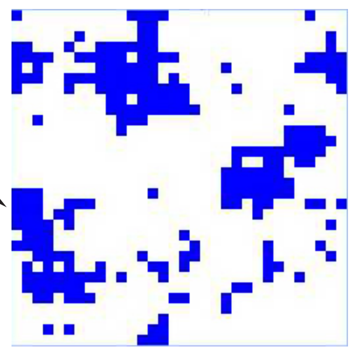

$$M(T,H) = \lim_{N\to\infty} \frac{1}{N} \left\langle \sum_j s_j \right\rangle$$

effective magnetization

energy is lowered when nearby spins align with each other, forming **magnetic domains**

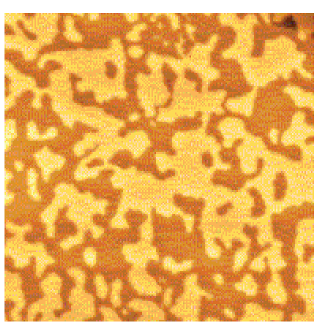

magnetic domains in cobalt

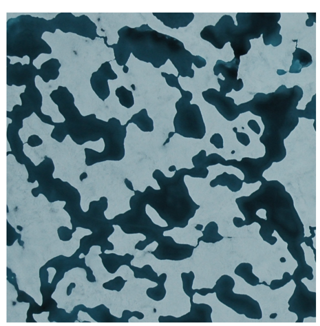

melt ponds (Perovich)

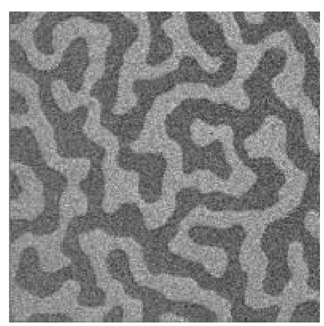

magnetic domains in cobalt-iron-boron

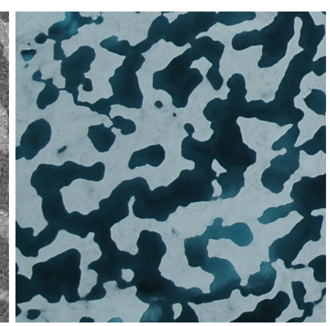

melt ponds (Perovich)

Ising model for ferromagnets $\longrightarrow$ Ising model for melt ponds

Ma, Sudakov, Strong, Golden, *New J. Phys.*, 2019

$$\mathcal{H} = -\sum_{i}^{N} H_i\, s_i - J \sum_{<i,j>}^{N} s_i s_j \qquad s_i = \begin{cases} \uparrow & +1 \quad \text{water} \quad \text{(spin up)} \\ \downarrow & -1 \quad \text{ice} \quad \text{(spin down)} \end{cases}$$

random magnetic field represents snow topography

magnetization M

pond area fraction $F = \dfrac{(M+1)}{2}$

~ albedo

only nearest neighbor patches interact

Starting with random initial configurations, as Hamiltonian energy is minimized by Glauber spin flip dynamics, system "flows" toward metastable equilibria.

Order from Disorder

Ising model for ferromagnets $\longrightarrow$ Ising model for melt ponds

Ma, Sudakov, Strong, Golden, *New J. Phys.*, 2019

$$\mathcal{H} = -\sum_{i}^{N} H_i\, s_i - J \sum_{<i,j>}^{N} s_i s_j \qquad s_i = \begin{cases} \uparrow & +1 \quad \text{water} \quad \text{(spin up)} \\ \downarrow & -1 \quad \text{ice} \quad \text{(spin down)} \end{cases}$$

random magnetic field represents snow topography

magnetization M

pond area fraction ***~ albedo***

$$F = \frac{(M+1)}{2}$$

only nearest neighbor patches interact

Starting with random initial configurations, as Hamiltonian energy is minimized by Glauber spin flip dynamics, system "flows" toward metastable equilibria.

Order from Disorder

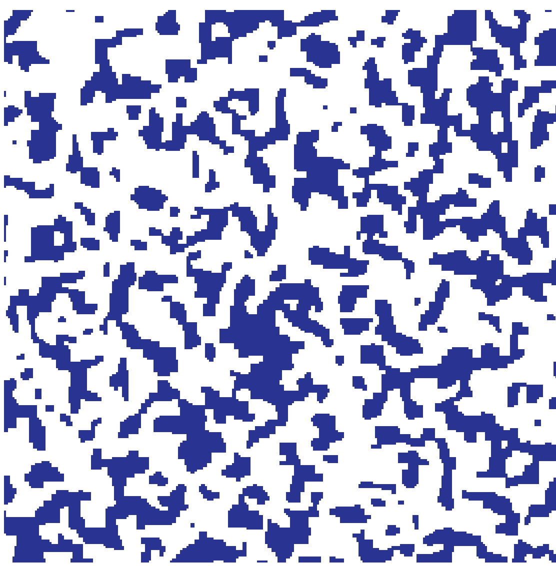

Ising model

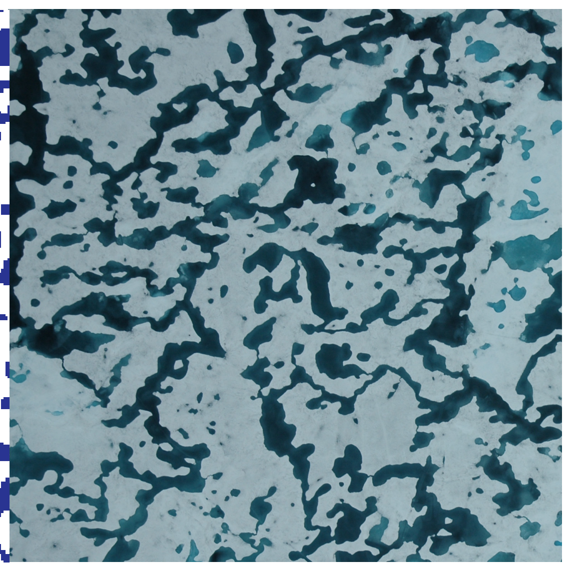

melt pond photo (Perovich)

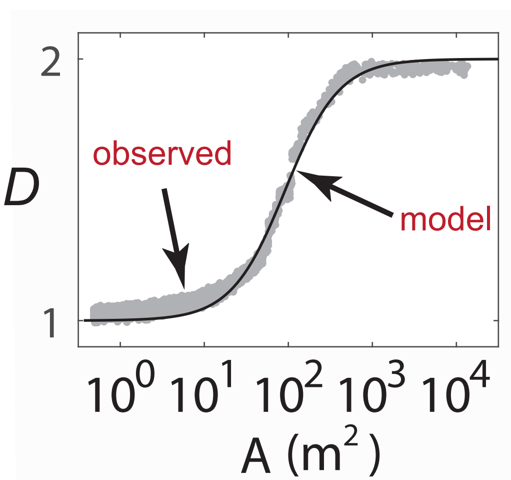

pond size distribution exponent

observed -1.5

(Perovich, *et al.* 2002)

model -1.58

Scientific American EOS, PhysicsWorld, ...

ONLY MEASURED INPUT = LENGTH SCALE (GRID SIZE) from snow topography data

Perovich

Melt ponds control transmittance of solar energy through sea ice, impacting upper ocean ecology.

WINDOWS

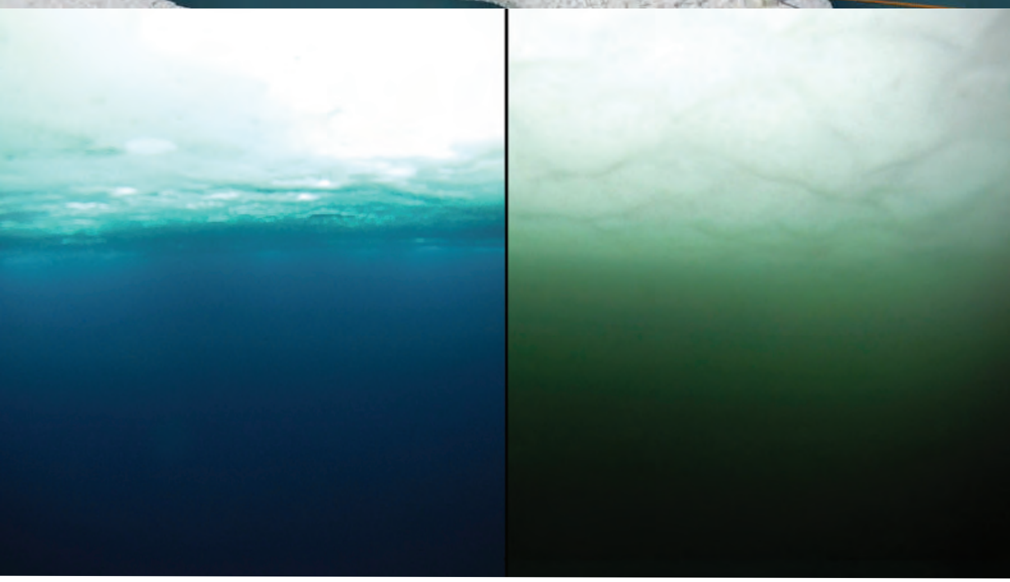

no bloom bloom

massive under-ice algal bloom

Arrigo et al., *Science* 2012

Have we crossed into a new ecological regime?

The frequency and extent of sub-ice phytoplankton blooms in the Arctic Ocean

Horvat, Rees Jones, Iams, Schroeder, Flocco, Feltham, ***Science Advances*** 2017

The effect of melt pond geometry on the distribution of solar energy under first year sea ice

Horvat, Flocco, Rees Jones, Roach, Golden

Geophys. Res. Lett. 2019

(2015 AMS MRC)

Uncertainty quantification and ecological dynamics in a model of a sea ice algae bloom, in prep. 2022

Jody Reimer, Fred Adler, Ken Golden, and Akil Narayan

Next week!

macroscale

Anomalous diffusion in sea ice dynamics

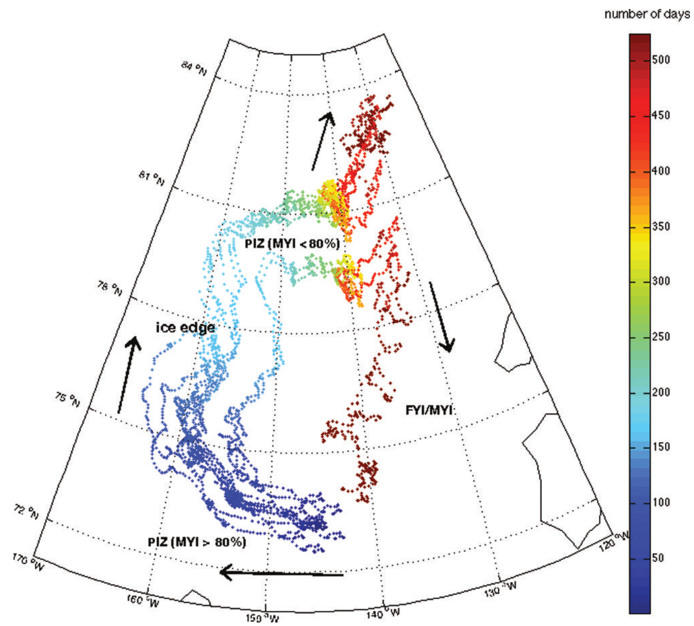

Ice floe diffusion in winds and currents

observations from GPS data:

Jennifer Lukovich, Jennifer Hutchings,
David Barber, *Ann. Glac.* 2015

- **On short time scales floes observed (buoy data) to exhibit Brownian-like behavior, but they are also being advected by winds and currents.**

- **Effective behavior is purely diffusive, sub-diffusive or super-diffusive depending on ice pack and advective conditions - Hurst exponent.**

modeling:

Huy Dinh, Ben Murphy, Elena Cherkaev,
Court Strong, Ken Golden 2022

floe scale model to analyze transport regimes in terms of ice pack crowding, advective conditions

Delaney Mosier, Jennifer Hutchings, Jennifer Lukovich,
Marta D'Elia, George Karniadakis, Ken Golden 2022

learning fractional PDE governing diffusion from data

Floe Scale Model of Anomalous Diffusion in Sea Ice Dynamics

Huy Dinh, Ben Murphy, Elena Cherkaev, Court Strong, Ken Golden 2022

$$\left\langle \left|\mathbf{x}(t) - \mathbf{x}(0) - \langle \mathbf{x}(t) - \mathbf{x}(0)\rangle\right|^2 \right\rangle \sim t^{\alpha}$$

$\alpha =$ Hurst exponent

diffusive $\alpha = 1$

sub-diffusive $\alpha < 1$

super-diffusive $\alpha > 1$

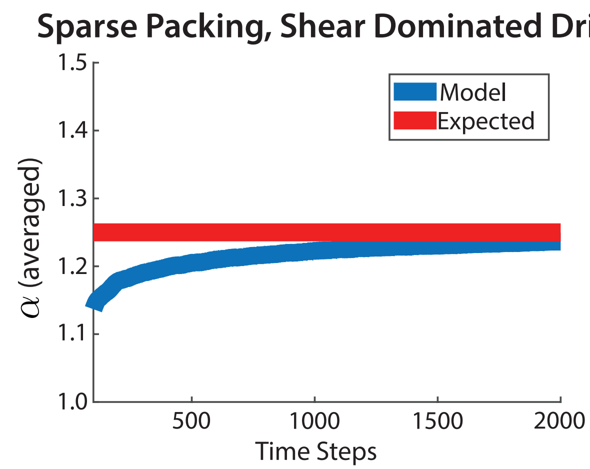

Model Approximations

Power Law Size Distribution: $N(D) \sim D^{-k}$

D. A. Rothrock and A. S. Thorndike Journal of Geophysical Research 1984

Floe-Floe Interactions: Linear Elastic Collisions

Advective Forcing: Passive, Linear Drag Law

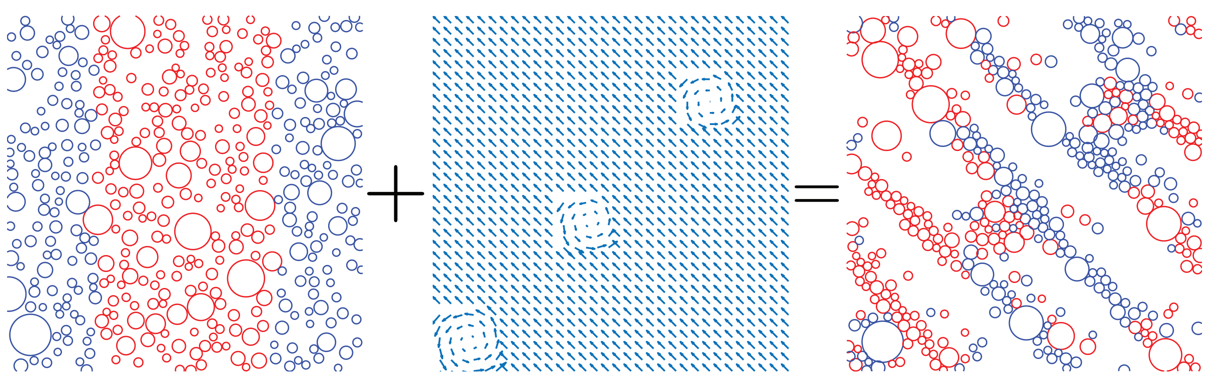

$\psi = 0.3$ **Vorticity Dominated Drift**

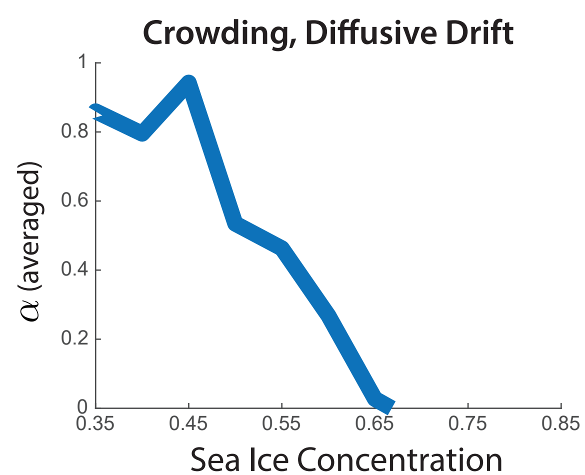

Marginal Ice Zone

MIZ

- biologically active region
- intense ocean-sea ice-atmosphere interactions
- region of significant wave-ice interactions

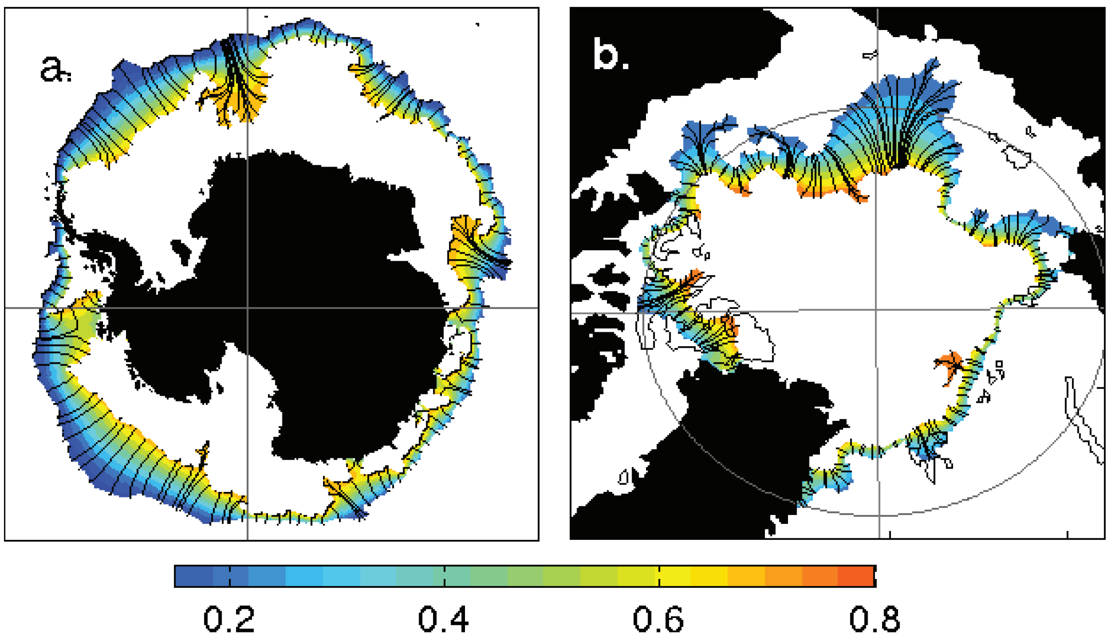

transitional region between
dense interior pack ($c > 80\%$)
sparse outer fringes ($c < 15\%$)

MIZ WIDTH
fundamental length scale of
ecological and climate dynamics

Strong, *Climate Dynamics* 2012
Strong and Rigor, *GRL* 2013

How to objectively measure the "width" of this complex, non-convex region?

Objective method for measuring MIZ width motivated by medical imaging and diagnostics

Strong, *Climate Dynamics* 2012
Strong and Rigor, *GRL* 2013

39% widening
1979 - 2012

streamlines of a solution to Laplace's equation

"average" lengths of streamlines

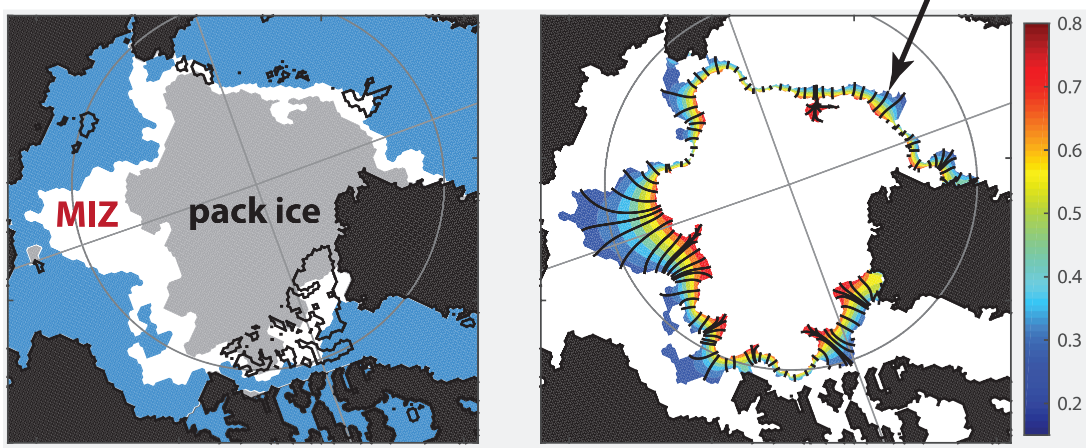

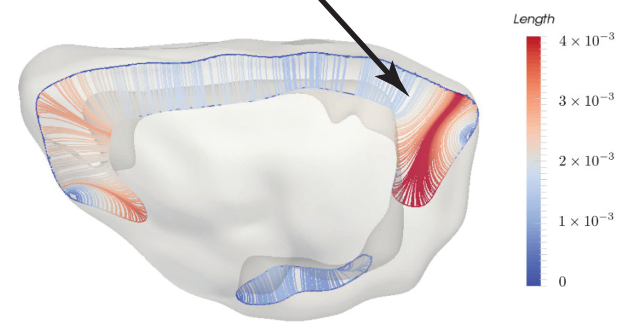

Arctic Marginal Ice Zone

crossection of the cerebral cortex of a rodent brain

analysis of different MIZ WIDTH definitions

Strong, Foster, Cherkaev, Eisenman, Golden
J. Atmos. Oceanic Tech. 2017

Strong and Golden
Society for Industrial and Applied Mathematics News, April 2017

Model larger scale effective behavior
with partial differential equations that
homogenize complex local structure and dynamics.

Arctic MIZ

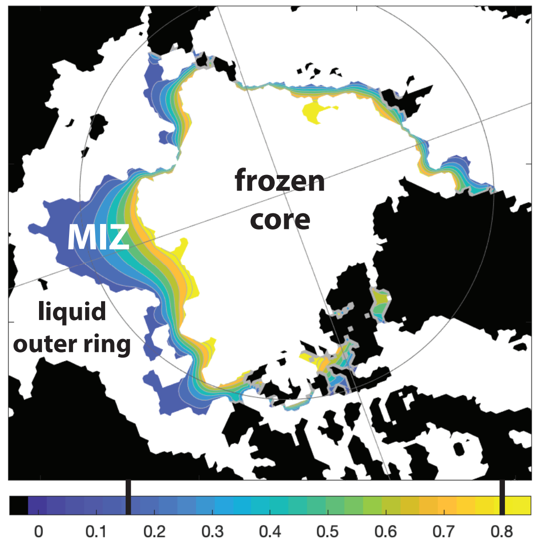

sea ice concentration ψ

Predict MIZ width and location with basin-scale phase change model.

dynamic transitional region - mushy layer - separating two "pure" phases

seasonal and long term trends

C. Strong, E. Cherkaev, and K. M. Golden,
Annual cycle of Arctic marginal ice zone location
and width explained by phase change front model, 2022

MIZ as a moving phase transition region

$$\rho c \frac{\partial T}{\partial t} = \nabla \cdot (k \nabla T) + S$$

$$S = [\rho(c_l - c_s)T + \rho L] \frac{\partial \psi}{\partial t}$$

$$\psi = 1 - \left(\frac{T - T_s}{T_l - T_s} \right)^{\alpha}$$

$$k_x = \left(\frac{\psi}{k_s} + \frac{1 - \psi}{k_l} \right)^{-1}$$

homogenization

$$k_z = \psi k_s + (1 - \psi) k_l$$

ρ effective density

T temperature

c specific heat

L latent heat of fusion

S models nonlinear phase change

ψ sea ice concentration

k effective diffusivity

l liquid, s solid

Classical small-scale application

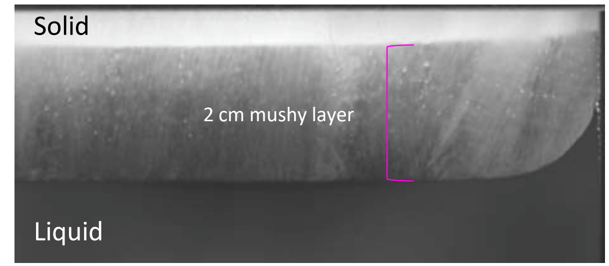

NaCl-H_2O in lab
(Peppin et al., 2007;, J. Fluid Mech.)

Macroscale application

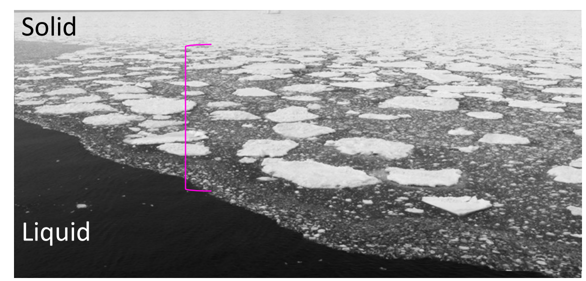

- Develop multiscale PDE model for simulating phase transition fronts to predict MIZ seasonal cycles and decadal trends
- Model simulates MIZ as a large-scale mushy layer with effective thermal conductivity derived from physics of composite materials

Model captures basic physics of MIZ dynamics

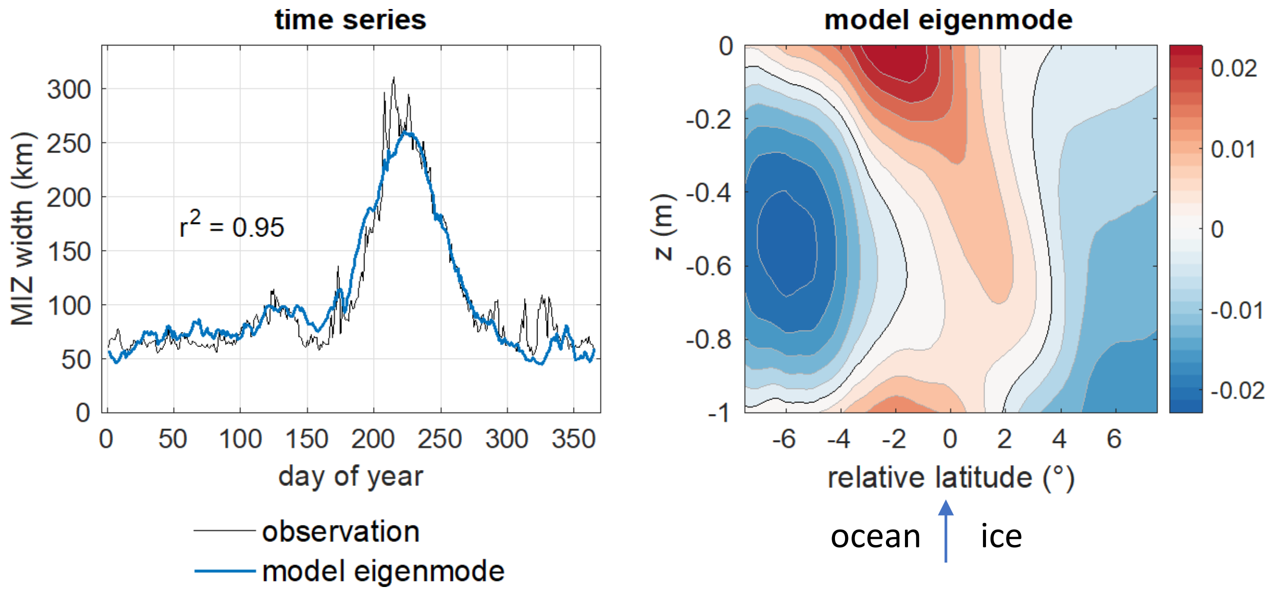

- Eigenmodes of temperature solution skillfully capture seasonal cycle of MIZ location and width.
- Eigenmode explaining MIZ width captures heat flux convergence into the MIZ layer from atmosphere above and oceanic mixed layer below.
- Model could ultimately be used to explain long term trends toward a wider and more poleward MIZ. Develop more sophisticated homogenization calculations; explore forcing scenarios and how to “drive” MIZ dynamics

Learning the velocity field in an advection diffusion model for sea ice concentration

Eric Brown, Delaney Mosier, Bao Wang, Ken Golden, 2022

Goal: Develop PDE model to describe evolution of sea ice concentration field.

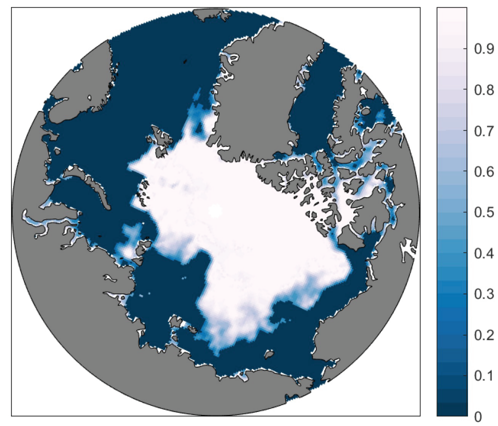

National Snow and Ice Data Center

discretized satellite concentration data

Figure 1. Arctic sea ice concentration in early August 2012.

advection diffusion model for sea ice concentration:

$$\frac{\partial \psi}{\partial t} = -\mathbf{v} \cdot \nabla \psi + k \Delta \psi$$

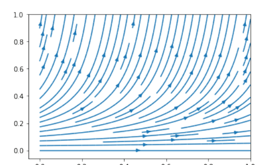

learned velocity

2.5% absolute error in preliminary study

Use two-layer neural network to infer advective fields based on satellite imagery

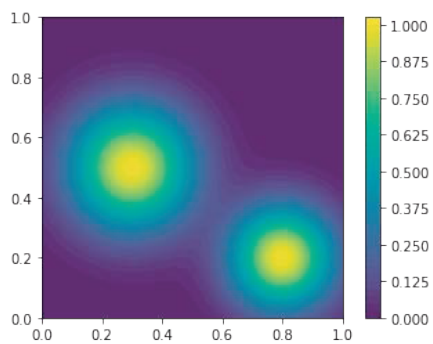

initital test concentation

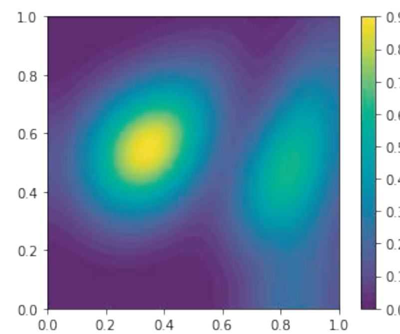

predicted concentation

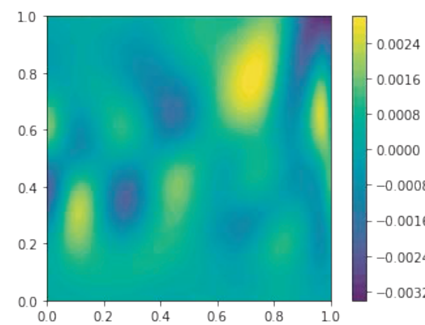

error

Filling the polar data gap with partial differential equations

hole in satellite coverage of sea ice concentration field

previously assumed ice covered

Gap radius: 611 km
06 January 1985

Gap radius: 311 km
30 August 2007

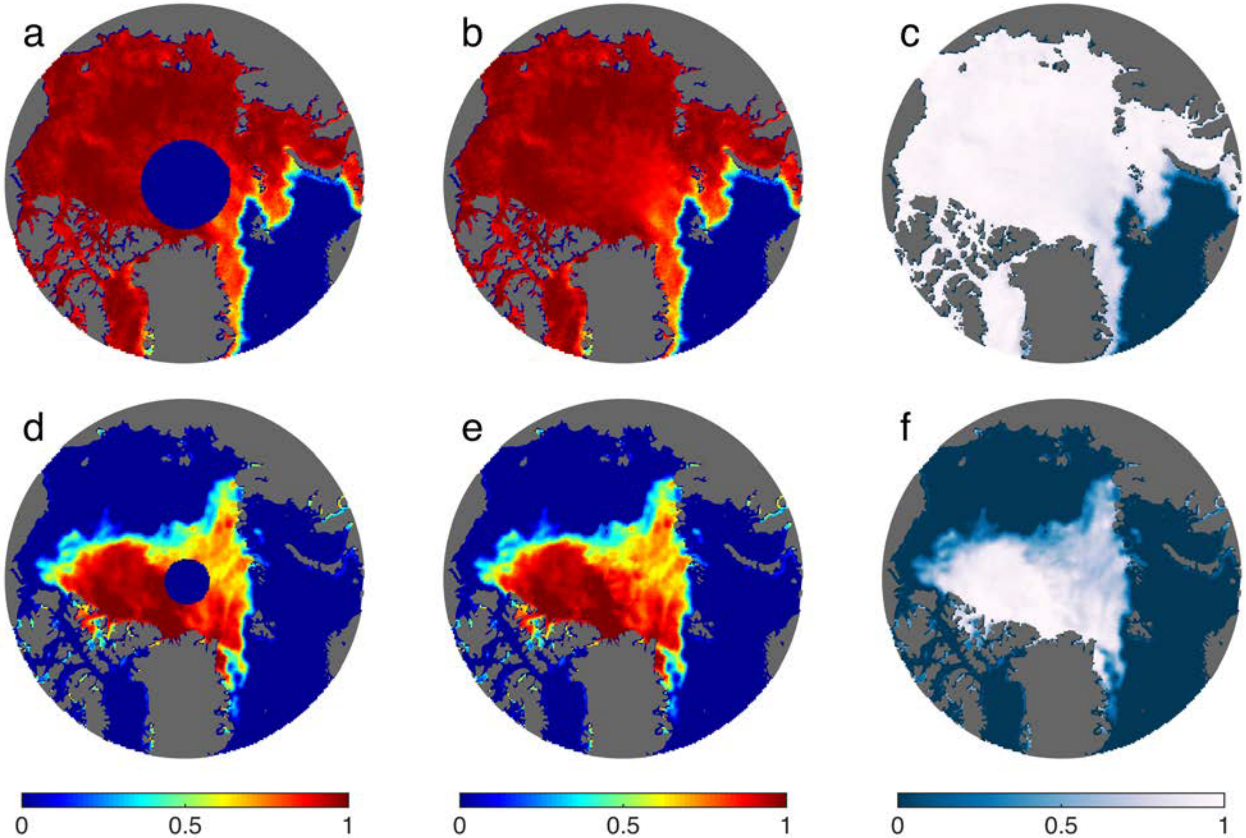

$$\Delta\psi=0$$

fill = harmonic function with learned stochastic term

Strong and Golden, *Remote Sensing* 2016
Strong and Golden, *SIAM News* 2017

NOAA/NSIDC Sea Ice Concentration CDR product update will use our PDE method.

Conclusions

1. Sea ice is a fascinating multiscale composite with structure similar to many other natural and man-made materials.

2. Mathematical methods developed for sea ice advance theories of composites and inverse problems in science and engineering.

3. Homogenization and statistical physics help ***link scales in sea ice and composites***; provide rigorous methods for finding effective behavior; advance sea ice representations in climate models.

4. Inverse problems of many types arise naturally in studying sea ice and the impact of climate change in Earth's polar regions.

5. Field experiments are essential to developing relevant mathematics.

6. Our research is helping to improve projections of climate change, the fate of Earth's sea ice packs, and the ecosystems they support.

University of Utah Sea Ice Modeling Group (2017-2021)

Senior Personnel: Ken Golden, Distinguished Professor of Mathematics
Elena Cherkaev, Professor of Mathematics
Court Strong, Associate Professor of Atmospheric Sciences
Ben Murphy, Adjunct Assistant Professor of Mathematics

Postdoctoral Researchers: Noa Kraitzman (now at ANU), Jody Reimer

Graduate Students: Kyle Steffen (now at UT Austin with Clint Dawson)
Christian Sampson (now at UNC Chapel Hill with Chris Jones)
Huy Dinh (now a sea ice MURI Postdoc at NYU/Courant)
Rebecca Hardenbrook
David Morison (Physics Department)
Ryleigh Moore
Delaney Mosier
Daniel Hallman

Undergraduate Students: Kenzie McLean, Jacqueline Cinella Rich,
Dane Gollero, Samir Suthar, Anna Hyde,
Kitsel Lusted, Ruby Bowers, Kimball Johnston,
Jerry Zhang, Nash Ward, David Gluckman

High School Students: Jeremiah Chapman, Titus Quah, Dylan Webb

---

Sea Ice Ecology Group Postdoc Jody Reimer, Grad Student Julie Sherman,
Undergraduates Kayla Stewart, Nicole Forrester

ISSN 0002-9920 (print)
ISSN 1088-9477 (online)

Notices

of the American Mathematical Society

November 2020 | Volume 67, Number 10

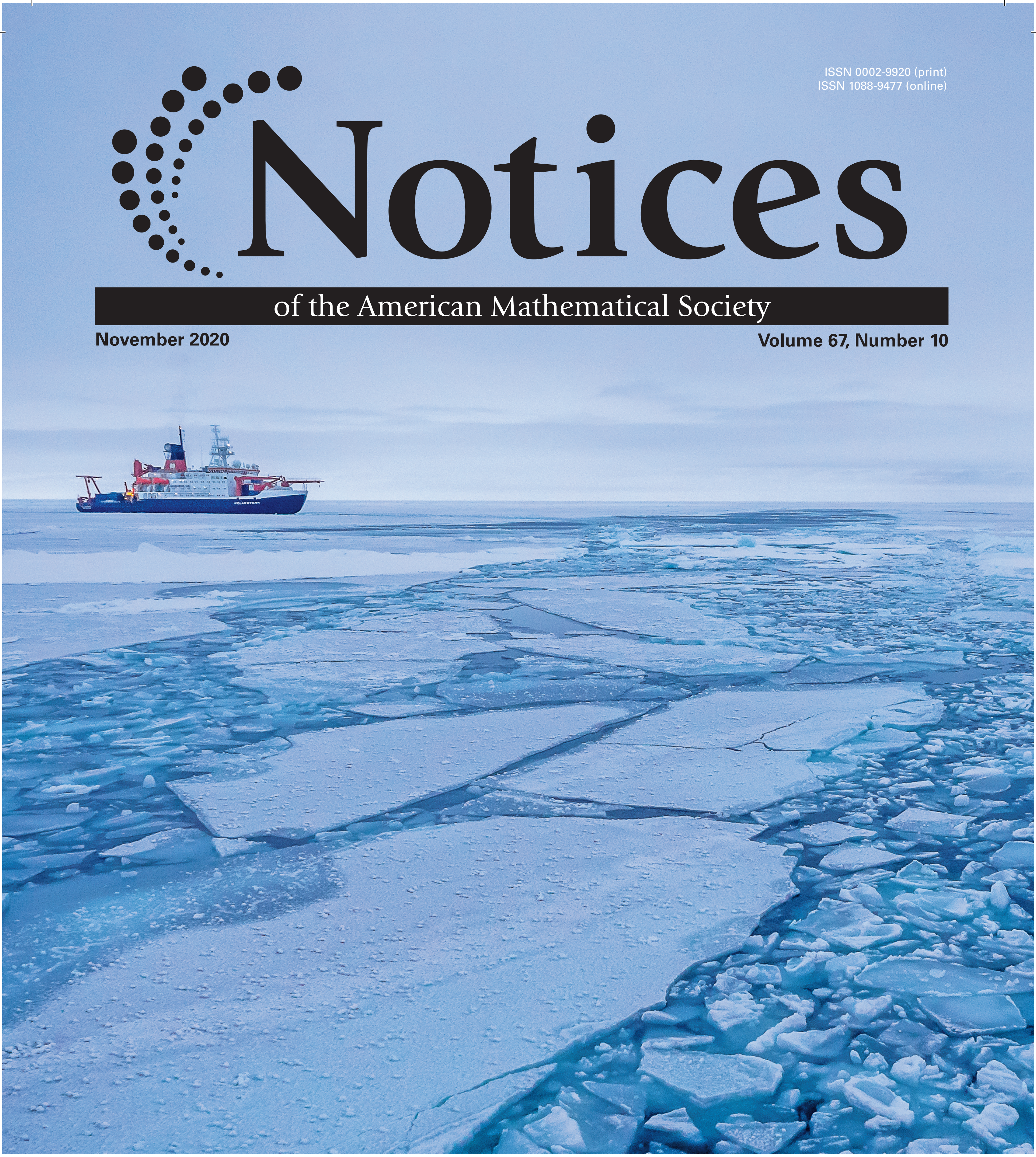

AMERICAN MATHEMATICAL SOCIETY

Advancing research. Creating connections.

The cover is based on "Modeling Sea Ice," page 1535.

Modeling Sea Ice

Kenneth M. Golden, Luke G. Bennetts, Elena Cherkaev, Ian Eisenman, Daniel Feltham, Christopher Horvat, Elizabeth Hunke, Christopher Jones, Donald K. Perovich, Pedro Ponte-Castañeda, Courtenay Strong, Deborah Sulsky, and Andrew J. Wells

Kenneth M. Golden is a Distinguished Professor of Mathematics at the University of Utah. His email address is golden@math.utah.edu.

Luke G. Bennetts is an associate professor of applied mathematics at the University of Adelaide. His email address is luke.bennetts@adelaide.edu.au.

Elena Cherkaev is a professor of mathematics at the University of Utah. Her email address is elena@math.utah.edu.

Ian Eisenman is an associate professor of climate, atmospheric science, and physical oceanography at the Scripps Institution of Oceanography at the University of California San Diego. His email address is eisenman@ucsd.edu.

Daniel Feltham is a professor of climate physics at the University of Reading. His email address is d.l.feltham@reading.ac.uk.

Christopher Horvat is a NOAA Climate and Global Change Postdoctoral Fellow at the Institute at Brown for Environment and Society at Brown University. His email address is christopher_horvat@brown.edu.

Elizabeth Hunke is a deputy group leader, T-3 fluid dynamics and solid mechanics group at the Los Alamos National Laboratory. Her email address is eclare@lanl.gov.

Christopher Jones is a Bill Guthridge Distinguished Professor of Mathematics at the University of North Carolina, Chapel Hill. His email address is ckrtj@unc.edu.

Donald K. Perovich is a professor of engineering at the Thayer School of Engineering at Dartmouth College. His email address is donald.k.perovich@dartmouth.edu.

Pedro Ponte-Castañeda is a Raymond S. Markowitz Faculty Fellow and professor of mechanical engineering and applied mechanics and of mathematics at the University of Pennsylvania. His email address is ponte@seas.upenn.edu.

Courtenay Strong is an associate professor of atmospheric sciences at the University of Utah. His email address is court.strong@utah.edu.

Deborah Sulsky is a professor of mathematics and statistics and of mechanical engineering at the University of New Mexico. Her email address is sulsky@math.unm.edu.

Andrew J. Wells is an associate professor of physical climate science at the University of Oxford. His email address is Andrew.Wells@physics.ox.ac.uk.

Communicated by Notices *Associate Editor Reza Malek-Madani.*

For permission to reprint this article, please contact: reprint-permission@ams.org.

THANK YOU

Office of Naval Research

Applied and Computational Analysis Program

Arctic and Global Prediction Program

National Science Foundation

Division of Mathematical Sciences

Division of Polar Programs

United States Coast Guard · Semper Paratus · 1790

Department of the Navy · ONR · Science & Technology · USN

MCRN · Mathematics and Climate Research Network · NSF

Australian Government
Department of the Environment and Water Resources
Australian Antarctic Division

ace CRC
ANTARCTIC CLIMATE & ECOSYSTEMS
COOPERATIVE RESEARCH CENTRE

NSF

Antarctica New Zealand

UAF · UNIVERSITY OF ALASKA FAIRBANKS

THE UNIVERSITY OF UTAH

Buchanan Bay, Antarctica   Mertz Glacier Polynya Experiment   July 1999

Newsjournal of the Society for Industrial and Applied Mathematics sinews.siam.org

siam news

Volume 53/ Issue 9
November 2020

Special Issue on the Mathematics of Planet Earth

Read about the application of mathematics and computational science to issues concerning invasive populations, Arctic sea ice, insect flight, and more in this Planet Earth ***special issue****!*

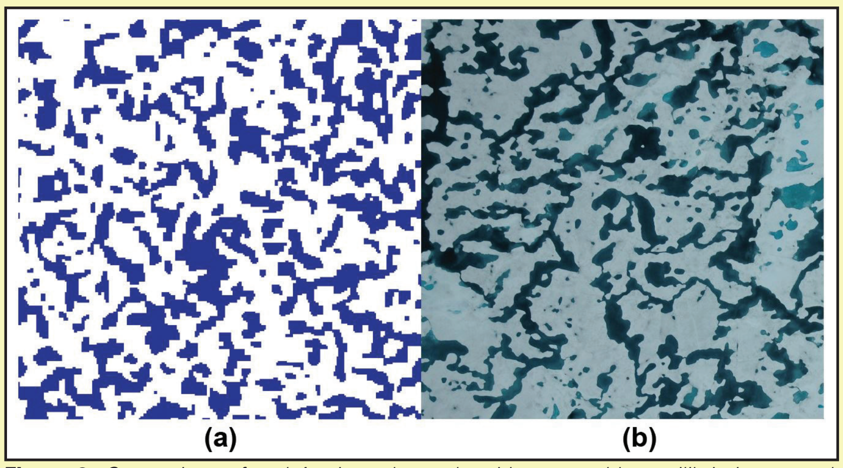

Figure 3. *Comparison of real Arctic melt ponds with metastable equilibria in our melt pond Ising model.* **3a.** *Ising model simulation.* **3b.** *Real melt pond photo. Figure 3a courtesy of Yiping Ma, 3b courtesy of Donald Perovich.*

Vast labyrinthine ponds on the surface of melting Arctic sea ice are key players in the polar climate system and upper ocean ecology. Researchers have adapted the Ising model, which was originally developed to understand magnetic materials, to study the geometry of meltwater's distribution over the sea ice surface. In an article on page 5, Kenneth Golden, Yiping Ma, Courtenay Strong, and Ivan Sudakov explore model predictions.

Controlling Invasive Populations in Rivers

By Yu Jin and Suzanne Lenhart

Flow regimes can change significantly over time and space and strongly impact all levels of river biodiversity, from the individual to the ecosystem. Invasive species in rivers—such as bighead and silver carp, as well as quagga and zebra mussels—continue to cause damage. Management of these species may include targeted adjustment of flow rates in rivers, based on recent research that examines the effects of river morphology and water flow on rivers' ecological statuses. While many previous methodologies rely on habitat suitability models or oversimplification of the hydrodynamics, few studies have focused on the integration of ecological dynamics into water flow assessments.

Earlier work yielded a hybrid modeling approach that directly links river hydrology with stream population models [3]. The hybrid model's hydrodynamic component is based on the water depth in a gradually varying river structure. The model derives the steady advective flow from this structure and relates it to flow features like water discharge, depth, velocity, cross-sectional area, bottom roughness, bottom slope, and gravitational acceleration. This approach facilitates both theoretical understanding and the generation of quantitative predictions, thus providing a way for scientists to analyze the effects of river fluctuations on population processes.

When a population spreads longitudinally in a one-dimensional (1D) river with spatial heterogeneities in habitat and temporal fluctuations in discharge, the resulting hydrodynamic population model is

$$\begin{aligned} N_t &= -A_t(x,t)\frac{N}{A(x,t)} + \\ &\frac{1}{A(x,t)}\Big(D(x,t)A(x,t)N_x\Big)_x - \\ &\frac{Q(t)}{A(x,t)}N_x + rN\left(1-\frac{N}{K}\right) \\ N(0,t) &= 0 \quad \text{on } (0,T), x=0, \\ N_x(L,t) &= 0 \quad \text{on } (0,T), x=L, \\ N(x,0) &= N_0(x) \quad \text{on } (0,L), t=0 \end{aligned} \qquad (1)$$

See **Invasive Populations** *on page 4*

Modeling Resource Demands and Constraints for COVID-19 Intervention Strategies

By Erin C.S. Acquesta, Walt Beyeler, Pat Finley, Katherine Klise, Monear Makvandi, and Emma Stanislawski

As the world desperately attempts to control the spread of COVID-19, the need for a model that accounts for realistic trade-offs between time, resources, and corresponding epidemiological implications is apparent. Some early mathematical models of the outbreak compared trade-offs for non-pharmaceutical interventions [3], while others derived the necessary level of test coverage for case-based interventions [4] and demonstrated the value of prioritized testing for close contacts [7].

Isolated analyses provide valuable insights, but real-world intervention strategies are interconnected. Contact tracing is the lynchpin of infection control [6] and forms the basis of prioritized testing. Therefore, quantifying the effectiveness of contact tracing is crucial to understanding the real-life implications of disease control strategies.

Contact Tracing Demands

Contact tracers are skilled, culturally competent interviewers who apply their knowledge of disease and risk factors when notifying people who have come into contact with COVID-19-infected individuals. They also continue to monitor the situation after case investigations [1].

Case investigation consists of four steps:

1. Identify and notify cases
2. Interview cases
3. Locate and notify contacts
4. Monitor contacts.

Most health departments are implementing case investigation, contact identification, and quarantine to disrupt COVID-19 transmission. The timeliness of contact tracing is constrained by the length of the infectious period, the turn-around time for testing and result reporting, and the ability to successfully reach and interview patients and their contacts. The European Centre for Disease Prevention and Control approximates that contact tracers spend one to two hours conducting an interview [2]. Estimates regarding the timelines of other steps are limited to subject matter expert elicitation and can vary based on cases' access to phone service or willingness to participate in interviews.

Bounded Exponential

The fundamental structure of our model follows traditional susceptible-exposed-infected-recovered (SEIR) compartmental modeling [5]. We add an asymptomatic population A, a hospitalized population H, and disease-related deaths D, as well as corresponding quarantine states. We define the states $\{S_i, E_i, A_i, I_i, H, R, D\}_{i=0,1}$ for our compartments, such that $i=0$ and $i=1$ correspond to unquarantined and quarantined respectively. Rather than focus on the dynamics that are associated with the state transition diagram in Figure 1, we introduce a formulation for the real-time demands on contact tracers' time as a function of infection prevalence, while also respecting constraints on resources.

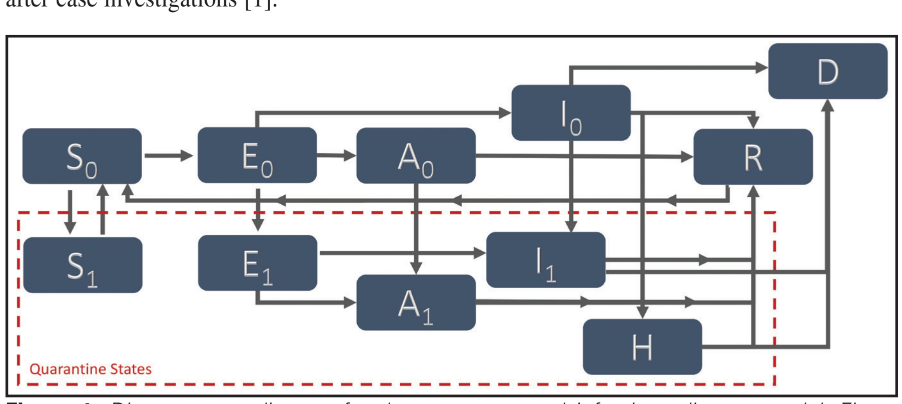

Figure 1. *Disease state diagram for the compartmental infectious disease model. Figure courtesy of the authors.*

When the work that is required to investigate new cases and monitor existing contacts exceeds available resources, a backlog develops. To simulate this backlog, we introduce a new compartment C for tracking the dynamic states of cases:

$$\frac{dC}{dt} = [flow_{in}] - [flow_{out}].$$

Flow into the backlog compartment, represented by $[flow_{in}]$, reflects case identification that is associated with the following transitions in the model:

– The rate of random testing: $q_{rA}(t)A_0(t) \to A_1(t)$ and $q_{rI}(t)I_0(t) \to I_1(t)$

– Testing triggered by contact tracing: $q_{tA}(t)A_0(t) \to A_1(t)$, $q_{tI}(t)I_0(t) \to I_1(t)$, and $q_{tE}(t)E_1(t) \to \{A_1(t), I_1(t)\}$

– The population that was missed by the non-pharmaceutical interventions that require hospitalization: $\tau_{IH}(t)I_0(t) \to H(t)$.

Here, $q_{r*}(t)$ defines the time-dependent rate of random testing, $q_{t*}(t)$ signifies the time-dependent rate of testing that is triggered by contact tracing, and τ_{IH} is the inverse of the expected amount of time for which an infected individual is symptomatic before hospitalization. These terms collectively provide the simulated number of newly-identified positive COVID-19 cases. However, we also need the average number of contacts per case. We thus define function $\mathcal{K}(\kappa, T_S, \phi_\kappa)$ that depends on the average number of contacts a day (κ), the average number of days for which an individual is infectious before going into isolation (T_S), and the likelihood that the individual

See **COVID-19 Intervention** *on page 3*

Nonprofit Org
U.S. Postage
PAID
Permit No 360
Bellmawr, NJ

siam
SOCIETY for INDUSTRIAL and APPLIED MATHEMATICS
3600 Market Street, 6th Floor
Philadelphia, PA 19104-2688 USA